Dissertation

submitted to the

Combined Faculty of Natural Sciences and Mathematics

of the Ruperto Carola University Heidelberg, Germany

for the degree of

Doctor of Natural Sciences

presented by:

Sonja Maria Krausert, M.Sc.

born in: Bad Tölz, Germany

Oral examination: March 18th, 2022

TARGETING HIGH-RISK PEDIATRIC BRAIN TUMOR ENTITIES

Referees:

Prof. Dr. Michael Boutros

Prof. Dr. Stefan M. Pfister

The work and results of the following dissertation were performed and obtained from August 2017 until December 2021 under the supervision of Dr. Marcel Kool and Prof. Dr. Stefan M. Pfister in the Division of Pediatric Neurooncology at the German Cancer Research Center (DKFZ), Heidelberg, Germany and the Hopp Children's Cancer Center (KiTZ), Heidelberg, Germany.

Declaration

I hereby declare that I have written and submitted this dissertation myself and have not used any other sources than those indicated. Furthermore, I declare that I have not applied to be examined at any other institution, nor have I used the dissertation in this or any other form at any other institution as an examination paper, nor submitted it to any other faculty as a dissertation.

The parts of this dissertation about the *Target Actionability Review* were accepted for publication by the *European Journal of Cancer* in November 2021 and were obtained in close collaboration with my co-shared first authors Kaylee M. Keller (Princess Máxima Center for Pediatric Oncology, Utrecht, The Netherlands) and Apurva Gopisetty (Hopp Children's Cancer Center, Heidelberg, Germany). The sections about the generation and characterization of a SMO-inhibitor resistant patient-derived xenograft medulloblastoma model were submitted for publication (in revision) to *Neuro-Oncology* in August 2021. The text of the chapters 3.2.1. and 3.2.2. and the figures in the chapters 3.2.1., 4.2. and 6.2. have been taken from the above mentioned submitted manuscripts. The used text sections have either been written in close collaboration with Kaylee M. Keller and Apurva Gopisetty (for chapters 3.2.1. and 4.2.) or by myself (for chapters 3.2.2. and 6.2.). Similar figures to Figure 22D+E in chapter 6.2. were already shown in the thesis of Sebastian Brabetz, the co-first author of the submitted manuscript and Figure 22D+E were prepared based on the same data.

_____

Sonja Krausert

Abstract

Treatment of pediatric tumors remains challenging and even though research has made a lot of progress and about 80% of diagnosed patients can nowadays be cured, for 20% of patients curative therapy is lacking and this ratio has not much improved in the last >20 years. For several pediatric tumors of the central nervous system, which account for 20-25% of all cancers in children and which are the second most common group of tumors after leukemia, outcome is explicitly poor. To improve survival of pediatric patients with high-risk brain tumors, new treatment strategies need to be developed and tested. In the thesis described here, which consists of three projects, not only new treatment strategies were tested but also already published research findings were evaluated.

In the **first project** a target actionability review (TAR) was prepared. A systematic literature search for literature published between 2014 and 2021 was performed to evaluate the process of replication stress as a therapeutic target for treatment of 16 different solid pediatric tumor entities. By using pre-defined search terms that were either general keywords of geno- and phenotypes observed with replication stress or specific genes that play a major role for replication stress, 319 papers were identified and included for further review based on abstract and title. The papers were evaluated by two reviewers independently and findings related to target activation in clinical series, from *in vitro* and *in vivo* preclinical experiments or from clinical trials were summarized. Data was scored for quality and outcome and reviews documented in the web portal R2. After evaluation of papers with discrepant scores by a third reviewer, in total 145 publications addressing 37 different drug targets were included for analysis and scores were visualized by heatmaps that are publicly available within the R2 TAR platform (https://hgserver1.amc.nl/cgi-bin/r2/main.cgi?option=imi2_targetmap_v1). Besides identification of 31 alternative potential targets to target replication stress in pediatric solid tumors, the targets ATM, ATR, CHK1, DNA-PK, PARP, and WEE1, were analyzed in more detail. The analysis revealed that the targets ATR, CHK1, PARP, and WEE1, were the most promising targets for monotherapy or combination therapies with chemo-/radiotherapy for treatment of neuroblastoma, osteosarcoma, high-grade glioma and medulloblastoma. The evidence scores for the targets ATM and DNA-PK were positive for treatment of high-grade glioma or neuroblastoma and osteosarcoma, respectively, however, the results were based on a limited amount of literature and need to be studied in more detail for a comprehensive analysis. An intensively studied module with 114/401 evidence entries (28%) was “combinations” and within this the most studied strategy was combining a PARP-inhibitor with chemo- or radiotherapy, which yielded positive appraisal scores for treatment of neuroblastoma, rhabdomyosarcoma, Ewing sarcoma, osteosarcoma, nephroblastoma, high-grade glioma and ependymoma.

The **second project** was performed to target replication stress *in vitro* and *in vivo* in cell lines and patient-derived xenograft (PDX) models, respectively of medulloblastoma (MB), ependymoma (EPN) and embryonal tumors with multilayered rosettes (ETMR). With an *in vitro* drug screen on the MB Group 3 cell line HD-MB03 and the ETMR cell line Bt183 the most synergistic combination partner for Irinotecan, respectively the active metabolite SN-38, was evaluated using a drug library with 76 compounds, which revealed the PARP-inhibitors Olaparib and Talazoparib as the most synergistic combination partners. The synergistic effect was also confirmed when using the brain penetrant PARP-inhibitor Pamiparib, while fetal Astrocytes, as a control cell line, did not respond effectively to the combination treatment. To verify the effect of the treatment with Pamiparib and Irinotecan *in vivo*, five different PDX models representing ETMR (Bt183), Sonic Hedgehog (SHH) MB (med-1712FH and BT084), Group 3 MB (nch2194) and *ZFTA*-fusion positive ependymoma (Bt165) were injected subcutaneously or orthotopically into immunodeficient NSG mice. Subcutaneous tumors of the ETMR model showed complete regression when treated with Irinotecan and Pamiparib in combination, however, for the other models no synergistic effect was observed when injected orthotopically. Nevertheless, Irinotecan alone was able to induce a significant survival benefit and tumor growth inhibition for the MB Group 3 and the *ZFTA*-fusion positive EPN model. Refinements of the treatment strategy including dose adaptations of Irinotecan and Pamiparib and using a nanoformulated version of SN-38 (peg-SN-38), which is characterized by a longer half-live and accumulation in the tumor, showed no significant differences when applied to the MB Group 3 model nch2194. The observed effect on tumor growth and survival was solely based on Irinotecan or peg-SN-38 and adding the PARP-inhibitor Pamiparib could not further increase the effect.

The **third project** focused on the generation and molecular characterization of SHH MB PDX models that are resistant to the treatment with the Smoothened (SMO) inhibitor Sonidegib. For treatment of patients diagnosed with a SHH MB, especially adult patients, use of inhibitors that target the transmembrane protein SMO, a key component of the SHH pathway, is promising. However, even though patients typically show initial tumor regression, they often develop resistance to the treatment. To understand the mechanisms of resistance and to develop new treatment strategies that overcome resistance, preclinical models that are resistant to SMO inhibition with the same molecular characteristics as seen in patients are needed. For generation of resistant models, mice harboring tumors of a *PTCH1*-mutated SHH MB PDX model that is sensitive to SMO inhibition were treated *in vivo* with the SMO-inhibitor Sonidegib using intermitted treatment cycles until tumors became resistant to therapy. Vehicle-treated and the nine generated resistant tumors were analyzed with whole genome and RNA sequencing to evaluate the underlying mechanism of resistance and confirmed target engagement of Sonidegib. Eight models acquired resistance due to a missense

mutation in *SMO* and one model became resistant due to an inactivating point mutation in *MEGF8*, which is a negative regulator of the SHH signaling pathway. For development of further treatment strategies, an *in vitro* drug screen with 76 drugs was performed with a sensitive, treatment-naïve and a resistant model and revealed the XPO1-inhibitor Selinexor as one of the top hits being effective in both models. To confirm efficacy *in vivo*, a sensitive, vehicle-treated and two resistant models, one *SMO*-mutated and the *MEGF8*-mutated, were intracranially injected into NSG mice and treated with Selinexor. Treatment of the two resistant models resulted in tumor growth inhibition and significant survival benefit.

The results of the three projects described in this thesis will support the improvement of treatment strategies for high-risk pediatric brain tumor entities. Evaluation of published literature helps to streamline the best treatment strategies and identify knowledge gaps. Applying one of the most promising approaches, a combination of a topoisomerase-inhibitor with a PARP-inhibitor, in *in vitro* and *in vivo* preclinical studies revealed further information on responding and non-responding tumor entities. In addition, the generation of new, clinically relevant preclinical medulloblastoma models may improve translational research for medulloblastoma patients and can be considered as a paradigm how to predict resistance to targeted monotherapy in clinically relevant models.

Zusammenfassung

Die Behandlung von pädiatrischen Tumoren stellt die Wissenschaft und Ärzte vor große Herausforderungen, und obwohl die Forschung große Fortschritte gemacht hat und etwa 80% der diagnostizierten Patienten geheilt werden können, fehlt für 20% der Patienten eine erfolgreiche Therapiestrategie und dieser Anteil konnte in den letzten 15-20 Jahren nicht wesentlich verringert werden. Etwa 20-25% der pädiatrischen Tumore befinden sich im zentralen Nervensystem und sind somit die zweithäufigste Tumorart nach den Leukämien und durch eine besonders schlechte Prognose charakterisiert. Um die Überlebenschancen der pädiatrischen Patienten zu verbessern müssen neue Therapiestrategien erforscht und etabliert werden. In dieser Dissertation, welche aus drei Projekten besteht, wurden nicht nur neue Therapien getestet, sondern auch schon publizierte Therapiestrategien evaluiert und bewertet.

Das **erste Projekt** beschreibt die Erstellung eines *Target Actionability Reviews* (TAR). Dafür wurde Literatur, welche zwischen 2014 und 2021 publiziert wurde, systematisch analysiert um den Prozess des Replikationsstresses als Therapietarget für 16 verschiedene pädiatrische Tumorentitäten zu evaluieren. Definierte Suchbegriffe, die entweder generelle Geno- oder Phänotypen von Replikationsstress beschreiben oder spezifische Gene, die wichtig für Replikationsstress sind, wurden genutzt um die publizierte Literatur zu durchsuchen und 319 relevante Publikationen wurden ausfindig gemacht, welche für die weitere Analyse verwendet wurden. Jede der Publikationen wurde von zwei unabhängigen Personen analysiert und Ergebnisse, welche sich aus klinischen Studien, *in vitro* oder *in vivo* präklinischen Experimenten ergaben, wurden zusammengefasst, in Bezug auf Qualität und Ergebnis bewertet und im Webportal R2 gepeichert. Publikationen mit unterschiedlichen Bewertungen wurden von einem dritten Reviewer analysiert und schlussendlich wurden 145 Publikationen mit 37 unterschiedlichen Therapietargets für die abschließende Analyse eingeschlossen. Die Bewertungen wurden durch Heatmaps visualisiert und sind über die Plattform „R2 TAR“ öffentlich zugänglich. Von den 37 unterschiedlichen Therapietargets, von denen 31 Targets alternative und noch wenig erforschte Targets sind, wurden die sechs Targets ATM, ATR, CHK1, DNA-PK, PARP und WEE1 genauer und detaillierter evaluiert. Die Analyse ergab, dass ATR, CHK1, PARP und WEE1 die vielversprechendsten Targets für Monotherapien oder Kombinationstherapien mit Chemo- oder Radiotherapien sind und besonders relevant für die Behandlung von Neuroblastomen, Osteosarkomen, hochgradigen Gliomen oder Medulloblastomen sind. Die Analyse der Targets ATM und DNA-PK ergab positive Bewertungen für die Behandlung von hochgradigen Gliomen bzw. Neuroblastomen und Osteosarkomen, jedoch beruht diese Wert nur auf wenigen Publikationen und weitere Studien werden benötigt um diese Targets vollständig zu evaluieren. Ein Modul, welches

intensiv erforscht wurde (mit 114/401 Bewertungen; 28%) bezieht sich auf Kombinationstherapien. Die am häufigsten angewendete Kombination war Chemo- oder Radiotherapie mit PARP-Inhibitoren und ergab positive Bewertungen für die Behandlung von Neuroblastomen, Rhabdomyosarkomen, Ewing-Sarkomen, Osteosarkomen, Nephroblastomen, hochgradigen Gliomen und Ependymomen.

Im **zweiten Projekt** wurde Replikationsstress als Target in *in vitro* und *in vivo* Experimenten mit Zelllinien bzw. PDX- (*patient-derived xenograft*) Modellen für Medulloblastome (MB), Ependymome (EPN) und embryonale Tumore mit mehrschichtigen Rosetten (ETMR) evaluiert. Mit Hilfe eines *in vitro* Screens und den Zelllinien HD-MB03 (MB Gruppe 3) und Bt183 (ETMR) wurde der synergistischste Kombinationspartner für Irinotecan, bzw. den aktiven Metabolit SN-38, unter 76 Medikamenten analysiert. Dabei wurden die PARP-Inhibitoren Olaparib und Talazoparib als beste Kombinationspartner identifiziert. Der synergistische Effekt konnte auch mit dem hirngängigen PARP-Inhibitor Pamiparib bestätigt werden und zugleich konnte gezeigt werden, dass normale Astrozyten, welche als Kontroll-Zelllinie verwendet wurden, nicht auf die Behandlung ansprechen. Um den positiven Effekt der Behandlung auch *in vivo* zu bestätigen wurden fünf verschiedene PDX-Modelle, welche die Entitäten ETMR (Bt183), MB „Sonic Hedgehog“ (SHH) (med-1712FH und BT084), MB Gruppe 3 (nch2194) und *ZFTA*-fusionspositive Ependymome (Bt165) repräsentieren, subkutan oder intrakraniell in immundefiziente NSG-Mäuse transplantiert. Durch die Behandlung mit Irinotecan und Pamiparib bildeten sich subkutane ETMR-Tumore vollständig zurück, jedoch konnte für die anderen Tumormodelle, welche orthotop injiziert wurden, kein derartiger synergistischer Effekt der Medikamente festgestellt werden. Dennoch führte die Behandlung mit Irinotecan alleine zu signifikant längerem Überleben und gehemmtem Tumorwachstum im MB Gruppe 3-Modell, sowie im *ZFTA*-fusionspositiven Ependymom-Modell. Auch durch Anpassung der Behandlung, wie veränderte Dosierung oder Verwendung einer nanoformulierten Version von SN-38 (peg-SN-38), welche eine längere Halbwertszeit hat und im Tumor akkumuliert, konnten keine signifikanten Unterschiede bei der Behandlung des MB Gruppe 3-Models nch2194 festgestellt werden. Die Wirkung auf Tumorwachstum und Überlebensdauer basierte allein auf der Wirkung von Irinotecan oder peg-SN-38 und durch die Kombination mit dem PARP-Inhibitor Pamiparib konnte kein zusätzlicher Effekt erzielt werden.

Im **dritten Projekt** wurden SHH MB PDX-Modelle, welche gegen die Behandlung mit dem *Smoothened* (SMO) –Inhibitor Sonidegib resistent sind, generiert und molekular charakterisiert. Für die Behandlung von Patienten mit einem MB SHH-Tumor, vor allem erwachsene Patienten, ist die Verwendung von Inhibitoren die das Transmembranprotein SMO des HH-Signalweges inhibieren, vielversprechend. Jedoch, obwohl die Patienten zuerst gut auf die Behandlung ansprechen und sich der Tumor

verkleinert, werden die Patienten oft resistent gegen die Behandlung. Um die zugrunde liegenden Mechanismen der entwickelten Resistenz zu verstehen und neue Behandlungsstrategien zu entwickeln um die Resistenz zu überwinden, sind präklinische Modelle, die die gleichen Resistenzmechanismen aufweisen die auch im Tumor des Patienten vorliegen, notwendig. Für die Generierung der resistenten Modelle wurden Mäuse mit Tumoren des *PTCH1*-mutierten MB SHH-Modells, welche sensitiv für die Behandlung mit einem SMO-Inhibitor sind, *in vivo* mit Sonidegib in Zyklen behandelt bis die Tumore resistent gegen die Behandlung waren. Tumore der Kontrollgruppe und die neun generierten resistenten Tumore wurden durch Sequenzierung des ganzen Genoms und der RNA analysiert um die Mechanismen der Resistenzen zu identifizieren und zu überprüfen, dass Sonidegib den HH-Signalweg inhibiert. Acht Modelle entwickelten die Resistenz durch eine Mutation in *SMO*, ein Modell wurde resistent durch eine inaktivierende Mutation in *MEGF8*, einem Regulator des HH-Signalweges. Um weitere Behandlungsstrategien zu untersuchen wurde ein *in vitro* Screen mit 76 Medikamenten und einem sensitiven sowie einem resistenten Modell durchgeführt. Eines der effizientesten Medikamente, welches in beiden Tumormodellen gute Wirkung zeigte, war der XPO1-Inhibitor Selinexor. Um die Wirkung von Selinexor auch *in vivo* zu bestätigen, wurde ein Tumor der Kontrollgruppe, sowie zwei resistente Tumore, einer mit Mutation in *SMO* und der mit Mutation in *MEGF8*, intrakraniell in NSG-Mäuse transplantiert und mit Selinexor behandelt. Die Behandlung führte zu langsamerem Tumorwachstum und signifikant längerem Überleben in beiden resistenten Modellen.

Die Ergebnisse der drei Projekte werden dazu beitragen die Behandlungsstrategien für aggressive pädiatrische Hirntumore zu verbessern. Die Evaluation der publizierten Literatur hilft die besten Behandlungsstrategien zu identifizieren. Die Anwendung einer der vielversprechendesten Strategien, die Kombination eines topoisomerase-Inhibitors und eines PARP-Inhibitors *in vitro* und *in vivo* lieferte mehr Einblick, welche Tumorentitäten von der Behandlung profitieren können. Darüberhinaus kann durch die Generierung von klinisch relevanten Medulloblastom-Modellen die translationale Forschung für diese Patienten verbessert werden und dient als Beispiel, wie die Resistenzbildung bei klinisch relevanten Modellen nachempfunden werden kann.

Contents

List of Abbreviations

APC	Adenomatous-polyposis-coli
ATM	Ataxia telangiectasia mutated serine/threonine kinase
ATR	Ataxia telangiectasia and Rad3 related
ATRT	atypical teratoid rhabdoid tumors
BBB	blood-brain-barrier
BCA – Assay	Bicinchoninic acid - assay
BCC	basal cell carcinoma
BCOR	BCL6 Corepressor
BID	“bis in die”; two times per day
BSA	bovine serum albumin/Fraction V
C19MC	microRNA-cluster on chromosome 19
CDK6	cyclin dependent kinase 6
CHK1	checkpoint kinase 1
CNS	central nervous system
CREBBP	(cAMP-response element binding) binding protein
CTDNEP1	CTD Nuclear Envelope Phosphatase 1
DDX3X	Dead box helicase 3 X-linked
DHH	Desert Hedgehog
DNA	deoxyribonucleic acid
DNA-PK	DNA-dependent protein kinase catalytic subunit
DNMT3B	DNA Methyltransferase 3 Beta
dsDNA	double-stranded DNA
DSS	drug Sensitivity Score
ELP1	Elongator Complex Protein 1
EPN	ependymoma
EPR	enhanced permeability and retention
ERBB4	Erb-B2 Receptor Tyrosine Kinase 4
ES	Ewing Sarcoma
ETMR	embryonal tumor with multilayered rosettes
EZHIP	EZH Inhibitory Protein
FACS	fluorescence Activated Cell Sorting

FDA	Food and Drug Administration
FFPE	Formalin fixed paraffin embedded
FIMM	Institute for Molecular Medicine Finnland
GCT	germ cell tumor
GEMM	genetically engineered mouse models
GFI1	growth Factor Independent 1 Transcriptional Repressor
GFP	green fluorescent protein
GLI	glioma-associated protein
GSEA	Gene Set Enrichment Analysis
H2AX	H2A Histone Family Member X
H3K27	histone 3 lysine 27
H3K27me3	histone 3 lysine 27 trimethylation
HB	hepatoblastoma
HE	Hematoxylin and Eosin
HGG	high-grade glioma
HH	hedgehog
ICGC	International Cancer Genome Consortium
IHC	immunohistochemistry
IHH	Indian Hedgehog
IMT	inflammatory myofibroblastic tumor
InDel	Insertion/Deletion
i.p.	intraperitoneal
IPA	Ingenuity Pathway Analysis
IRN	Irinotecan
ITCC-P4	Innovative Therapies for Children with Cancer – Pediatric Preclinical Proof of Concept Platform
IVC	individually ventilated cages
IVIS	*in vivo* imaging system
KBTBD4	Kelch Repeat And BTB Domain Containing 4
KDM6A	lysine Demethylase 6A
KiTZ	Kinder-Tumorzentrum, Heidelberg
KMT2D	histone-Lysine N-Methyltransferase 2D
L1CAM	L1 cell adhesion molecule
LCA	large cell and/or anaplastic

LGG	low-grade glioma
LIN28A	Lin-28 Homolog A
LoF	loss of function
MAML2	Mastermind Like Transcriptional Coactivator 2
MB	medulloblastoma
Mb	Megabase
MBEN	medulloblastoma with extensive nodularity
MEGF8	multiple epidermal growth factor-like domains protein 8
MoA	mechanism-of-action
MPNST	malignant peripheral neve sheath tumor
MRT	malignant rhabdoid tumor
MTD	maximum tolerated dose
NBL	neuroblastoma
NF2	Neurofibromin 2
NF-κB	nuclear factor-κB
NGS	next-generation sequencing
NSC	neural stem cells
NSG	NOD-*scid* IL2Rgamma^{null}
OS	osteosarcoma
OS	overall survival
OTX2	Orthodenticle Homeobox 2
PAR	poly (ADP-ribose)
PARP	poly (ADP-ribose) polymerase
PBS	phosphate-buffered saline
PD	pharmacodynamics
PDOX	patient-derived orthotopic xenograft
PDX	patient-derived xenograft
PF	Posterior fossa
PF-EPN-A	Posterior fossa ependymoma A
PF-EPN-B	Posterior fossa ependymoma B
PFS	progression free survival
pGF1	pGreenFire1
PK	pharmacokinetics
PMID	PubMed IDs

po	per oral
PoC	Proof of Concept
PRDM6	PR/SET Domain 6
PTCH1	patched 1
PTEN	Phosphatase and tensin homolog
RB	retinoblastoma
RIN	RNA integrity number
RMS	rhabdomyosarcoma
RNA	ribonucleic acid
RP2D	recommended phase II dose
RTK	receptor-tyrosine-kinase
s.c.	subcutan
SCNA	somatic copy number alterations
SEM	standard error of the mean
SHH	Sonic Hedgehog
SMARCA4	SWI/SNF-Related Matrix-Associated Actin-Dependent Regulator Of Chromatin Subfamily A Member 4
SMO	smoothened
SNCAIP	Synuclein Alpha Interacting Protein
SNV	single nucleotide variation
SoC	standard-of-care
SP-EPN	spinal anaplastic ependymoma
SP-MPE	spinal myxopapillary ependymoma
SS	synovial sarcoma
ssDNA	Single stranded DNA
ST	supratentorially
ST-EPN-RELA	supratentorial ependymoma, type RELA
ST-EPN-YAP1	supratentorial ependymoma, type YAP1-fusion positive
SUFU	suppressor of fused homolog
SV	structural variation
TAR	Target Actionability Review
TBS-t	Tris-buffered saline with 0.05% Tween20
TDSU	Translational Drug Screening Unit
TERT	telomerase reverse transcriptase

TTYH1	tweety family member 1
WGS	whole genome sequencing
WHO	World Health Organization
WNT	wingless-type
WT	Wilms tumor/Nephroblastoma
ZFTA	Zinc Finger Translocation Associated
ZMYM3	Zinc Finger MYM-Type Containing 3

List of Figures

List of Tables

1. General Introduction

1.1. Pediatric brain cancer entities

1.1.1. Overview

Pediatric central nervous system (CNS) tumors are the second most common group of tumors in children after leukemia and account for 20-25% of all cancers in children [1,2]. Even though leukemia is the leading cause of cancer-related death for young children aged 1-4 years, for children aged 0-18 years brain tumors are the leading cause of cancer-related deaths [3]. In the US, the incidence rate for childhood brain tumors is 5.14/100.000 in the age range 0-14 and the 5-year overall survival rate is 72.3% [3,4]. The survival is highly dependent on the diagnosis and, if applicable, the subgroup within an entity. Since the mutational burden of pediatric brain cancers is significantly lower than of adult brain tumors - the only exception are high-grade gliomas with mutations in the DNA repair machinery – pediatric brain tumors are among many other reasons, not comparable to brain tumors in adults [5].

Pediatric brain tumors can be grouped into cancers derived from glial cells like astrocytes or oligodendrocytes or from non-glial cells such as neurons or stem cells (Figure 1) [6,7]. Tumor entities that originate from glial cells are ependymoma (EPN) and low- and high-grade glioma (LGG and HGG, respectively). Tumors that develop from a non-glial origin can be further divided into embryonal tumors, meningioma, and other tumors such as craniopharyngioma or germ cell tumors. Embryonal tumor entities comprise among others medulloblastoma (MB) with various molecular groups and tumor entities such as atypical teratoid rhabdoid tumors (ATRT), embryonal tumors with multilayered rosettes (ETMR) and various CNS tumors with e.g. *FOXR2*-activation or *BCOR* internal tandem duplication. Besides these entities and groups, more groups were defined in the most recent WHO classification published in 2021 but for easier presentation and overview not all molecular groups defined for e.g. glioma, meningioma or other non-glial tumors were listed in Figure 1 and tumor entities and groups not relevant for the project described here were not added [8]. Within the group of patients younger than 14 years, medulloblastoma is the most common malignant tumor type accounting for 15-20% of all brain tumors [9,10]. However, recent tumor statistics report that high-grade glioma are the most common malignant pediatric brain tumor type with incidence rates of 25-30% [11].

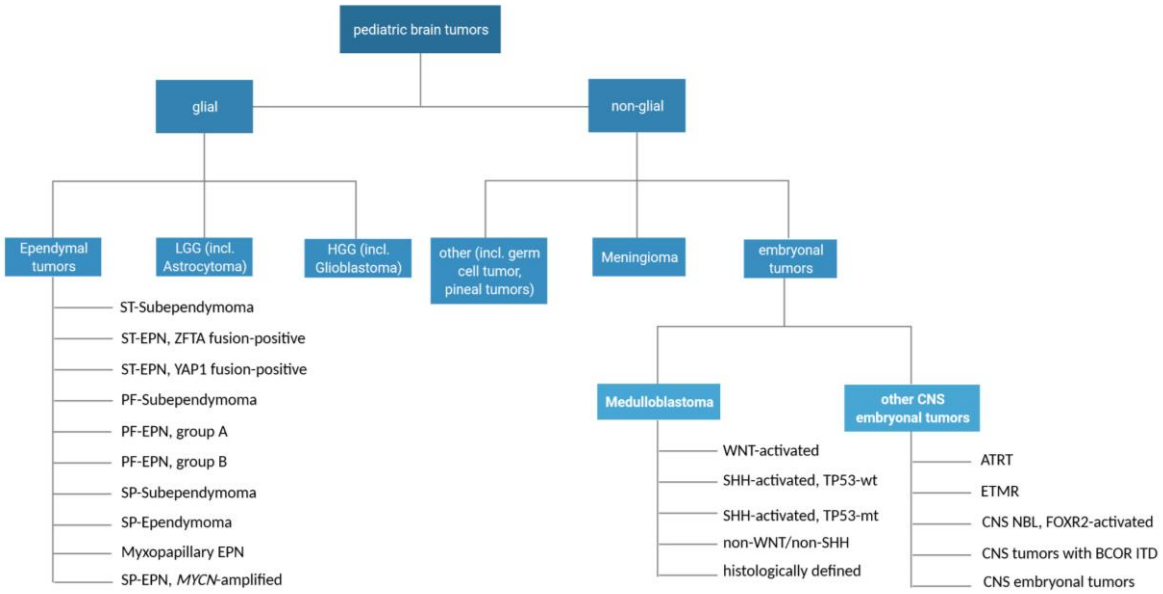

Figure 1: Overview of pediatric brain tumors.

Pediatric brain tumors can be grouped into glial and non-glial tumors and are then further subdivided into different entities. For better overview not all further subdivided groups are listed; adapted from Pfister *et al*. 2018 [6] and Louis *et al*. 2021 [8]; created with BioRender.com.

In my PhD project the focus was on the tumor entities medulloblastoma, ependymoma and ETMR and these three entities will be further introduced here.

1.1.2. Medulloblastoma

Medulloblastoma (MB) is a common malignant brain tumor occurring in childhood, is typically classified as World Health Organization (WHO) grade IV and accounts for roughly 20% of all CNS malignancies and 63% of intracranial embryonal tumors [9,12-14]. Histologically, the entity presents as classic, desmoplastic nodular, MB with extensive nodularity (MBEN), or as large cell/anaplastic (LCA), which also come along with variable prognosis with MBEN and desmoplastic histology indicating better prognosis than the other two histologies, of which tumors with LCA histology mostly do worse than the ones with classic histology [8,15-18]. The standard-of-care (SoC) therapy, however it is age dependent, includes maximal safe resection followed by high-dose chemotherapy or by low-dose chemotherapy in combination with radiotherapy [19-21]. About 70% of diagnosed patients survive but the treatment can lead to severe long-term side effects such as neurocognitive deficits, increased chance of secondary tumors, endocrine dysfunction, loss of hearing and other organ toxicities [17,22-25]. Already starting in 2006 different researchers identified several molecular groups of MB but the

studies varied in number and composition of the groups and between four and six groups were identified initially [26-29]. In 2012 a consensus was reached and four main molecular groups named Wingless-type (WNT), Sonic Hedgehog (SHH), Group 3 and Group 4 were defined, which differ in clinical and molecular characteristics (Figure 2).

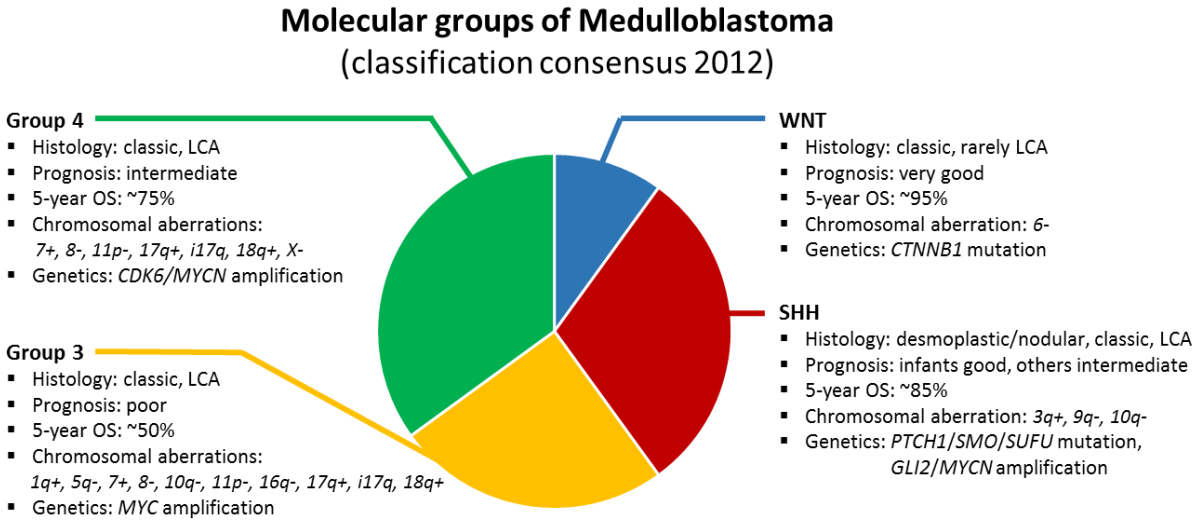

Figure 2: Overview of the four main molecular groups of medulloblastoma of the consensus reached in 2012.

The published consensus of molecular groups of medulloblastoma (reached in 2012) defined the WNT, SHH, Group 3 and Group 4 group which present differences in histology, prognosis and genetics [30,31].

Tumors of the WNT and SHH group are driven by mutations that lead to constitutive activity of the respective pathway but the oncogenic driver and the biology is less clear for Group 3 and Group 4 tumors. However, some drivers are known as e.g. *GFI/GFI1B* activation or *MYC*-amplification for Group 3 or aberrant SRC signaling and *PRDM6* activation in Group 4 tumors [32-34]. Based on the WHO guidelines for classification of CNS tumors published in 2016, a molecular categorization of MBs into a WNT, a SHH-TP53^{wildtype}, a SHH-TP53^{mutant} and a non-WNT/non-SHH-group was suggested [12].

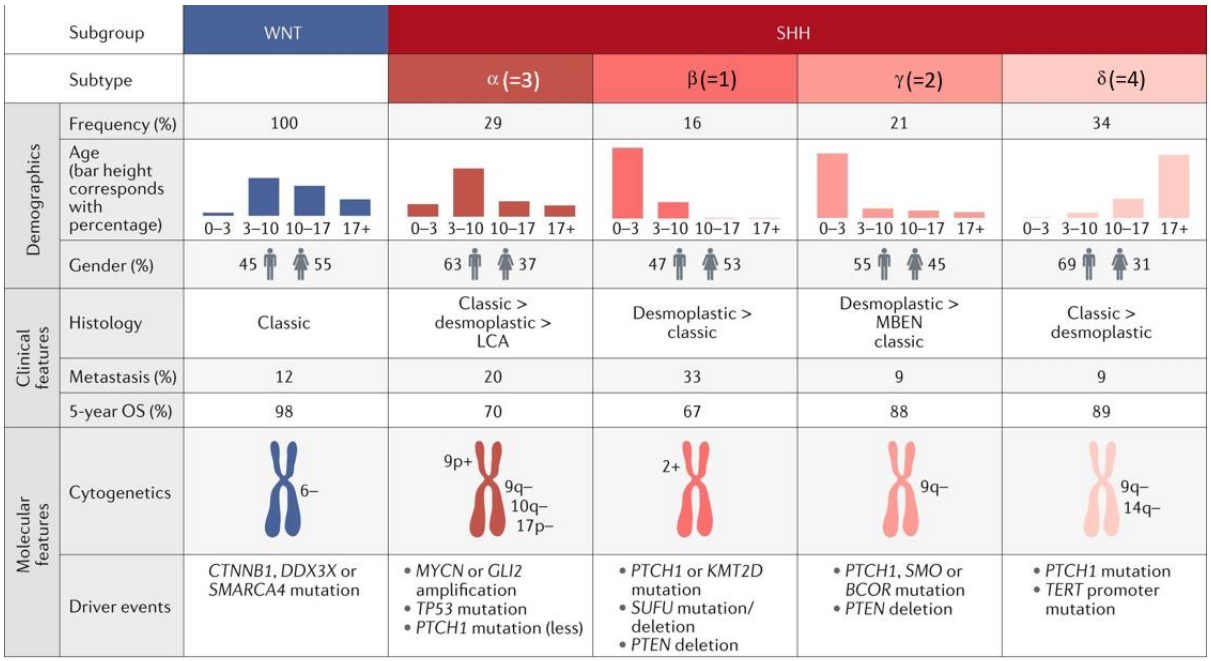

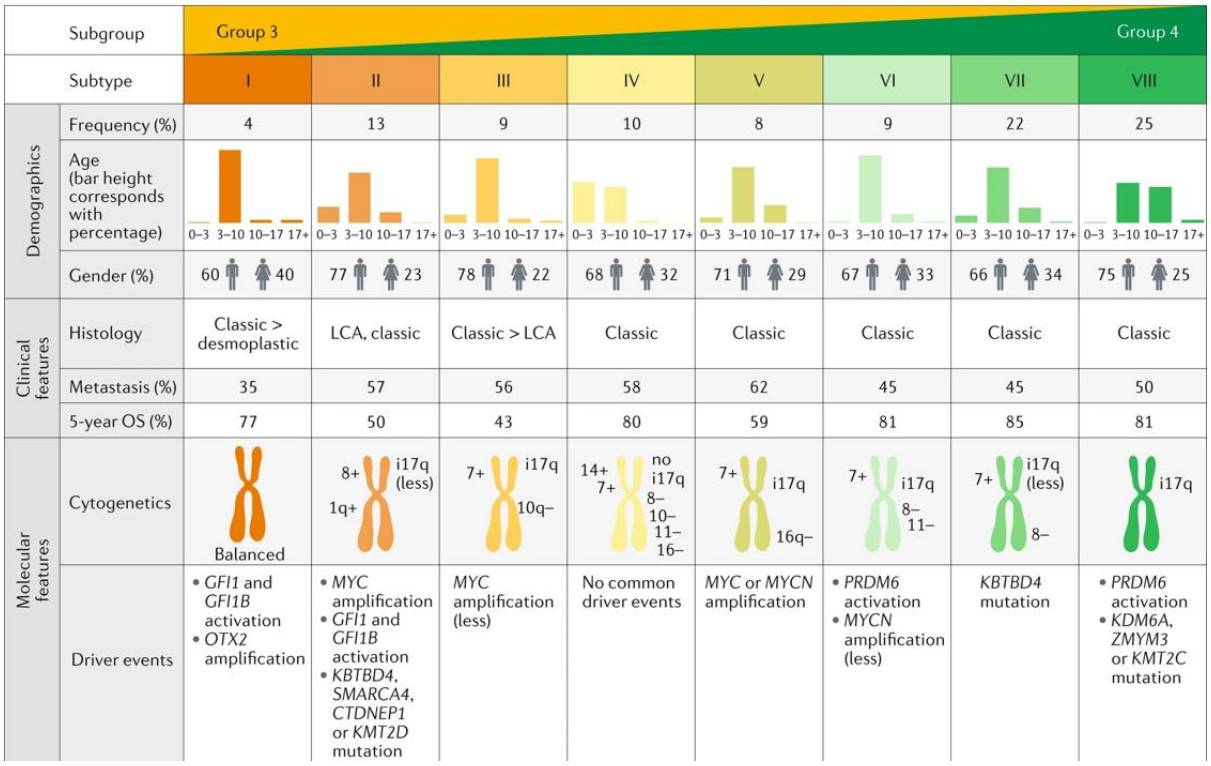

Figure 3: Overview of the four main molecular groups and additional subgroups of medulloblastoma with demographic, clinical and molecular characteristics.

Each of the molecular groups and subgroups is characterized by unique age and gender distribution, histology and cytogenetics. For most subgroups driver events are known and established, however for some driver events are not identified or established. Recently the SHH subgroups α, β, γ and δ were renamed into SHH-3, SHH-1, SHH-2 and SHH-4 respectively [35]. Figure taken from Hovestadt *et al.* 2020 [36].

WNT group

The WNT group accounts for ~10% of all MB and these tumors mostly arise in children between 3 and 17 years with equal frequencies for males and females [30,37]. Patients with WNT MB tumors have the best outcome (10-year survival rate: ~95%) among all MB groups (Figure 3) [4]. The most common mutation (90% of cases) detected in this group of tumors is a somatic mutation occurring in exon 3 of *CTNNB1*, which encodes β-catenin. Patients that have wildtype β-catenin have a germline mutation occurring within the gene *adenomatous-polyposis-coli (APC)* (Turcot-syndrome), which is an inhibitor of the WNT pathway [14,38-40]. The mutations in *CTNNB1* and *APC* both lead to aberrant activation of the WNT pathway. Patients with mutation in *APC* are also at risk to develop other tumors as e.g. colon cancer [41]. Mutated *CTNNB1* leads to stabilization of β-catenin by preventing its degradation by *APC* [42]. Besides the characteristic activation of the WNT pathway, tumors of the WNT group are very commonly characterized by monosomy 6. Other somatic mutations that occur frequently within the WNT group are mutations in *TP53*, *SMARCA4 (SWI/SNF-related matrix-associated actin-dependent regulator of chromatin subfamily A member 4*) or *DDX3X (dead box helicase 3 X-linked),* which encodes an RNA helicase. None of these mutations seem to have an effect the outcome of WNT MB patients [14,37,43]. The good survival rate of WNT MB, which also impacts that these tumors are not designated as WHO grade IV anymore, might be explained by the fact that these tumors show a disruption of the blood-brain-barrier (BBB), since constitutive activation of the WNT pathway leads to secretion of WNT antagonists, which do not affect tumor cells, because β-catenin is mutated, but do affect endothelial cells. In endothelial cells the WNT pathway gets inhibited by the secreted antagonists and results in porous vasculature since endothelial cells cannot maintain intercellular contacts anymore, which subsequently leads to a better accumulation of chemotherapeutics within the tumor [44,45].

SHH group

About 30% of all MB tumors are of the SHH subgroup. Interestingly, SHH MB tumors show a bimodal age distribution in young children <10 years and in adults, respectively. They can arise due to different germline mutations that predispose patients to SHH MB (>40% of cases) or they can also occur sporadically [35,46]. Germline mutations in *Patched 1 (PTCH1)* (Gorlin-syndrome), *Suppressor of fused homolog (SUFU)* or *TP53* (Li-Fraumeni-syndrome) or, very rarely *Smoothened (SMO)* (Curry-Jones-syndrome) are known so far [40,47-53]. In addition, recent studies reported germline loss-of-function (LoF) mutations within the *Elongator Complex Protein 1* (*ELP1*) gene and within the *G protein-coupled receptor 161* (*GPR161*) [54,55]. Besides the genetic predisposition, SHH MB tumors can arise sporadically by somatic mutations in *PTCH1* (present in ~40% of the SHH MB tumors), *SMO* (9%), *SUFU* (10%) or amplifications of g*lioma-associated protein 1/2 (GLI1/2)* (9%) or *MYCN* (7%) [14,30,56,57]. Several studies,

where cohorts of SHH MB tumors were sequenced, showed age-associated differences in the distribution of mutations (Figure 3) [14,36,58,59]. Adult patients mostly harbor mutations upstream in the SHH pathway, older children more often have amplifications downstream of *SMO,* namely in *MYCN* or *GLI* co-occurring with mutations in *TP53*. Very young children frequently have mutations in *PTCH1* or *SUFU*. In about 40% of the SHH MB tumors, but mostly in adults, *telomerase reverse transcriptase* (*TERT)* acts as an oncogenic driver with the recurrent mutations C228T and C250T that are located in the promoter and increase expression of *TERT* [60,61]. Another characteristic of SHH MB tumors is the deletion of chromosome 9q, where *ELP1* (chr.9q31) and also *PTCH1* (chr.9q22) are located [28]. Over the course of the past years, more and more samples were subjected to DNA methylation profiling. This data allowed to further classify SHH MB tumors into four different subgroups (SHHα, SHHβ, SHHγ, SHHδ), which were recently renamed into SHH-3, SHH-1, SHH-2, and SHH-4, respectively (Figure 3) [35,46]. The SHH-1 subgroup includes infants (≤3 years) and is characterized by mostly desmoplastic histology, metastasis in more than 30% of cases and mutations in *PTCH1*, *histone-lysine N-methyltransferase 2D (KMT2D)*, *SUFU* or *Phosphatase and tensin homolog (PTEN)* deletions. Tumors of the SHH-2 subgroup also mostly occur in infants, however, they are less frequently metastasized (<10% of cases) than SHH-1 tumors [62]. Nevertheless, they also often have mutations in *PTCH1*, but also in *SMO* or *BCL6 Corepressor (BCOR)* and deletion of chromosome 9q. MB tumors that occur in children older than 3 years are mostly classified as SHH-3, have frequently classic histology and mutually exclusive germline mutations in *TP53* or *ELP1* and amplification of *MYCN* and/or *GLI2* in the context of *TP53* mutant cases. Adult SHH MB frequently belong to the SHH-4 subgroup with classic histology and low rates of metastasis (<10% of cases). Identified driver events in this subgroup are mutations in *PTCH1, SMO* or the *TERT* promoter region [58]. The 5-year overall survival is higher for subgroups SHH-2 and SHH-4 (~90%) than for SHH-1 and SHH-3 (~70%) [35,36]. However, the outcome for SHH-3 tumors is dependent on the status of *TP53* and *ELP1*, which are mutated mutually exclusively and can either indicate poor outcome for *TP53*-mutated cases or favorable outcome for cases harboring a mutation in *ELP1* [54].

Group 3 and Group 4

Group 3 and Group 4 MB tumors are grouped together as non-WNT/non-SHH-tumors by the WHO and together account for 60% of all MBs [8,30]. Group 3 MBs mostly occur during infancy and childhood (<10 years of age) but very rarely in adults (>17years), while Group 4 tumors occur in all age groups. For both groups tumors occur at least two times more often in males than in females [36]. Diagnosis is mostly based on the DNA methylation profile and whether a tumor clusters with other tumors of a subgroup in unsupervised analysis of the methylation data [26-28]. Biology and characteristics of Group

3 and Group 4 MB are less clear than for the other groups and the oncogenic drivers are not fully known yet. Common features of Group 3 MBs are *MYC*-amplifications, present in around 12% of the cases and which is also linked to poor outcome, or amplification/high expression of *Orthodenticle Homeobox 2* (*OTX2)*, as well as activation of g*rowth factor independent 1 transcriptional repressor* (*GFI)* and *GFI1B* [27,34,63,64]. In Group 4 tumors *MYCN*- and *cyclin dependent kinase 6 (CDK6)*-amplification is common and identified in around 4% and 2% of the cases, respectively [34].In addition, these tumors are characterized by activation of *PRDM6* [14]. In more than 50% of cases in both groups isochromosome 17q is detected [36]. Further subgrouping of Group 3 and Group 4 MB tumors has been discussed often and the number of defined subgroups varied during the last years between three and four subgroups for each group [46,65]. The recent consensus is based on common analysis of DNA methylation profiles of a large set of Group 3 and Group 4 tumors (n=1501) and classifying them into eight subgroups named I – VIII [14,66]. A tumor classified as a subgroup with a low number (I-IV) is more likely a Group 3 tumor and with higher number (V-VIII) the likelihood increases that the tumor has characteristics of a Group 4 tumor (Figure 3). Tumors of the subgroup I occur only very rarely (4% of Group 3/Group 4 tumors), the 5-year overall survival is intermediate within the Group 3/Group 4 tumors (77%), they have a balanced genome and established driver events are amplification of *OTX2* and activation of *GFI1* and *GFI1B* [36]. *GFI1/B* are known as transcriptional repressors that play a role in T- and B-cell development but were also identified as oncogenes in hematopoietic tumors [67]. The subgroup II and III occur in 13% and 9% of Group 3/Group 4 cases, respectively, and have the lowest 5-year overall survival (OS) within the group (50% vs. 43% respectively). Both subgroups are characterized by amplification of *MYC* but for subgroup II other identified driver events are *GFI1/B* activation or mutations of *Kelch repeat and BTB domain containing 4* (*KBTBD4)*, *SMARCA4*, *CTD nuclear envelope phosphatase 1 (CTDNEP1)* or *KMT2D* [36]. For subgroup IV driver events are not known yet but tumors show high level of genomic rearrangements with loss of chromosomes 8, 10, 11, 16 and gain of chromosome 7 and 14. However, they do not have isochromosome 17q which is common for most of the other subgroups [36]. Subgroup V occurs in less than 10% of Group 3/Group 4 tumors, the 5-year OS is approximately 60% and driver events are amplification of *MYC* or *MYCN*. Also tumors classified as subgroup VI occur in less than 10% of Group 3/Group 4 tumors but do have a more favorable 5-year OS (>80%). Possible driver events are activation of *PR/SET domain 6 (PRDM6)* and less frequently amplification of *MYCN* [36]. The last two subgroups, VII and VIII, occur most frequently in Group 3/Group 4 tumors with >20% each and are within the groups with the best outcome (5-year OS: 85% and 81% respectively). Molecular features of subgroup VII are mutations in *KBTBD4* and of subgroup VIII mutations in l*ysine demethylase 6A (KDM6A)*, *zinc finger MYM-type containing 3 (ZMYM3)*, *KMT2C* or activation of *PRDM6* [36]. Subgroup VIII is the only subgroup that almost exclusively

consists of Group 4-tumors, also occurs in older children (up to 17 years) and, besides subgroup I, has not many cytogenetic aberrations apart from isochromosome 17q. Overall recurrent mutations, in e.g. *SMARCA4* for Group 3 tumors and *KDM6A*, *ZMYM3* or *KMT2C* for Group 4 tumors, are rare and occur only in less than 10% of cases [36,68]. However, Group 3 and Group 4 tumors show many somatic copy number alterations (SCNA) and structural variants (SVs) with SVs mostly affecting chromosome 9q34, which is specific for these subgroups [69]. Through the analysis of larger cohorts, *GFI1/B* were characterized as novel oncogenes which, in combination with *MYC*, led to aggressive Group-3 like tumors in mice [69]. *GFI1/B* gets activated by enhancer hijacking, which describes the process when an active enhancer promotes expression of a normally repressed gene by SV-dependent misappropriation [36,70]. In about 15% of Group 3 and Group 4 MB tumors *GFI1/B* and in about 17% of Group 4 tumors *PRDM6* are activated by enhancer hijacking [14,69,71]. Other than that receptor-tyrosine-kinase (RTK) signaling can be activated by deregulated expression of *Erb-B2 receptor tyrosine kinase 4* (*ERBB4)* and phosphorylated tyrosin-kinase *SRC* [33].

1.1.3. Ependymal tumors

Ependymal tumors can be histologically categorized into ependymoma (EPN) and subependymoma and are neuroepithelial tumors of the CNS that can occur in adults and children [72]. They account for 10% of all brain tumors in children, are more likely to occur in males than in females (ratio 1.77:1) and can arise at any age but the highest incidence is within children aged 0 – 4 years [73,74]. The tumors can arise in the hemispheres, hindbrain or the spinal cord but in children 90% of the ependymal tumors are located intracranially with 2/3 arising in the posterior fossa and 1/3 supratentorially [10,75,76]. The standard-of-care therapy includes maximal safe resection and radiotherapy, however the clinical outcome is highly variable and the 10-year survival is about 65% in pediatric patients [72,77-79]. Histopathological analysis can classify EPN tumors into grade I, II and III with grade I being subependymomas and myxopapillary EPNs. Grade II comprises classic EPNs with different histological features; e.g., perivascular and true ependymal rosettes [12]. EPN tumors grade III are anaplastic with hypercellularity with abundant mitotic activity, pseudopalisading necrosis and microvascular proliferation [80]. However, differences in histology are not easy to standardize, and especially the differentiation between grade II and III tumors is difficult and leads to high inter-observer variability and thus is only of limited relevance [10,81-83]. Better classification of EPN tumors can be achieved by taking the genetic and molecular features into account and a study in 2015 with 500 primary samples identified nine distinct molecular groups (Figure 4) [84]. In this study, for each compartment of the CNS three groups were identified with one group in each compartment comprising subependymomas,

which only rarely occur in children. The remaining ependymomas in the spine, which are also more common in adults and only very rarely occur in children, are myxopapillary ependymoma (SP-MPE) and ependymoma (SP-EPN). The distribution for spinal EPN mostly matches the histopathology, however, in the recent WHO classification a group for spinal EPNs with *MYCN* amplification was added [8]. EPN in the posterior fossa (PF) other than subependymomas can be classified as group A (PF-A) or group B (PF-B) tumors. PF-A ependymomas are more common in infants and young children, have a poor clinical outcome and are characterized by a loss of H3K27me3 even though mutations in H3K27 are rare [85-88]. In a majority of cases, aberrant expression of *EZH Inhibitory Protein (EZHIP)* mimics the mutation [89-92]. PF-B tumors occur more often in adolescents and young adults and do have a better prognosis than PF-A tumors. The two groups, besides subependymoma, of posterior fossa tumors have also been identified and confirmed in retrospective and prospective studies [85,86]. Based on the original classification of ependymoma into nine groups by Pajtler *et al*. 2015, tumors occurring supratentorially (ST) that are not grade I are either ST-EPN-RELA or ST-EPN-YAP1 tumors, which are both characterized by the expression of specific fusion genes [84]. More than 70% of tumors in the ST-EPN-RELA group have chromothripsis and express a fusion gene between *Zinc Finger Translocation Associated (ZFTA; C11orf95)* and the nuclear factor kappa B effector *RELA*, which activates the immune regulatory nuclear factor-κB (NF-κB) signaling [84,93,94]. In addition, ST-EPN-RELA tumors are associated with frequent recurrences and poor clinical outcome and occur in children and adults [88,95]. ST-EPN-YAP1 tumors occur mainly in children and express gene fusions with the oncogene *YAP1* [84,94].

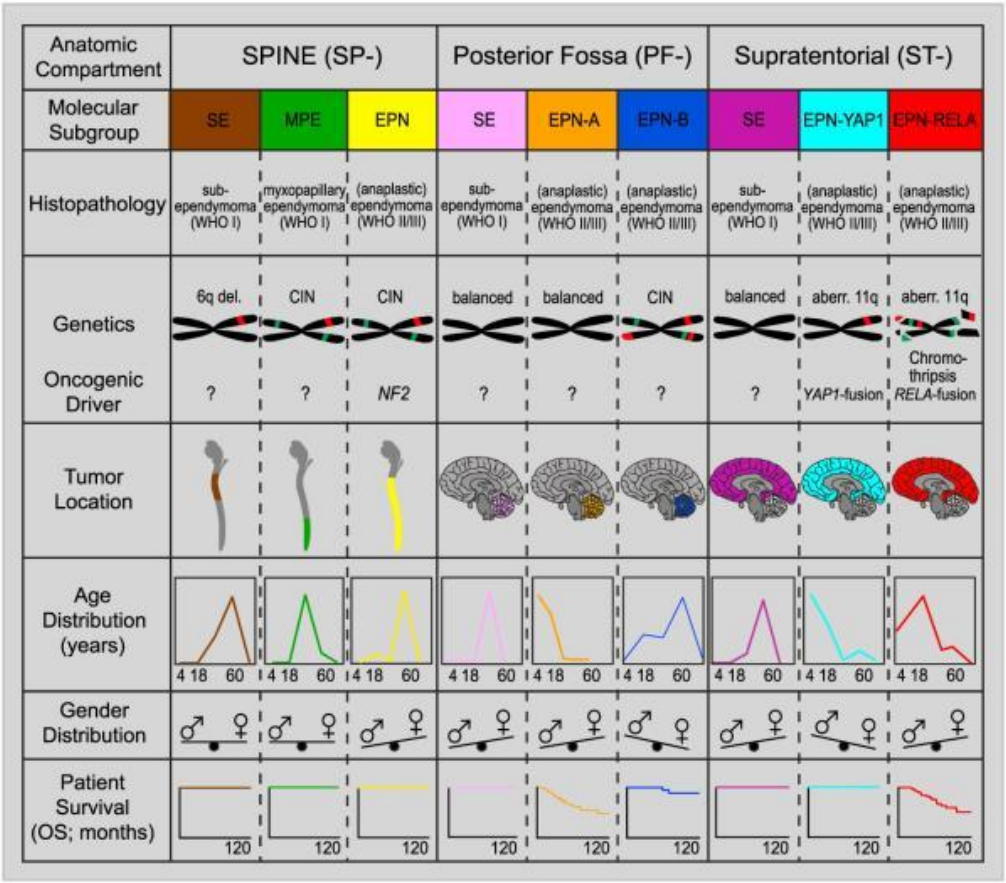

Figure 4: Overview and classification of ependymal tumors.

Ependymoma can occur in three different anatomic compartments (spine, posterior fossa, supratentorial) and can be divided in three subgroups per compartment. Each subgroup is characterized by distinct genetic and clinical features. Figure taken from Pajtler *et al*. 2015 [84]

In the past only histology-based classification of EPN tumors was included in the WHO, but based on the latest version released in 2021, location, histology and molecular features are taken into account for classification and ten molecular groups were defined [8,96]. The recognized groups are based on the findings of Pajtler *et al*. 2015 but, as mentioned above, one group for spinal EPNs with *MYCN* amplification was added [8,84]. EPN tumors arising in the spine can now be classified as SP-Subependymoma, SP-MPE, SP-EPN or as SP-EPN with *MYCN*-amplification, which was detected recently as oncogenic driver in a distinct subset of aggressive spinal EPN tumors [97]. The molecular group ST-EPN-RELA was renamed into *ZFTA*-fusion positive ST-EPN since *ZFTA* can also be fused to other genes than RELA as e.g. *mastermind like transcriptional coactivator* 2 (*MAML2)* [98]. Important diagnostic gene alterations that are characteristic for a specific molecular group of EPN are *Neurofibromin 2* (*NF2)* and *MYCN* for spinal EPN, H3K27me3 and *EZHIP* for EPN occurring in the posterior fossa and *ZFTA*, *RELA*, *YAP1* and *MAML2* for supratentorial EPN [8].

The project described here encompasses treatment strategies for tumors that are highly aggressive and show characteristics as e.g. high levels of *MYC(N)* or R-loops, which is explained in more detail below. Of the ependymal tumors only *ZFTA*-fusion positive tumors do have high levels of R-loops and for this reason will be introduced in more detail.

As mentioned above the subgroup is genetically characterized by chromothripsis and especially structural rearrangements on chromosome 11q. The characteristic oncogenic driver of the entity is a fusion gene between *ZFTA,* typically with *RELA*, which is a downstream effector of NF-κB signaling [94]. Normally the two genes are 1.9 Megabases (Mb) apart from each other, however the translocation and fusion leads to high expression of the two genes as well as high expression of *CCND1*, a direct transcriptional target of NF-κB, and *L1 cell adhesion molecule (L1CAM)*, which is associated with NF-κB signaling, invasion and cell-cell adhesion and is in addition used as a diagnostic marker [12,94,99-102]. Mouse studies confirmed that *ZFTA:RELA* is a genetic driver and its expression leads to aberrant NF-κB signaling, which transforms neural stem cells (NSC) to cancer cells [94]. The 10-year overall survival of patients with an EPN-ZFTA tumor is 50%, but the 10-year progression-free-survival is only 20% [84]. Up to now there is no specific treatment recommendation for these fusion-positive tumors [103].

1.1.4. ETMR

Embryonal tumor with multilayered rosettes (ETMR) is an aggressive, WHO-grade IV brain tumor that usually occurs in children younger than three years of age (Figure 5) [104,105]. The entity is one of the most aggressive pediatric brain tumors, is overall rare (incidence 1.35/1 million children aged 1-4 years) and 5-year overall survival is between 0-30% [7,106,107]. It was also only categorized as separate entity in recent years but has quite intensively been studied since then [12,106,108]. Histology and location of the tumors can be highly variable with 70% occurring supratentorially and 30% infratentorially [104,109,110]. A recently published study included 35 patients and reported that about 75% had an ETMR tumor supratentorially, about 15% in the cerebellum and 10% in the brainstem [107]. Common characteristics for ETMRs are large areas of neuropil with unmyelinated axons, dendrites and glial cells as well as multilayered rosette structures of proliferating neuroepithelial cells [106,110,111].

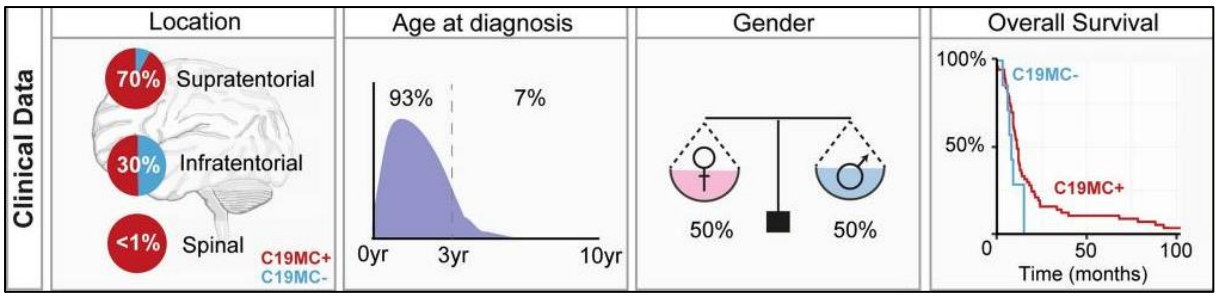

Figure 5: Clinical characteristics of ETMR.

Most of ETMRs occur supratentorially (70%) and 30% occur infratentorially with different distributions for *C19MC*-positive (red) and *C19MC*-negative (blue) tumors (left panel); patients are almost always younger than 3 years (second to left panel) and equally affects female and male pediatrics (second to right panel); overall survival is very poor for all patients, independent of *C19MC*-status (right panel); Figure taken from Lambo *et al*. 2020 [106].

However, as histology can be variable, ETMRs can be better characterized by molecular features such as amplification of the microRNA-cluster on chromosome 19 (*C19MC*), which is present in about 90% of cases [108,112-115]. The expression of *C19MC* is further enhanced by fusion of *C19MC* and the promoter of *Tweety family member 1 (TTYH1)* [116]. Tumors without the amplification often have a biallelic mutation in *DICER1*, where the first hit often is in the germline [108,115]. Another reliable biomarker is increased expression of *Lin-28 Homolog A* (*LIN28A),* which can be verified by staining [104,105,117]. In addition, ETMRs have a distinctive epigenome and *DNA methyltransferase 3 beta (DNMT3B)*, an isoform of DNA methyltransferase, is typically upregulated [104,116]. ETMR tumors grow rapidly, even during aggressive treatment, and local recurrence is common [104,118]. The standard-of-care treatment involves surgical resection, which is often challenging due to the young age of patients and the localization of the tumor. Recent studies analyzed that high-dose chemotherapy can improve survival compared to standard chemotherapy, however outcome is still poor and evaluation of new therapies is needed [107]. Overall better survival is linked to absence of metastasis, non-brainstem location, gross total resection, high-dose chemotherapy and cranio-spinal irradiation for patients older than 3 years [119,120].

1.2. Treatment strategies

1.2.1. From chemotherapy to mechanism-of-action based treatment

In pediatrics, cancers are the most frequent cause of disease-related deaths and treatment remains challenging [121]. Since less than 1% of all cancers are diagnosed in pediatrics, patient numbers are limited and due to the small market size, drug development is mostly focused on adult malignancies [122]. For children with newly diagnosed tumors the overall cure rate is 80%, however this proportion has plateaued over the last >20 years despite improvements in research and diagnosis [123,124]. Furthermore, cure rates are dismal for patients with relapsed tumors [125]. In many cases, no established second-line therapy is available and overall survival is low. Even though research is making progress and new therapy options are developed, patients with very-high risk disease or at relapse remain to have a dismal outcome [126,127].

The standard-of-care therapy mostly includes surgery to remove the tumor bulk followed by radio- and/or chemotherapy [127,128]. Nevertheless, these conventional treatment strategies have severe side effects especially for pediatric patients as e.g. impaired growth and development or endocrine and neurocognitive dysfunction [129]. To prevent long-term side effects of chemo- and radiotherapy, mechanism-of-action based therapies are being explored, which is only possible with improved understanding of molecular genetics, epigenetics and biology of the different tumors. The exploitation of sequencing methods such as next-generation sequencing (NGS) and DNA methylation profiling has tremendously improved the knowledge about genetic drivers and tumor genetics and opened up classification and diagnosis of different molecular groups and subgroups [7,84,130-132]. In 2016, more molecular findings were already included into the WHO classification but the latest version from 2021 made major changes to enhance the role of molecular diagnostics for tumor classification, prognosis assessment, and treatment prediction [8,12,133-135].

1.2.2. Strategies of mechanism-of-action based treatment

By gaining deeper knowledge of the underlying biology of the different tumor entities, mechanism-of-action (MoA) based treatment approaches were designed. In general, MoA based therapies or precision medicine are based on targeting proteins that are relevant for growth, division or spreading of cancer cells [136]. However, MoA based therapies can not only stop the growth of cancer cells by inhibiting pathways relevant for proliferation but can also induce apoptosis of the tumor cells by reactivation of relevant pathways or inhibit angiogenesis and thereby harm the tumor. Another known mechanism of MoA based therapies is to support the immune system in destroying tumor cells by

either marking cancer cells to make them visible for the immune system or by strengthen the immune system to work against the cancer cells [137].

Promising targets for therapy can either be proteins that are more abundant in cancer cells than in normal cells, mutated proteins that are solely expressed by tumor cells or fusion proteins that are also only expressed in the tumor but not in the normal cells throughout the body. A prominent example for a protein that is detected more abundantly on cancer cells than on normal cells is the *human epidermal growth factor receptor 2* (*HER2,* also *ERBB2*), which is overexpressed in 25-30% of patients with breast cancer [138,139]. *HER2* belongs to the family of *epidermal growth factor* (*EGF*)-receptors and can be specifically downregulated by e.g., the targeted drug Trastuzumab (Herceptin). A hallmark of chronic myeloid leukemia (CML) is the Philadelphia-chromosome, which is present in about 95% of the cases [140]. The Philadelphia-chromosome describes the translocation of the q-arms of chromosome 9 and 22 and thereby giving rise to a gene fusion of *BCR* (*breakpoint cluster region protein*) and *ABL* (*Abelson tyrosine-protein kinase 1*) [141]. The expression of the fusion-protein BCR-ABL leads to a deregulated tyrosine kinase, however it can be inhibited by e.g. the targeted drug Imatinib (Gleevec), which prevents phosphorylation of proteins that are involved in signal transduction of BCR-ABL [142-144]. The treatment leads to growth arrest and apoptosis of CML cells, but has little effect on normal cells since BCR-ABL is not expressed by them. A well-studied example for a mutated protein expressed by tumor but not normal cells is BRAF V600E. The gene with the missense mutation was initially detected in melanoma, but is also present in a subset of colorectal carcinoma and primary tumors of the nervous system [145]. The V600E mutation mimics phosphorylation of the protein and leads to constitutive activation of the RAS/RAF/MEK/ERK-pathway with effects on cell proliferation, differentiation and survival of the cell [146]. Besides several inhibitors for the pathway also inhibitors specifically targeting the mutated version of BRAF are known [147]. An example among others is the small molecule Vemurafenib, which specifically binds to the ATP-binding domain of the mutated BRAF V600E protein [148]. Since the drug only binds to the altered protein, signaling pathways in healthy cells are not targeted and thereby side effects of the treatment can be reduced.

In general side effects of MoA based therapies depend on the applied treatment, but common side effects are diarrhea, fatigue, dermatological and hepatic toxicity [137]. However, typically the side effects disappear as soon as the treatment is discontinued. Even though research has made good progress, the development of targeted drugs for any target is still not possible due to e.g. the structure of the target or its function in the cell. Another downside of MoA based therapies is that cancer cells can develop resistance to the treatment either by acquired mutations of the target that hinder the drug to bind or by upregulation of other pathways that circumvent the targeted pathway as e.g.

amplification of *MET* or upregulation of *HGF*, the ligand of MET, to bypass EGFR inhibition [149,150]. A possibility to prevent resistance can be combinatorial treatment approaches that either combine targeted drugs with chemotherapeutics to add more stress to the metabolism of the cell or to use two drugs to inhibit the same pathway, which was shown to be effective for melanoma with BRAF V600E mutation and BRAF-mutant brain tumors that were treated with a MEK- and a BRAF-inhibitor and showed enhanced progression-free survival [151,152].

1.3. Models to test treatment strategies

1.3.1. *In vitro* models

In vitro models are the most common model system for preclinical drug testing and the efficacy of the tested compound is mostly evaluated by clonogenic survival, cell proliferation, or cell viability [153]. And even though *in vitro* growth of cells does not mimic the physiological situation of human cells in the body, it also has many advantages as there are many well-characterized cell lines available, it is typically easy to culture and comparably low in cost [154]. In addition, *in vitro* drug screening can be easily performed in a high-throughput manner and modeling of genetic mutations is rather simple.

However, *in vitro* experiments do not mimic the human disease due to e.g. lack of microenvironment and related signaling pathways [155,156]. By isolating cells from an organism and putting them into culture dishes gene signatures change. In addition, culture-specific limitations as e.g. lack of complex metabolism, alteration of growth and invasion, loss of specific cell populations and interaction with other cell types and microenvironment are being observed. Another limitation for brain tumor research is the lack of a blood-brain barrier [157-161]. Moreover, it is known that cell lines have a limited predictive value since direct translation into clinical usage remains difficult and even though a drug might be highly effective *in vitro* it can still be ineffective in patients [162].

1.3.2. *In vivo* models

Since mice and humans are genetically and physiologically highly similar, *in vivo* mouse models are essential for research [163]. The genomes of mice and human are 90% identical [164,165] and *in vivo* models are important for better understanding of physiological processes in tumors within a complex organism. Across the species, especially the human and mouse CNS is highly conserved and molecular and cellular mechanisms are well preserved [164,166-170].

For *in vivo* models, two different model types are broadly used: genetically engineered mouse models (GEMM) and xenografts for which tissue or cells from one species are injected into another species, mostly human cells into immunodeficient mice. GEMMs are used for tumor models that have a simplified genetic background and only mimic the key events of a tumor and have the advantage that the mice have an intact immune system. The expression of oncogenes can be combined with the loss of tumor suppressor genes in only specific tissues or throughout the whole organism [171]. With inducible systems it is even possible to have temporal and/or tissue-specific regulation of expression of the gene of interest [172]. For xenograft models, typically low passages of cells are used to conserve original tumor characteristics and to ensure reduction of clonal selection compared to cell culture. The

standard injection method of xenograft models is subcutaneously where cells are injected into the flank of the animal and tumor volumes can easily be determined [172]. A more elaborate method is when tumor cells are injected into the mice at the anatomic region where the cells were growing in the patient. In these orthotopic models the microenvironment may better reflect the original tumor location in the patient [173]. To more reliably predict clinical activity and reflect the patient's situation better, patient-derived orthotopic xenograft models (PDX or PDOX) that were generated by injecting tumor cells from a patient's surgery or biopsy directly into the brain of immunodeficient mice, mostly NOD-*scid* IL2Rgamma^{null} (NSG) mice can be used (Figure 6).

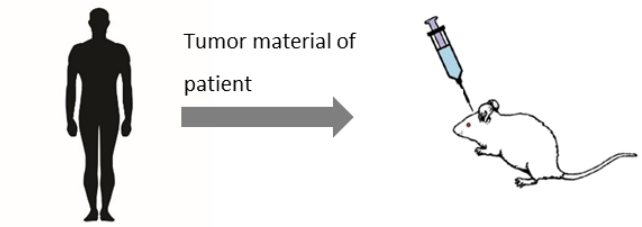

Figure 6: Generation of an orthotopic PDX model by injecting tumor material from a patient directly into the brain of immunodeficient mice.

By keeping the cells only for minimal time *in vitro* or not at all the generated model is genetically stable and similar to the original tumor [174-176]. Established PDX models are known to maintain genetic and histological characteristics of the donor tumor [176]. Moreover, the localization and microenvironment mirrors the original tumor and translation into clinical use can be more predictive. However, generation of PDX models is so far only possible for aggressive tumors as more benign tumors often do not engraft [177]. Additionally, immunocompromised mice are needed to ensure engraftment, which limits the use of immune mediating drugs as vaccines or immune modulators, and treatments that rely on the immune system. Nevertheless, PDX models are the preferred preclinical models in industry and academia as they can predict clinical outcome and improve therapy development [175,178,179].

1.3.3. Translation from preclinical to clinical research

Even though the use of sequencing techniques tremendously increased knowledge of genetic alterations and molecular drivers in tumors, the success of translation of research findings into clinical situations is still limited [180]. In fact, clinical trials in oncology have one of the highest failure rates among clinical trials across disease entities [181]. Problems are inappropriately selected cell lines and models that do not cover the respective subgroups and consequently inadequate patient selection [182,183]. Moreover, for preclinical studies often only one model is used compared to 20-30 different

tumors in a patient cohort and the interpretation of results of preclinical studies is not as rigorous as in clinical trials where inhibition of tumor growth indicates a failed treatment, whereas it is seen as success in preclinical studies.

In addition, preclinical studies only barely include research about predictive biomarkers. For successful translation of new treatment strategies into clinical use good trial design and identification of patients who might benefit from new drugs or treatment strategies play a major role. However, successful translation into clinical use starts with a reasonable selection of preclinical models to evaluate biological processes as well as to develop new treatment strategies [184,185]. It is important to use appropriate preclinical models and to prioritize new anticancer agents as there are many new compounds under evaluation, while the number of patients, especially for some subgroups, can be low [186]. Instead of running clinical trials based on histology and entity, patient selection should be performed based on the presence of the target/biology of interest for the mechanism-of-action of the drug(s)/treatment. For example, clinical trials should not be planned for MB in general but be more specific for molecular group and subgroup of the entity itself. In addition and for faster and more comprehensive research preclinical studies should be performed in a standardized manner and endpoints as well as desired degrees of efficacy should be well defined [176]. Results can then be incorporated more easily into clinical development.

2. Objective of the project

My PhD project about targeting high-risk pediatric brain tumors comprised three different subprojects. In one project a systematic literature research about targeting replication stress was performed. The second project focused on testing a combination therapy approach that targets replication stress in *in vitro* and *in vivo*. In the third project PDX models that are resistant to treatment with a SMO-inhibitor were molecularly characterized and evaluated for further treatment strategies in order to overcome resistance.

2.1. Target actionability review

Within the *Innovative Therapies for Children with Cancer – Pediatric Preclinical Proof of Concept Platform* (ITCC-P4) consortium preclinical models are being established and mechanism-of-action-based therapies for solid pediatric tumors are being tested. One work package aims at performing systematic literature searches to specific, pre-defined pathways or processes relevant in pediatric cancer entities that can be targeted for therapy. These *Target Actionability Reviews* (TAR) aim to evaluate therapeutic targets in pediatric cancers based on published data from (pre-)clinical studies. These TAR results will form a strong basis to choose the most promising targets for further evaluation, fill gaps in preclinical knowledge, and ultimately will facilitate translation into clinical applications. The systematic literature research performed as part of the project described here concerns the process replication stress in solid pediatric cancer entities. The literature search was performed systematically with pre-defined keywords and all papers were scored by at least two independent reviewers with respect to *in vitro* and *in vivo* preclinical experiments, clinical trials and target activation in clinical series.

The results of this study are summarized in the publication “Keller K. M.*, Krausert S.*, Gopisetty A.* *et al*. (2021); Target Actionability Review: a systematic evaluation of replication stress as a therapeutic target for pediatric solid malignancies” and were accepted for publication by the *European Journal of Cancer*.

2.2. Targeting replication stress *in vitro* and *in vivo*

In this part of the project a hypothesis-driven approach was used to target replication stress *in vitro* and *in vivo*. Tumors with *MYC(N)*-amplification or high expression levels of *MYC(N)* have high proliferation rates leading to replication stress and a possible accumulation of DNA:RNA-hybrids called R-loops. Cells want to keep levels of R-loops low as high levels could lead to DNA damage. To resolve R-loops, the enzyme Topoisomerase I is needed. Previously, it was shown that when inhibiting Topoisomerase I in ETMR cells with high levels of R-loops more DNA damage occurs. When inhibiting the DNA repair machinery at the same time, for instance through PARP-inhibition, cells go into apoptosis [108].

A combination treatment of topoisomerase and PARP-inhibition has already been shown to be effective in Ewing Sarcoma, a tumor entity that has also high levels of R-loops [187]. In the project described here, this combination was tested *in vitro* and *in vivo* in pediatric brain tumors that have high levels of *MYC(N)*, including ETMR, Group 3 medulloblastoma and *ZFTA*-fusion positive EPN.

2.3. Generation and molecular characterization of SMO-inhibitor resistant SHH MB PDX models

Treatment with SMO-inhibitors reveals good results in the clinic for tumors that harbor a mutation in the SHH pathway downstream of *SMO*, but patients often acquire resistance to the drug quickly. To understand mechanisms of resistance better and test new treatment strategies to overcome resistance, good preclinical models are of need. As part of the project described here SMO-inhibitor resistant SHH MB PDX models were generated and molecularly characterized. Mice with tumors of a *PTCH1*-mutated MB SHH PDX model were treated in cycles with the SMO-inhibitor Sonidegib and the generated nine resistant models were sequenced to identify the mechanisms of resistance. This project was initiated by Sebastian Brabetz, a former PhD student in the group, and the generation of the resistant models was part of his work. In the project described here the models were molecularly characterized and used for evaluation of further treatment strategies in order to overcome resistance.

This part of the project is submitted for publication (Krausert S.*, Brabetz S.* *et al.* (2021); Predictive modeling of resistance to SMO-inhibition in a patient-derived orthotopic xenograft model of SHH medulloblastoma) to *Neuro-Oncology* and is in revision.

3. Material and Methods

3.1. Material

3.1.1. Cell lines and PDX models

Cell line/PDX	Entity	Supplier
Astrocytes	Fetal Astrocytes	Sciencell Research Laboratories, Carlsbad, USA
BT084	MB SHH	Generated by Till Milde, Heidelberg, Germany
Bt165	ST-EPN-ZFTA	Generated by Till Milde, Heidelberg, Germany
Bt183	ETMR	Generated by Jennifer Chen, Calgary, Canada
HD-MB03	MB Group 3	Generated by Till Milde, Heidelberg, Germany
HEK 293T	Human embryonal kidney	ATCC®, Manassas, USA
Med-1712FH	MB SHH	Generated by James M. Olson, Seattle, USA
NCH2194	MB Group 3	Generated by Till Milde, Heidelberg, Germany

3.1.2. Plasmids

Plasmids	Catalog No.	Supplier
pGF1 Reporter Vector	#TR011-PA1	System Biosciences, Palo Alto, USA
pMD2.G	#12259	Addgene, Cambridge, USA
psPAX2	#12260	Addgene, Cambridge, USA

3.1.3. (Bio-)chemicals and inhibitors

Article	Catalog No.	Supplier
Agar	05039	Sigma-Aldrich, Munich, Germany
Agarose	A9539	Sigma-Aldrich, Munich, Germany
Albumin fraction V	T844.3	Carl Roth GmbH, Karlsruhe, Germany
Ampicillin	10835242001	Roche Diagnostics, Mannheim, Germany
B-27 supplement (50x)	17504044	Thermo Fisher Scientific, Waltham, USA

CellTiter-Glo® Cell Viability Assay	G7570	Promega, Madison, WI, USA
Citrate buffer (10 mM sodium citrate tribasic dehydrate + 0.05% Tween20)	C8532; 9127.1	Sigma-Aldrich, St. Louis, USA; Carl Roth GmbH, Karlsruhe, Germany
DAB-2V, Histofine®	425312F	Nichirei Bioscience, Tokyo, Japan
Dako Pen	S2002	Agilent, Santa Clara, USA
DNA ladder, 100 bp, GeneRuler	SM0243	Thermo Fisher Scientific, Waltham, USA
DNA loading dye (6x)	R0611	Thermo Fisher Scientific, Waltham, USA
ECL western blotting reagents	W1001	Merck, Darmstadt, Germany
Eosin-Y Solution, 0.5%	1024390500	Carl Roth GmbH, Karlsruhe, Germany
Ethanol	32205	Sigma-Aldrich, Munich, Germany
Eukitt® mounting medium	600010001040102	Orsatec GmbH, Bobingen, Germany
Irinotecan hydrochloride	HY-16562A	MedChemExpress LLC, Monmouth Jct., USA
LB medium (Luria-Miller)	X968.1	Carl Roth GmbH, Karlsruhe, Germany
Magnesium chloride ($MgCl_2$)	208337	Sigma-Aldrich, Munich, Germany
Mayer's Hematoxylin, 100%	H9627	AppliChem GmbH, Darmstadt, Germany
Menzel Microscope Coverslips	A113MNZ	Thermo Fisher Scientific, Waltham, USA
Methanol	34860	Sigma-Aldrich, Munich, Germany
NaCl 0.9% solution (10 ml)	2350748	B. Braun, Melsungen, Germany
Normal Donkey Serum	566460	Merck, Darmstadt, Germany
NP-40 lysis buffer	FNN0021	Thermo Fisher Scientific, Karlsruhe, Germany
Nuclease-free water, Ambion®	AM9916	Thermo Fisher Scientific, Waltham, USA
NuPAGE™ 4-12% Bis-Tris gel	10247002	Thermo Fisher Scientific, Karlsruhe, Germany
NuPAGE™ antioxidant	NP0005	Thermo Fisher Scientific, Karlsruhe, Germany
NuPAGE™ LDS sample buffer (4x)	NP0007	Thermo Fisher Scientific, Karlsruhe, Germany

NuPAGE™ MES SDS running buffer (20x)	NP0002	Thermo Fisher Scientific, Karlsruhe, Germany
OptiView DAB IHC Detection Kit	06396500001	Ventana Medical Systems, Oro Valley, USA
Pamiparib		BeiGene, Beijing, China
Paraformaldehyde solution 4% in PBS	sc-281692	Santa Cruz Biotechnology, Dallas, USA
PARP in vivo pharmacodynamics assay II	4520-096-K	Trevigen Inc., Gaithersburg, USA
Pierce™ BCA Protein Assay Kit	#23225	Thermo Fisher Scientific, Waltham, USA
Pierce™ DAB substrate with chromogen	34002	Thermo Fisher Scientific, Waltham, USA
PLX038A		ProLynx, San Francisco, CA, USA
Proteinase K, recombinant, PCR grade	EO0491	Thermo Fisher Scientific, Waltham, USA
Restore™ Western Blot Stripping Buffer	21059	Thermo Fisher Scientific, Waltham, USA
RIPA lysis buffer (10x)	20-188	Merck, Darmstadt, Germany
Selinexor		Karyopharm Therapeutics, Newton, MA, USA
SN-38	HY-13704	MedChemExpress LLC, Monmouth Jct., USA
Sodium chloride (NaCl)	S3014	Sigma-Aldrich, Munich, Germany
Topotecan hydrochloride	HY-13768A	MedChemExpress LLC, Monmouth Jct., USA
Tween®20	817072	Merck, Darmstadt, Germany
VectaStain Elite ABC Kit	VEC-PK-6100	Vector Laboratories, Burlingame, USA
Xylene	XX0020	VWR International GmbH, Darmstadt, Germany

3.1.4. Cell culture reagents and materials

Article	Catalog No.	Supplier
Accumax™	00-4666-56	eBioscience, Inc., San Diego, USA
Corning® Plate. 96-Well, white	#3610	Corning, New York, USA
Dimethyl sulfoxide (DMSO)	472301	Sigma-Aldrich, Munich, Germany
Dimethyl sulfoxide (DMSO)	472301	Sigma-Aldrich, Munich, Germany
DMEM (Dulbecco's modified eagle medium)	D6046	Sigma-Aldrich, Munich, Germany
Dulbecco's PBS	21600010	Thermo Fisher Scientific, Waltham, USA
Dulbecco's PBS	21600010	Thermo Fisher Scientific, Waltham, USA
EGF	AF-100-15	Peprotech
Fetal Bovine Serum (FBS), heat-inactivated	10082147	Gibco®, Thermo Fisher Scientific, Waltham, USA
FGF	100-18C	Peprotech
GlutaMAX™	13462629	Thermo Fisher Scientific, Waltham, USA
L-Glutamine	25030081	Gibco®, Thermo Fisher Scientific, Waltham, USA
N-2 Supplement (100x)	17502048	Thermo Fisher Scientific, Waltham, USA
Neurobasal™-A Medium	10888022	Gibco®, Thermo Fisher Scientific, Waltham, USA
NeuroCult™ NS-A basal Medium (Human)	05750	STEMCELL Technologies, Vancouver, Canada
NeuroCult™ NS-A Proliferation Supplement Medium (Human)	05751	STEMCELL Technologies, Vancouver, Canada
Nunc® CryoTubes® (1.8 ml)	V7884	Sigma-Aldrich, Munich, Germany
Opti-MEM I reduced serum medium	31985062	Thermo Fisher Scientific, Waltham, USA
Penicillin/Streptomycin (10,000 U/ml, 100 µg/ml)	15140122	Gibco®, Thermo Fisher Scientific, Waltham, USA
Gibco™ RPMI-1640 medium	11530586	Thermo Fisher Scientific, Waltham, USA
Sodium Pyruvate (100 mM)	11360070	Thermo Fisher Scientific, Waltham, USA
T-75 adhesion flask	90076	TPP, Schaffhausen, Switzerland

TransIT®-LT1 transfection reagent	MIR2300	Mirus Bio, Madison, USA
Trypan Blue Dye (0.4%)	1450021	Bio-Rad, Munich, Germany
Trypsin EDTA solution (0.5%)	T3924	Sigma-Aldrich, Munich, Germany

3.1.5. Antibodies

Article	Catalog No.	Supplier
Alexa Fluor®-568, donkey anti-rabbit IgG	A10042	Thermo Fisher Scientific, Waltham, USA
Biotin-SP-conjugated anti-rabbit IgG	711-065-125	Jackson Immuno Research Laboratories, West Grove, USA
Cleaved Caspase 3 (Asp175); rabbit	#9661	Cell Signaling Technology, Danvers, USA
IgG-HRP goat anti-rabbit	#7074	Cell Signaling Technology, Danvers, USA
Ki-67, clone MIB-1	M724001-2	Dako Agilent, Santa Clara, USA
Poly/Mono-ADP Ribose (E6F6A); Rabbit mAb	#83732	Cell Signaling Technology, Danvers, USA
HRP Anti-beta Actin [AC-15]	ab49900	Abcam, Cambridge, UK
Phospho-Histone H2A.X (Ser139) (20E3); rabbit mAb	#9718	Cell Signaling Technology, Danvers, USA

3.1.6. Mice

Mouse strain	Supplier
NOD.Cg-Prkdc^{scid} Il2rg^{tm1Wjl}/SzJ (Nonobese diabetic/severe combined immunodeficiency gamma, NOD-SCID gamma®)	In-house breeding facility, DKFZ, Heidelberg, Germany

3.1.7. *In vivo* reagents and materials

Article	Catalog No.	Supplier
AccuLux ThermoLux (heating pad)	561170-NA	Conrad, Mannheim, Germany
Bepanthen®	00829388	Bayer Vital, Leverkusen, Germany
Fine-Ject® Needles	4710003012	Henke-Sass Wolf, Tuttlingen, Germany
Hamilton syringe, sub-microliter injection system		World Precision Instruments, Friedberg, Germany
Histacryl® tissue adhesive	HS5649	Braun, Melsungen, Germany
Isoflurane	1214	cp-pharma, Burgdorf, Germany
Metamizol	793-333	WDT, Garbsen Germany
Precision Scale PLS/PLJ	6200-2A	Kern®, Balingen, Germany
Reusable feeding needle, 50 mm length	18060-20	Fine Science Tools®, Heidelberg, Germany
Rimadyl® (Carprofen)		Zoetis, Berlin, Germany
Scalpel	2-7125	NeoLab, Heidelberg, Germany
Soft-Ject® Syringes, 1 ml	110586	Henke-Sass Wolf, Tuttlingen, Germany
Stereotaxic Instrument, Model 900		David Kopf Instruments, Tujunga, USA
VivoGlo™ luciferin	P1041	Promega, Madison, USA

3.1.8. Equipment

Article	Supplier
Biofuge Fresco table top centrifuge	Haraeus Instruments, Hanau, Germany
Bruker 1 Tesla MRI	Bruker, Billerica, USA
Chemiluminescence imager	Intas, Göttingen, Germany
Cytostatics Hood Maxisafe 2020	Sigma-Aldrich, Munich, Germany
Electrophoresis chamber	NeoLab, Heidelberg, Germany

Epredia™ STP120 Dehydration machine	Thermo Fisher Scientific, Waltham, USA
Heating Block QBT	Grant Instruments, Cambridge, UK
HistoStar™ Embedding machine	Thermo Fisher Scientific, Waltham, USA
Incubator HERA cell 150	Thermo Fisher Scientific, Waltham, USA
Intas Chemostar ECL Imager	Intas Science Imaging, Göttingen, Germany
IVIS Lumina Series III	PerkinElmer, Waltham, USA
L8-M ultracentrifuge	Beckmann Coulter, Krefeld, Germany
Mithras LB 940 plate reader	Berhold Technologies, Bad Wilbad, Germany
PHERAstar FS microplate reader	BMG Labtech, Ortenberg, Germany
Sonicator water bath	Arrayit Microarray Technology, Sunnyvale, USA
T20 Automated cell counter	Bio-Rad Laboratories, Munich, Germany
Tissue Master TM125-220	Omni International, Kennesaw, USA
Ventana BenchMark Ultra Immunostainer	Ventana Medical Systems, Oro Valley, USA
Vortex Genie 2	Scientific Industries Inc., New York, USA

3.1.9. Other materials

Article	**Catalog No.**	**Supplier**
Cell strainer 40 µm	GF-0059	NeoLab Migge, Heidelberg, Germany
Chromatography Paper, 3 mm, Whatman®	WHA3030861	Sigma-Aldrich, Munich, Germany
Corning 384-well plate	#3830	Sigma-Aldrich, Munich, Germany
Eppendorf tube 1.5 ml and 2 ml	0030120086; 0030120094	Eppendorf, Hamburg, Germany
Falcon® tubes (15 ml and 50 ml)	11507411; 10788561	Thermo Fisher Scientific, Karlsruhe, Germany

Infinium Human-MethylationEPIC BeadChip Kit	WG-317-1003	Illumina, San Diego, USA
One shot TOP10 chemically competent E.coli	C404010	Thermo Fisher Scientific, Karlsruhe, Germany
PCR tubes (0.2 ml)	21-402-168	Molecular BioProducts, San Diego, USA
PVDF transfer membrane	88518	Thermo Fisher Scientific, Karlsruhe, Germany
SafeSeal-tips® professional (10-1000 µl)	770005 - 770600	Biozym, Hessisch Oldendorf, Germany
Spectra™ multicolor broad range protein ladder	26623	Thermo Fisher Scientific, Karlsruhe, Germany
Stripetten, Corning® Costar® (5,10,25, 50 ml)	10041591	Sigma-Aldrich, Munich, Germany
SW41 ultracentrifuge tubes	331362	Beckman Coulter, Krefeld, Germany
Tissue Culture flask	Z707481	TPP, Klettgau, Germany

3.1.10. Databases and Software

Database/Software	**Weblink/Supplier**
Affinity Designer 1.6.5.135	Serif, West Bridgford, UK
Biorender	http://app.biorender.com
BREEZEe	https://breeze.fimm.fi
EndNote X7	Thomson, ResearchSoft, Carlsbad, USA
FACS-Diva	BD Biosciences, Heidelberg, Germany
Gene Cards (Human Genes Database)	https://www.genecards.org
GSEA 4.1.0	https://www.gsea-msigdb.org
GraphPad Prism 5	GraphPad, San Diego, USA
Ingenuity Pathway Analysis	Qiagen, Hilden, Germany
ProteinPaint	https://proteinpaint.stjude.org
PubMed	http://pubmed.ncbi.nlm.nih.gov
R version 3.6.1	https://cran.r-project.org

R2 Microarray Analysis and Visualization Platform	https://r2.amc.nl
Studylog 4.2.1.3	Studylog Systems Inc. San Francisco, USA

3.2. Methods taken from publications

The methods described in this chapter have been entirely taken from the joint publications below, are annotated by separate headings and, if not entirely written by me, are put in quotation marks.

Kaylee M. Keller*, **Sonja Krausert***, Apurva Gopisetty*, Dan Luedtke, Jan Koster, Nil A. Schubert, Ana Rodríguez, Sander R. van Hooff, Damian Stichel, Emmy M. Dolman, Gilles Vassal, Stefan M. Pfister, Hubert N. Caron, Louis F. Stancato, Jan J. Molenaar**, Natalie Jäger**, and Marcel Kool**. **Target Actionability Review: a systematic evaluation of replication stress as a therapeutic target for pediatric solid malignancies**; European Journal of Cancer; in press.

* Kaylee M. Keller, Sonja Krausert and Apurva Gopisetty are joint first authors.

** Jan J. Molenaar, Natalie Jäger and Marcel Kool are joint senior authors.

Sonja Krausert*, Sebastian Brabetz*, Norman L. Mack, Felix Schmitt-Hoffner, Benjamin Schwalm, Heike Peterziel, Aileen Mangang, Tim Holland-Letz, Laura Sieber, Andrey Korshunov, Ina Oehme, Natalie Jäger, Olaf Witt, Stefan M. Pfister and Marcel Kool. **Predictive modeling of resistance to SMO-inhibition in a patient-derived orthotopic xenograft model of SHH medulloblastoma**; Neuro-Oncology; *in revision*.

* Sonja Krausert and Sebastian Brabetz are joint first authors.

3.2.1 Methods taken from "Target Actionability Review: a systematic evaluation of replication stress as a therapeutic target for pediatric solid malignancies"

3.2.1.1. Systematic literature research

"The TAR methodology we established—which is outlined in Figure 7—consisted of four major steps with minor deviations from the original appraisal approach established by Schubert *et al.* (2020)[188]. Using specific and general keywords, literature related to replication stress in 16 different types of pediatric solid tumors (Table 1) was collected (step 1). If individual papers addressed one of the defined PoC modules (Table 2), it was included for further review. In step 2, each paper was scored by two separate reviewers using the publicly available web portal R2 [https://hgserver1.amc.nl/cgi-bin/r2/main.cgi?option=imi2_targetmap_v1]. Next, the key target addressed in the paper was identified, any discrepant scores were adjudicated by utilizing an independent third reviewer (step 3), and final scores were assigned and visualized (step 4)."

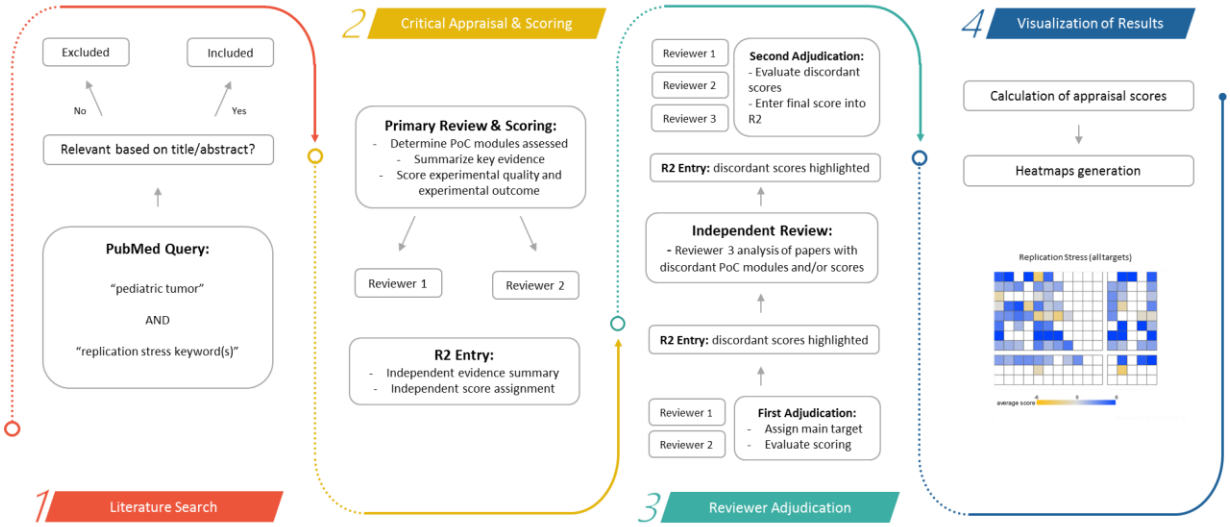

Figure 7: Overview of target actionability review (TAR) process [189].

Table 1: Keywords and tumor entities included in PubMed search queries [189].

Replication stress keywords		Tumor entities
General keywords:	replication stress	Neuroblastoma (NBL)
	genomic instability	Rhabdomyosarcoma (RMS)
	chromothripsis	Synovial sarcoma (SS)
	BRCA	Malignant peripheral nerve sheath tumor (MPNST)
	R-loops	Ewing's sarcoma (ES)
	mutational signature	Osteosarcoma (OS)
	MYC amplification	Atypical teratoid/rhabdoid tumor (AT/RT) & Malignant rhabdoid tumor (MRT)
	MYCN amplification	Wilms tumors/nephroblastoma (WT)
	high MYC expression	Hepatoblastoma (HB)
	high MYCN expression	Inflammatory myofibroblastic tumor (IMT)
	mitotic catastrophe	Retinoblastoma (RB)
	reactive oxygen species	Extracranial germ cell tumor (extracranial GCT)
	synthetic lethal treatment	Low-grade glioma (WHO grades I & II; LGG)
		High-grade glioma (WHO grades III & IV, incl. glioblastoma; HGG)
Specific keywords:	ATM	Ependymoma (EPN)
	ATR	Medulloblastoma (MB)
	DNA-PK/DNA-PKcs/PRKDC	
	CHK1/CHEK1	
	WEE1	
	PARP	

Table 2: Proof-of-concept (PoC) modules, critical appraisal questions and framework of experimental findings summarized in the TAR [188]

Proof of concept module (PoC)	Critical appraisal questions	Information to include in summary of experimental findings
PoC 1: target/pathway activation in pediatric clinical series	**Is the target pathway active in the tumor of interest?** Target/pathway evaluation in clinical series: DNA aberrations, (over)expression, methylation changes? Target DNA aberrations: mutation, translocation, amplification, InDel,, CNV Percent of samples with aberrant target/pathway in clinical series Correlation to clinical outcome Correlation to other tumor biology Target expression/pathway activity compared to normal tissue, other cancers and/or other reference tissue	Total size of cohort (only consider the number of patient samples, not cell lines) Methodology used Percent of samples expression the target (and associated alterations or mutation) or with activated target pathway
Tumor target dependence **PoC 2:** ***in vitro*** **PoC 3:** ***in vivo***	**Is the tumor of interest dependent on the target/pathway for survival?** ***In vitro*** Molecular target gene silencing in cells (RNAi, AOs, CRISPR, etc.) or ectopic expression; preferably ≥ 3 cell lines Phenotype analysis (apoptosis, cell viability, etc.) Biological effect of molecular silencing or ectopic expression of target Appropriate controls (use of multiple silencing tools, rescue experiments, control cell lines, etc.) Additional functional assays showing target or pathway dependence for mutated/translocated/amplified target genes ***In vivo*** Molecular silencing or overexpression of target gene in xenografts (inducible shRNA or expression vectors) Transgenic models (mice, zebrafish, etc.) for mutated/translocated/amplified target genes or for activated pathways	***In vitro/ in vivo*** Model system(s) Methodology used Results of initial experiment (cell viability or tumor growth) Rescue experiment used Validation (effects on apoptosis, proliferation, cell cycle, migration, gene or protein expression, etc.)

Sensitivity to compound/drug **PoC 4: *in vitro*** **PoC 5: *in vivo***	**Does the targeted compound reduce survival of the tumor of interest in preclinical models?** ***In vitro*** Preferably ≥ 4 cell lines with target dependence (preferably with ≥ 1 control cell line without target dependence) Cell viability: IC_{50}, GI_{50}, LC_{50}, dose-response curves Biological efficacy: preferably measured with pharmacodynamic (PD) assays intended for extrapolation to clinical studies Correlation of efficacy with tumor biology ***In vivo*** Xenografts/PDX/GEMM (both with dependency on evaluated target) Preferably measured with predictive biomarker to be used in clinical trial for patient selection Pharmacokinetics (PK; plasma and intra-tumoral) Pharmacodynamics in tumor: (1) target binding, (2) target inhibition, (3) pathway modulation, (4) biological effect PK-PD relationships: preferably use assays intended for extrapolation to clinical studies Response rates and survival measures (use established, measurable tumors) Efficacy-PD-PK relationships	***In vitro*** Type (establish cell line or patient-derived [i.e., *ex vivo*] and number of cell lines used [including controls]) Drug(s) used and concentration range tested; time point(s) used to assess cell viability Percent of sensitive lines (IC_{50} ≤ 500 nM of clinically relevant [if known/applicable]) Validation (effects on apoptosis, proliferation, cell cycle, migration, gene or protein expression, etc.) ***In vivo*** Model(s) (cell line or patient-derived xenografts, transgenic mice, orthotopic vs. subcutaneous, etc.) and *n/*arm Dosing schedule used Tumor growth inhibition and/or overall response extrapolation for each experiment Validation (effects on apoptosis, proliferation, cell cycle, migration, gene or protein expression, etc.)
PoC 6: predictive biomarkers	**Can biological compound efficacy be determined by a specific marker in preclinical models?** Evaluation of existing, validated biomarkers in PoC 4 and PoC 5 Predictive biomarker (intended for extrapolation to clinical studies and patient selection) Efficacy biomarkers (PD markers)	Biomarker(s) reported *In vitro/in vivo* correlation (include statistical values if available) Patient correlation (include statistical values if available)
PoC 7: resistance	**Are the mechanisms of resistance understood?** (Analyzed in preclinical models, use knowledge from adult studies, added observations in patient samples from trials) Target mutations Upregulation of alternative pathways	Model(s) (*in vitro/in vivo*) Methodology Resistance reported and drug concentration/validation (if applicable)

	Increased drug transporters Other mechanisms	
PoC 8: combinations	**Are synergistic combinations with other drugs/compounds established?** Rational combinations: based on pathway knowledge and/or resistance observations from PoC 7 Compound/drug + cytotoxic drug Compound/drug + targeted compound	Model(s) (*in vitro/in vivo*) Methodology for combination Drug(s) used and concentration range tested; time point(s) Results (combination index [CI]/method of determining combination effect, percent of models showing synergism) Validation (effects on apoptosis, proliferation, cell cycle, migration, gene or protein expression, etc.)
PoC 9: clinical evaluation	**Can the targeted compound safely be administered to children with cancer? (Phase I)** Has a formal phase I trial been conducted with a targeted compound in children with cancer? Has a recommended dose been established for single drug use? Has a recommended dose been established for use in combination in standard of care (SOC)? **Does the targeted compound show efficacy (clinical or biological) in relapsed/refractory disease (Phase II)** Has a formal phase II trial been performed with a targeted compound in children with cancer? In which diseases has efficacy been investigated? In which stage of disease (relapsed/refractory?, Treatment-naïve?) Were trials done with single drug or in combination? Has 'biological efficacy' (PD biomarkers) been shown? **Does the targeted compound add benefit to the standard-of-care treatment? (Phase III)** See EBM critical appraisal checklists for 'therapeutic interventions': https://www.cebm.net/	Number of patients included in the trial and tumor types considered Study design (phase, type of design [open label, randomized, controlled, other]) Toxicity profile Recommended phase II dose (RP2D); if applicable Efficacy observed (ORR, CR, PR, SD or PD); if applicable

3.2.1.2. Step 1: Literature search

"Using the R package RISmed version2.2, literature related to replication stress was collected via PubMed queries using replication stress keyword(s) combined with the pediatric tumor type of interest ([*"pediatric tumor"* AND *"replication stress keyword"*]; see Table 1 for search term overview and Table 3 for detailed search queries) [190]. Literature that was published between 2014-2021 (last literature search: 27-01-2021) and contained the search terms in the title and/or abstract were included. Next, abstracts were analyzed to determine if they should be included for critical review and scoring. Only literature that addressed one of the PoC modules outlined in Table 2, in a pediatric entity listed in Table 1 was included and all review articles were excluded. The final list of PubMed IDs (PMIDs) was uploaded into the R2 TAR platform where they were scored in step 2 of the TAR methodology."

Table 3: Detailed PubMed search queries. All search queries were conducted using RISmed version 2.2 and limited to publications between 2014-2021 [189].

PubMed Queries	
Search queriers (all tumor types)	**Tumor types (used in search queries)**
(tumor type[Title/Abstract]) AND (replication stress[Title/Abstract])	neuroblastoma
(tumor type [Title/Abstract]) AND (genomic instability[Title/Abstract])	rhabdomyosarcoma
(tumor type [Title/Abstract]) AND (chromothripsis[Title/Abstract])	synovial sarcoma
(tumor type [Title/Abstract]) AND (BRCA[Title/Abstract])	malignant peripheral nerve sheath tumor
(tumor type [Title/Abstract]) AND (R-loops[Title/Abstract])	ewing sarcoma
(tumor type [Title/Abstract]) AND (mutational signature[Title/Abstract])	osteosarcoma
(tumor type [Title/Abstract]) AND (MYC amplification[Title/Abstract])	atypical tetratoid rhabdoid tumor
(tumor type [Title/Abstract]) AND (MYCN amplification[Title/Abstract])	malignant rhabdoid tumor
(tumor type [Title/Abstract]) AND (high MYC expression[Title/Abstract])	wilms tumor
(tumor type [Title/Abstract]) AND (high MYCN expression[Title/Abstract])	nephroblastoma
(tumor type [Title/Abstract]) AND (mitotic catastrophe[Title/Abstract])	hepatoblastoma
(tumor type [Title/Abstract]) AND (reactive oxygen species[Title/Abstract])	inflammatory myofibroblastic tumor
(tumor type [Title/Abstract]) AND (synthetic lethal treatment[Title/Abstract])	retinoblastoma
(tumor type [Title/Abstract]) AND (ATM[Title/Abstract])	extracranial germ cell tumor
(tumor type [Title/Abstract]) AND (ATR[Title/Abstract])	low grade glioma
(tumor type [Title/Abstract]) AND (CHK1[Title/Abstract])	high grade glioma
(tumor type [Title/Abstract]) AND (CHEK1[Title/Abstract])	ependymoma
(tumor type [Title/Abstract]) AND (PARP[Title/Abstract])	medulloblastoma
(tumor type [Title/Abstract]) AND (WEE1[Title/Abstract])	
Additional search queriers for neuroblastoma	
((neuroblastoma[Title/Abstract]) AND (MYCN amplification[Title/Abstract])) AND (replication stress)	

((neuroblastoma[Title/Abstract]) AND (MYCN amplification[Title/Abstract])) AND (genomic instability)
((neuroblastoma[Title/Abstract]) AND (MYCN amplification[Title/Abstract])) AND (chromothripsis)
((neuroblastoma[Title/Abstract]) AND (MYCN amplification[Title/Abstract])) AND (BRCA)
((neuroblastoma[Title/Abstract]) AND (MYCN amplification[Title/Abstract])) AND (R-loops)
((neuroblastoma[Title/Abstract]) AND (MYCN amplification[Title/Abstract])) AND (mutational signature)
((neuroblastoma[Title/Abstract]) AND (MYCN amplification[Title/Abstract])) AND (ATM)
((neuroblastoma[Title/Abstract]) AND (MYCN amplification[Title/Abstract])) AND (ATR)
((neuroblastoma[Title/Abstract]) AND (MYCN amplification[Title/Abstract])) AND (CHK1)
((neuroblastoma[Title/Abstract]) AND (MYCN amplification[Title/Abstract])) AND (CHEK1)
((neuroblastoma[Title/Abstract]) AND (MYCN amplification[Title/Abstract])) AND (DNA-PK)
((neuroblastoma[Title/Abstract]) AND (MYCN amplification[Title/Abstract])) AND (DNA-PKcs)
((neuroblastoma[Title/Abstract]) AND (MYCN amplification[Title/Abstract])) AND (PRKDC)
((neuroblastoma[Title/Abstract]) AND (MYCN amplification[Title/Abstract])) AND (PARP)
((neuroblastoma[Title/Abstract]) AND (MYCN amplification[Title/Abstract])) AND (WEE1)

Additional search queriers for PARP

((neuroblastoma[Title/Abstract]) AND (PARP[Title/Abstract])) AND (replication stress)
((neuroblastoma[Title/Abstract]) AND (PARP[Title/Abstract])) AND (genomic instability)
((neuroblastoma[Title/Abstract]) AND (PARP[Title/Abstract])) AND (chromothripsis)
((neuroblastoma[Title/Abstract]) AND (PARP[Title/Abstract])) AND (BRCA)
((neuroblastoma[Title/Abstract]) AND (PARP[Title/Abstract])) AND (R-loops)
((neuroblastoma[Title/Abstract]) AND (PARP[Title/Abstract])) AND (mutational signature)
((neuroblastoma[Title/Abstract]) AND (PARP[Title/Abstract])) AND (MYC amplification)
((neuroblastoma[Title/Abstract]) AND (PARP[Title/Abstract])) AND (MYCN amplification)
((neuroblastoma[Title/Abstract]) AND (PARP[Title/Abstract])) AND (high MYC expression)
((neuroblastoma[Title/Abstract]) AND (PARP[Title/Abstract])) AND (high MYCN expression)
((neuroblastoma[Title/Abstract]) AND (PARP[Title/Abstract])) AND (mitotic catastrophe)
((neuroblastoma[Title/Abstract]) AND (PARP[Title/Abstract])) AND (reactive oxygen species)
((neuroblastoma[Title/Abstract]) AND (PARP[Title/Abstract])) AND (synthetic lethal treatment)
((osteosarcoma[Title/Abstract]) AND (PARP[Title/Abstract])) AND (replication stress)
((osteosarcoma [Title/Abstract]) AND (PARP[Title/Abstract])) AND (genomic instability)
((osteosarcoma [Title/Abstract]) AND (PARP[Title/Abstract])) AND (chromothripsis)
((osteosarcoma [Title/Abstract]) AND (PARP[Title/Abstract])) AND (BRCA)
((osteosarcoma [Title/Abstract]) AND (PARP[Title/Abstract])) AND (R-loops)
((osteosarcoma [Title/Abstract]) AND (PARP[Title/Abstract])) AND (mutational signature)
((osteosarcoma [Title/Abstract]) AND (PARP[Title/Abstract])) AND (MYC amplification)
((osteosarcoma [Title/Abstract]) AND (PARP[Title/Abstract])) AND (MYCN amplification)
((osteosarcoma [Title/Abstract]) AND (PARP[Title/Abstract])) AND (high MYC expression)
((osteosarcoma [Title/Abstract]) AND (PARP[Title/Abstract])) AND (high MYCN expression)
((osteosarcoma [Title/Abstract]) AND (PARP[Title/Abstract])) AND (mitotic catastrophe)
((osteosarcoma [Title/Abstract]) AND (PARP[Title/Abstract])) AND (reactive oxygen species)
((osteosarcoma [Title/Abstract]) AND (PARP[Title/Abstract])) AND (synthetic lethal treatment)

3.2.1.3. Step 2: Critical review and scoring

"Using the previously established critical appraisal PoC modules, each paper was evaluated by two separate reviewers and all relevant data were entered as separate evidence entries in the R2 TAR platform [188]. First, the key findings of each paper were briefly summarized by both reviewers 1 and 2 according to the guidelines presented in Table 2. Any studies evaluating micro- or long non-coding RNA, natural compounds or monotherapy with classical chemotherapy or radiotherapy were excluded. Then, using the scoring criteria outlined by Schubert *et al.* (2020), each module for each tumor type was assessed and quality and outcome scores were assigned. The experimental quality scores—reflecting the robustness of the reported findings—ranged from 1 to 3 (Table 4). The experimental outcome scores ranged from -3 to +3 and give an indication as to whether the study results warrant the targeting of a specific protein/pathway for the treatment of a pediatric solid or brain tumor (Table 5). Once the summary and appraisal scores from both reviewers were entered in the R2 TAR platform, each paper proceeded to the adjudication stage."

Table 4: Experimental quality scoring [188].

Proof of Concept (PoC) Module	**Description**	**Scoring and Criteria**	
PoC 1: target/pathway activation in pediatric clinical series	Number of pediatric samples Type of analysis	3	n ≥ 20 pediatric patient samples; ≥ 2 different methods OR next-generation sequencing
		2	20>*n* >10 pediatric patient samples; ≥ 1 reliable method
		1	n ≤ 10 pediatric patient samples; 1 method
PoC 2: tumor target dependence *in vitro*	Methodology Tumor cell viability Biological pathway readout	3	Different methods to alter target expression in ≥ 3 cell lines; phenotypic analysis of knockdown
		2	Single method to alter target expression in <3 cell lines
		1	Questionable alteration of gene expression
PoC 3: tumor target dependence *in vivo*	Model(s) used Tumor formation/growth Biological pathway readout	3	Transgenic mouse model or ≥ 2 different xenografts with appropriate controls and/or different methods of genetic modification *in vivo* (shRNA/CRISPR)
		2	≥ 2 different xenografts without appropriate control
		1	1 xenograft model without appropriate control
PoC 4: *in vitro* sensitivity to compound/drug	Number of cell lines Measurement of PD markers Phenotypic response	3	5+ cell lines and ≥ 2 appropriate controls; validation
		2	2-5 cell lines and ≥ 1 appropriate control; validation
		1	1 cell line and/or lack of control and/or validation

PoC 5: *in vivo* activity of compound/drug	Number and type of model(s) Measurement of PD markers Phenotypic response	3 2 1	≥ 2 xenograft models or 1 transgenic mouse model with appropriate controls; treatment with clinically relevant dose; validation 1 xenograft model with appropriate control; treatment with clinically relevant dose; validation 1 xenograft model OR use of supra-clinical dose levels; no appropriate control or validation
PoC 6: predictive biomarkers	Confirmation of correlation Patient selection	3 2 1	Correlation molecularly confirmed in ≥ 2 models (eg: silencing, overexpression, etc.); patient selection Correlation confirmed in 1 model Correlation not confirmed
PoC 7: resistance	Mechanism of resistance Molecular analysis Method to overcome resistance	3 2 1	Reported resistance and comprehensive analysis and reversing/overcoming resistance Reported resistance and analysis of molecular changes underlying/due to resistance Only reporting resistance
PoC 8: combinations	Concentrations tested *In vitro* combination index values *In vivo* combination	3 2 1	>4 concentrations of each compound are tested and combination index values calculated; combination evaluated *in vivo* 1-4 concentrations of each compound are tested and combination index values calculated; with or without evaluation of combination *in vivo* 1 concentration of each compound tested; no evaluation of combination *in vivo*
PoC 9: clinical evaluation	Pediatric patient selection Toxicity Efficacy	1	number of patients; tumor types included in study; study design

Table 5: Experimental outcome scoring rubric [188].

Proof of Concept (PoC) Module	Description	Scoring and Criteria	
PoC 1: target/pathway activation in pediatric clinical series	Prevalence of target/pathway in cohort	3 1 -3	>10% of cohort Between 2% and 10% ≤ 2% of cohort

PoC 2: tumor target dependence *in vitro*	Level of dependency and phenotypic recapitulation	3 1 -3	Full dependency (>75% cell death or transformation) Partial dependency (<75% cell death or altered growth) No dependency
PoC 3: tumor target dependence *in vivo*	Level of dependency and phenotypic recapitulation	3 1 -3	Full dependency (CR) after knockdown/knockout or transformation in GEMM Partial dependency (<75% response) No dependency
PoC 4: *in vitro* sensitivity to compound/drug	IC_{50} observed after 72-hour exposure	3 1 -1 -3	IC_{50} <500 nM or ≤ clinically relevant concentration IC_{50} = 500- 1000 nM IC_{50} >1500 nM No activity (IC_{50} >10 μM)
PoC 5: *in vivo* activity of compound/drug	*In vivo* tumor response	3 1 -1 -3	Response comparable to PR/CR Response comparable to SD Very minor response (between SD and PD, slight TGI) No activity or clear PD; growth comparable to control
PoC 6: predictive biomarkers	Correlation of biomarker status with anti-cancer activity of a targeted drug *in vitro*/*in vivo*	3 1 -3	Strong correlation (presence of biomarker results in significantly different drug response) Moderate correlation (presence of biomarker results in different drug response; not significant) No correlation (presence of biomarker does not correlate with drug response)
PoC 7: resistance	Reported resistance with drug exposure	3 1	Resistance reported at clinically relevant concentrations/dose and identification/description of mechanism Resistance reported with no mechanism
PoC 8: combinations	Synergy in combination testing at clinically relevant dosages in relevant *in vitro* and/or *in vivo* models	3 1 -1 -3	Strong synergy reported— CI <0.5 Moderate synergy/additive effect observed— CI 0.5 - 0.9 Very minor synergy/additive effect observed— CI 0.9 - 1.1 No combination benefit
PoC 9: clinical evaluation	Phase I	3 1	Toxicity profile acceptable, RP2D identified and early efficacy observed DLT observed with still acceptable safety and no efficacy reported

		-3	Toxicity profile not acceptable
	Phase II	3	Efficacy observed greater than historical ORR, DoR and/or PFS and acceptable toxicity
		1	Limited efficacy observed above the historical ORR, DoR and/or PFS and acceptable toxicity
	Phase III	-3	No efficacy observed and/or unacceptable toxicity
		3	Added efficacy over SOC in appropriate pivotal trial with acceptable benefit/risk profile; new drug now part of SOC
		1	Added efficacy over SOC but new agent not part of SOC due to trial design issues and/or benefit/risk assessment
		-3	Insufficient efficacy in pivotal trial

3.2.1.4. Step 3: Reviewer adjudication

"In the first step of the adjudication process, the collected evidence for each paper was re-evaluated by reviewer 1 and 2 together. The main target of each paper was identified and the addressed PoC modules and assigned quality and experimental scores were evaluated. Each module or score that was discrepant between the two reviewers was briefly discussed and adjusted if necessary. Papers with remaining discordant scores were sent to a third independent reviewer who then scored the paper while being blind to the original modules and scores given by reviewers 1 and 2. If the score given by the third reviewer was discordant with the scores given by the first reviewers, the paper then entered a second adjudication phase where discrepant scores were discussed by reviewer 1, 2 and 3 together and a single final consensus score was assigned to the paper."

3.2.1.5. Step 4: Visualization of results

"Once final experimental quality and outcome scores were entered in the R2 TAR platform, they were multiplied to create a single appraisal score for each data entry. The final scores ranged from -9 to +9, creating a gradient indicative of the importance of the study. Lastly, the scores for each PoC module within each of the 16 tumor types was averaged to create a heatmap of results. The interactive heatmap can be accessed using the publicly available R2 TAR platform [https://hgserver1.amc.nl/cgi-

bin/r2/main.cgi?option=imi2_targetmap_v1] where readers can view the number of papers and average appraisal score for each module in each malignancy type for replication stress overall as well as per specific target included in our study. Additionally, the summarized evidence, individual scores and PubMed links can be viewed for each entry by clicking on a tile in the heatmap."

3.2.2. Methods taken from "Predictive modeling of resistance to SMO-inhibition in a patient-derived orthotopic xenograft model of SHH medulloblastoma"

3.2.2.1. *In vivo* bioluminescence imaging

For bioluminescence imaging animals were anesthetized using inhaled isoflurane (1.5-2.5 Vol%) and injected with Luciferin solution (Promega) (i.p., 10 ml/kg, 15 mg/ml). Imaging was performed using an IVIS100 or IVIS Lumina luminescence imager with an exposure time of 5 min.

3.2.2.2. Tumor isolation

As soon as mice showed symptoms of tumor growth and termination criteria, they were euthanized and the tumor was extracted from the brain. It was put in medium (NeuroCult + 10% Proliferation Suupplement), mechanically dissociated to single cell suspension and filtered through a 40 µm strainer. Aliquots of $1.5x10^6$ cells were supplemented with 10% DMSO, frozen and stored in liquid nitrogen. Fresh-frozen tumor samples were prepared by freezing isolated tumor tissue immediately in liquid nitrogen. For formalin-embedded tissue, brain was cut in halves longitudinally, fixed in 10% formalin-solution and stored at 4°C until embedding.

3.2.2.3. FFPE tissue preparation and immunohistochemistry

For embedding formalin-fixed tissue the samples were dehydrated over a time period of 60 hrs with a dehydration machine (Epredia™ STP120, Thermo Fisher, USA) and afterwards paraffin embedded (HistoStar™, Thermo Fisher, USA). For stainings, 3 µm sections of the blocks were used and deparaffinized. Antigen retrieval was performed using boiling citrate buffer and sections were blocked for 1 hr with 10% normal donkey serum in PBS-T (0.1% Tween20 in PBS). Primary antibody was applied and incubated o/n at room temperature (anti-cleaved Capsase-3, 1:500, #9661, Cell Signaling, USA). After incubation with secondary antibody (anti-rabbit-biotin-SP-conjugated, 1:400, Jackson ImmunoResearch, USA), ABC-staining (Vectastain Elite ABC Kit, Vector Laboratories, USA) was added. Then sections were stained with DAB (DAB-2V, Nichirei Bioscience) and counterstained with Hematoxylin. Slides were rehydrated and mounted with Eukitt. Staining for Ki67 (clone MIB-1, Dako Agilent, USA) was done on a Ventana BenchMark ULTRA Immunostainer using the OptiView DAB IHC Detection Kit for Ki67 (Ventana Medical Systems, USA). Hematoxylin and Eosin (H&E) staining was performed for 1.5 min and 5 min, respectively.

3.2.2.4. DNA and RNA isolation

DNA and RNA isolation was performed as published previously [177]. In brief, by using TRIzol (Invitrogen) and the Qiagen miRNeasy Mini Kit (Qiagen) (for RNA) or the Qiagen DNeasy Blood & Tissue Kit (Qiagen) (for DNA), DNA and RNA were extracted from snap-frozen tumor tissue. The quality was assessed on an Agilent 2100 Bioanalyzer (Agilent Technologies) and only samples without ribosomla degradation and an RIN (RNA integrity number) >6.0 were used for further analysis.

3.2.2.5. Whole-exome and whole-genome sequencing

Whole-genome and whole-exome sequencing were performed as published previously [177]. In brief, libraries were prepared according to manufacturer's protocol with the Agilent SureSelectXT Target Enrichment System for Illumina Paired-End Sequencing. After quality assessment of the libraries (Agilent 2100 Bioanalyzer), sequencing was performed on an Illumina HiSeq2000 instrument with paired-end 100 bp or 125 bp runs (v3 and v4) at the DKFZ Genomics and Proteomics Core Facility, Heidelberg, Germany. For further processing of the data, a pipeline developed within the ICGC Pan-Cancer project (https://github.com/ICGC-TCGA-PanCancer) was adapted for alignment and variant calling. Using bwa-mem (v. 0.6.2), the reads were aligned to a reference genome based on merged human and murine genomes (hs37d5 and GRChm38mm10) and contaminating reads of mouse sequences was removed. Based on coordinates, the aligned reads were sorted and with biobambam bamSort and bammarkduplicates (c. 0.0.148) duplicates were highlighted. Identification of single-nucelotide variants (SNVs) was performed with SAMtools (v. 0.1.19) mpileup and annotated with ANNOVAR (http://annovar.openbioinformatics.org/en/latest/) [191]. Single-nucleotide polymorphisms and arifacts were removed.

3.2.2.6. RNA sequencing

RNA-sequencing was performed as published previously [177]. With the Illumina TruSeq RNA Kit v2 and poly(A)+RNA, the tumor DNA library was prepared and sequenced using a Illumina HiSeq2500 (paired-end 100 bp, rapid mode). To process the data, the reads were mapped by applying the STAR algorithm version 2.3.0e and as reference 1000 genomes were used [192]. Indexing was performed based on Gencode v.17 transcripts and for conversion of BAM files SAMtools (v. 0.1.17 (r973;277) was used [193]. Duplicates were annotated by Picard version tools (https://github.com/broadinstitute/picard (v. 190)). Raw counts of RNAseq data were normalized using DeSeq2 and used for Gene Set Enrichment analysis [194,195]. For gene expression analysis feature counts were used and pathway analyses were

performed using Gene Set Enrichment Analysis [194,195] and Ingenuity Pathway Analysis (Qiagen, Hilden, Germany).

3.2.2.7. DNA methylation analysis

Analysis of DNA methylation was performed as published previously [196] and EPIC (850k) BeadChip arrays (Illumina, San Diego, USA) were used according to the manufacturer's protocol at the Genomics and Proteomics Core Facility of the German Cancer Research Center (DKFZ), Heidelberg. Normalization of data was performed by background and dye bias correction and probes that were not uniquely mapped, due to e.g. targeting sex chormosomes of containing multiple SNPs, were removed.

3.3. Additional methods

3.3.1. *In vitro* drug screen

All used cell lines (respective media see Table 6) were kept in culture for at least one week after thawing before experiments were performed. Cultured cells were split, prepared as single cell suspension and counted using an automated cell counter (T20 Automated Cell Counter). The cells were seeded with the respective numbers (Table 6) in triplicates in a 96-well plate. After 24 hrs drugs were added and plates were incubated for 72 hrs. After incubation, readout was performed using CellTiterGlo® and luminescent signal was determined by a plate reader (Mithras LB 940 plate reader). All signals were averaged and normalized to DMSO-control.

Table 6: Overview of used cell lines, number of seeded cells and medium composition.

Cell line	# of seeded cells/well of 96-well plate	Medium
HD-MB03	3000	RPMI + 10% FCS (heat-inactivated) + 1% L-Glut + 1% Pen/Strep
Bt183	5000	Neurcult + 10% Proliferation Supplement + 0.1% hEGF (20 µg/ml) + 0.1% hFGF (20 µg/ml) + 0.1% Heparin (0.2% - solution)
Astrocytes	5500	DMEM high glucose + 10% FBS + 10% Pen/Strep + 1% Sodium Pyruvate + 1% N2 + 1% GlutaMax

The high-throughput drug screens using a library of 76 compounds was done in collaboration with Dr. Ina Oehme and Dr. Heike Peterziel of the Translational Drug Screening Unit at the Hopp Children Cancer Center, Heidelberg, Germany. For the (combination) drug screen with the library of 76 compounds cells were seeded in drug-preprinted 384-well round bottom plates (Corning #3830, 1000 cells/well, 25 µl/well). Cryopreserved PDX cells were thawed and kept in short-term culture in TSM complete medium before seeding [197]. After 72 hrs, luminescent signal (CellTiterGlo 2.0) was determined with a PHERAstar FS microplate reader. Drug sensitivity analysis was done with the drug-analysis pipeline BREEZE (https://breeze.fimm.fi), which has been developed at the Institute for Molecular Medicine Finnland (FIMM) [198].

For combination treatments the IC20 of one drug, which was determined in preceding experiments, was added to serial dilutions of the other drugs.

3.3.2. Animal experiments

All animal experiments for the projects were done in accordance with legal and ethical regulations and approved by the regional council (Regierungspräsidium Karlsruhe, Germany). The experiments were part of the following protocols: G259/14, G164/17, G227/19, G228/19, G91/20. For all *in vivo* experiments immunocompromised NSG-mice (NOD.Cg-Prkdc^{scid} Il2rg^{tm1Wjl}/SzJ) were used and obtained from the in-house breeding facility (German Cancer Research Center, Heidelberg, Germany). Housing of mice was in individually ventilated cages (IVC) and all animals were monitored daily for health status and tumor-related symptoms. Mice were euthanized as soon as they showed or any termination criteria listed in the animal protocol including symptoms of tumor growth.

3.3.3. Orthotopical injection of PDX cells in mice

For orthotopical intracranial injection of PDX models analgesia was administered to mice subcutaneously 20 min before surgery (5 mg/kg Carprofen or 200 mg/kg Metamizol; dependent on used animal protocol). Mice were anesthetized by inhaled isoflurane (1.5-2.5 Vol%) and checked by monitoring respiratory rate and toe pinch reflex. Then mice were transferred to a stereotactical frame and Bepanthen® was applied to both eyes. With a scalpel, an incision of ~0.5 cm was made along the mediolateral line using a scalpel. For local anesthesia 0.25% Bupivacain was applied. Afterwards the skull was exposed with a cotton-tipped applicator and cleaned of minor connective tissue or blood. With an 18G canula a hole was burred at the respective site, depending on the exact orthotopic location (Table 7). A Hamilton needle (10 µl Rainin Pipette-Lite fitted with a 2-10 µl ART tips barrier non-filtered pipette tip) was filled with 4 µl of cell suspension (PDX cells in Neurocult medium + 10% proliferation supplement), inserted into the stereotactical frame and brought to the respective site in the brain. Then the suspension was slowly injected within 1 min. Afterwards the needle was left in its place for 2 additional minutes to prevent reflux of the cells. When the needle was retracted the incision was closed with veterinary-grade surgical glue (3M, Vetbond). Then, the isoflurane inhalation was removed and mice were transferred back to their cages and monitored for the duration of recovery. For post-surgical analgesia Carprofen (s.c., 5 mg/kg, every 12 hrs for 48 hrs) or Metamizol (via drinking water, 800 mg/kg/day for 72 hrs) were administered.

Table 7: Overview of coordinates for intracranial injection of PDX models.

Injection site in mouse brain	Coordinate (mm; bregma)	Coordinate (mm; lateral left)	Coordinate (mm; depth)
Striatum	0	2.5	3
Cerebellum	-7	1	2

3.3.4. Virus production

For virus production $4x10^6$ HEK293T (low passage; p<10) cells were seeded in 10 cm dishes. After 24 hrs cells were transfected with packaging plasmids (pMD2.G and psPAX2) and the plasmid TR011-PA1 with pGreenFire1 (pGF1) using MirusIT according to manufacturer's protocol. After 72 hrs, supernatant was harvested and filtered with a 0.45 µm filter into a SW41 centrifuge tube and ultracentrifuged (15.000 rpm, 4°C, 90 min). Afterwards, supernatant was discarded and the pellet resuspended in 15 µl PBS. Solution was then aliquoted and stored at -80°C.

3.3.5. Luciferase-labelling of PDX models

For luciferase-labelling of PDX models, the established PDX model was transduced *in vitro* with the produced lentivirus containing the plasmid TR011-PA1 with pGF1 and green fluorescent protein (GFP). After 24 hrs *in vitro* the cells were injected orthotopically into mice at the respective site (Table 7). As soon as the mice show tumor-related symptoms, the mice were euthanized, the tumor taken out and a single-cell suspension prepared, which was then submitted to fluorescence-activated cell sorting (FACS) for GFP to pool the transduced cells. The positively sorted cells were then re-injected into mice to expand the labelled cells and be able to cryo-preserve aliquots for future experiments.

3.3.6. Preparation of drugs for *in vivo* treatments and application

Different drugs were used for preclinical *in vivo* studies and prepared for application as listed in Table 8. Pamiparib was applied in 1.5 mg/kg or 9 mg/kg per oral gavage twice per day on 5 days per week. The solution was stored at 4°C for a maximum of one week. Irinotecan (IRN) was applied in 2.5 mg/kg, 0.83 mg/kg and 0.27 mg/kg. The ready-to-use solution was stored at -80°C for up to 6 months and applied once per day intraperitoneally (i.p.) on 5 days per week. The used concentration of Selinexor was 5 mg/kg and was freshly prepared once per week. Liposomal and pegylated SN-38 (peg-SN-38)

was applied either at 15 µmol/kg or at 60 µmol/kg and aliquots were stored at -80°C. All drugs were applied at a volume of 10 ml/kg.

Table 8: Vehicles and dosing schedules of applied drugs.

Drug	Vehicle	Dosing schedule
Topotecan	0.9% NaCl	i.p., 1x/day, 5 days on/2 days off
Irinotecan	0.9% NaCl + 0.6% DMSO	i.p., 1x/day, 5 days on/2 days off
peg-SN-38	Isotonic acetate	i.p., 1x/week
Pamiparib	0.5% Methylcellulose (4000 cP)	p.o., 2x/day, 5 days on/2 days off
Selinexor	0.6% Plasdone PVP K-29/32 + 0.6% Poloxamer Pluronic F-68	p.o., 1x/day, 5 days on/2 days off

3.3.7. Protein lysis of tumor samples

Fresh-frozen tumor samples were thawed on ice and 200 µl RIPA buffer, containing 1% Protease-inhibitor and 1% EDTA, were added. Tissue was minced using a tissue mincer (Tissue Master TM125-220) and afterwards samples were sonicated for 30 sec on ice. Then samples were incubated on ice for 10 min and centrifuged (13.000 rpm, 10 min, 4 °C) afterwards. Supernatant was transferred to new Eppendorf tubes and protein concentration was determined by BCA-assay according to manufacturer's protocol.

3.3.8. Western blot analysis

Protein samples (50 µg protein) were mixed with NuPAGE™ reducing agent (10x) and NuPAGE™ LDS sample buffer (4x) and denaturated by boiling for 5 min (95 °C). Then, lysed samples were separated on a 4-12% Bis – Tris gradient gel (Invitrogen) (NuPAGE™ MES SDS running buffer w/o antioxidant; 130 V, 1.15 hrs) and afterwards transferred onto a 0.2 µm PVDF membrane (20 V, 1.15 hrs). The membrane was blocked with 5% milk in Tris-buffered saline with 0.05% Tween20 (TBS-T) and incubated with the primary antibody o/n at 4 °C, see dilutions and solvents in Table 9. On the next day, the membrane was washed with TBS-T (3x) and incubated with the HRP-linked secondary antibody for 1 hr at room temperature. Afterwards, the membrane was washed with TBS-T (3x), covered with ECL or ECL-prime Western Blotting Detection Reagent and chemiluminescent signal was detected using the Intas Chemostar ECL Imager. If necessary, antibodies were stripped using Restore™

Western Blot Stripping Buffer and membrane was again blocked and incubated with different antibodies.

Table 9: Overview of used antibodies with dilutions and solvents.

Antibody	Dilution	Solvent
IgG-HRP goat anti-rabbit	1:2500	5% milk in TBS-T
Poly/Mono-ADP Ribose (E6F6A); Rabbit mAb	1:1000	5% BSA in TBS-T
HRP Anti-beta Actin [AC-15]	1:10.000	5% milk in TBS-T

4. Target actionability review

Within my PhD project "Targeting high-risk pediatric brain tumor entities" one subproject was about a systematic literature research that was performed as part of the Innovative Therapies for Children with Cancer – Pediatric Preclinical proof-of-Concept Platform (ITCC-P4) consortium and I worked together with Kaylee M. Keller from the Princess Máxima Center for Pediatric Oncology in Utrecht, The Netherlands and Apurva Gopisetty from the Hopp Children's Cancer Center in Heidelberg, Germany on the conceptualization of the project, acted as a primary reviewer of the literature, and collaborated for data curation, visualization and writing of the TAR paper. The findings of this manuscript are summarized in a publication and were accepted by the *European Journal of Cancer* for publication. The figures displayed in this chapter were taken from this manuscript.

4.1. Introduction

Even though an increasing number of treatments for different cancer entities are being developed, cancer is still the leading disease-related cause, and second leading overall cause of death in children, and establishment of new therapeutic strategies are challenging [121]. A limitation is that only less than 1% of all cancer diagnoses occur in children and consequently patient numbers for clinical trials are often low [122]. Moreover, development of drugs for treating cancer is focused on adult tumor entities and for treatment of pediatric patients, physicians have to consider off-label use of drugs, which raises not only ethical questions but also concerns about systematic evaluation of efficacy. These limitations highlight the need for well-planned and well-structured collaborations to prioritize and develop new treatment strategies and therapeutics for pediatric cancer patients. To streamline research and development of new therapies, a methodology for systematic literature research was developed as part of the ITCC-P4 (Grant Agreement No. 116064) consortium [188,199]. By using this method, the current knowledge of publications should be evaluated, scored and summarized into different Proof-of-Concept (PoC) modules to help prioritizing promising treatment strategies as well as highlight potential gaps in a particular research field. Ultimately, the results are summarized in a target actionability review (TAR). The TAR described here was performed to evaluate all literature that relates to replication stress in any of 16 different predefined pediatric solid tumor entities.

A cell experiences replication stress during a cell cycle when the DNA replication fork is stalled [200]. However, neither only one specific pathway can lead to replication stress, nor one specific pathway is exclusively upregulated if replication stress occurs. A multitude of pathways and mechanisms can

result in slowing or stalling of the DNA replication fork which in turn typically leads to accumulation of DNA damage, genome instability and, if present to a higher extend, subsequently leads to cell death [201]. Since genomic instability and DNA damage are hallmarks of cancer and present in nearly all cancer cells, replication stress is characteristic for cancer cells as well. If processes leading to replication stress are targeted for therapeutic reasons, the effect of replication stress can even be increased in cells and push them towards cell death [202].

One possibility to induce and exacerbate replication stress is to use radiotherapy and/or chemotherapeutics such as DNA alkylating agents or topoisomerase-inhibitors, by which DNA replication is interrupted and replication stress is induced to an extent that the cell has to go into apoptosis [203]. Even though radiation and chemotherapeutics are commonly used in the clinic, the therapies have limitations since the mechanism of classic chemotherapies is based on a high rate of cell proliferation and DNA replication, which may also occur in non-tumorigenic healthy cells. Commonly cells of the gut epithelium and bone marrow are also susceptible for treatment with radiation or chemotherapeutics and toxic side effects as well as long-term side effects are the result for children who survive cancer [204].

Another possibility to induce and exacerbate replication stress is to apply targeted inhibition of pathways to prevent that the cell can resolve the induced replication stress. By this, replication stress is also accumulated over time and leads to cell death. In healthy as well as tumor cells, stalling of a replication fork due to any damage leads to activation of numerous signaling pathways and proteins that support resolving of the damage and restarting the replication fork [205]. Since tumor cells often can be characterized by loss of cell cycle control and/or overexpression or aberrant activation of oncogenes which leads to high proliferation and replication, cancer cells frequently experience replication stress, and the stress response network for resolving accumulated replication stress is highly important for the cell and its survival [206,207]. Moreover, treatment strategies that aim to inhibit one or more pathways of this network can be especially successful for killing of cancer cells and may be less toxic in normal cells. Since many different pathways and proteins are cooperating within the replication stress response process, a multitude of possibilities and targets can be inhibited for therapeutic approaches and many different strategies for therapy of pediatric and adult malignancies are currently being studied.

For the TAR described here, publications that reported preclinical studies or clinical trials focusing on replication stress as a target for treatment of intra- or extracranial pediatric solid tumors were systematically evaluated and scored. Besides underlining the knowledge but also gaps of replication

stress as a target for pediatric solid tumors, promising treatment strategies were highlighted as well as the limitations of published data.

4.2. Results

Literature that was published between 2014 and 2021 was evaluated with respect to targeting replication stress in 16 different pediatric solid tumor entities. The systematic literature research was performed as a stepwise process which consists of the literature search, critical appraisal and scoring of the papers, reviewer adjudication and visualization of the results (Figure 8). Firstly, in the literature search pre-defined keywords were used for Pubmed queries and publications were evaluated based on abstract and title whether they fit in the scope of the TAR. For step 2, papers were read in detail by two independent reviewers and scores and evidence entries were entered in the R2 portal. Papers with discrepant scores were analyzed by a third independent reviewer in step 3 and afterwards the results were illustrated in the R2 portal as heatmaps (step 4).

The first literature search was done as described in detail in the methods section and yielded in total 708 unique papers. In a next step, all papers were individually checked for addressing at least one of the Proof-of-Concept (PoC) modules (Table 2) in title or abstract. This resulted in the exclusion of 389 papers (55%), while the remaining 319 papers were used as basis for the next steps (Figure 8). In step 2 the remaining papers were analyzed in more detail and 174 papers that did not fulfil the criteria for the TAR (e.g. used micro or long non-coding RNA, natural compounds or chemotherapeutics or radiation in monotherapy) were also excluded. Finally, 145 papers were scored independently by two reviewers each with respect to the defined PoC modules and 392 evidence entries were registered in the R2 portal. For 68 papers (47%) at least one discrepancy in the scores (module, quality or experimental outcome) was noted and these papers were scored by a third, independent reviewer. Ultimately, 58 scoring discrepancies (from 145 papers) remained and these were all discussed and resolved in a final adjudication step. In total, 37 drug targets were identified to be addressed in at least one of the scored papers. Using the R2 portal, all results were summarized and visualized in heatmaps, displaying the scores for 145 publications, 16 pediatric solid tumor entities, and 37 drug targets.

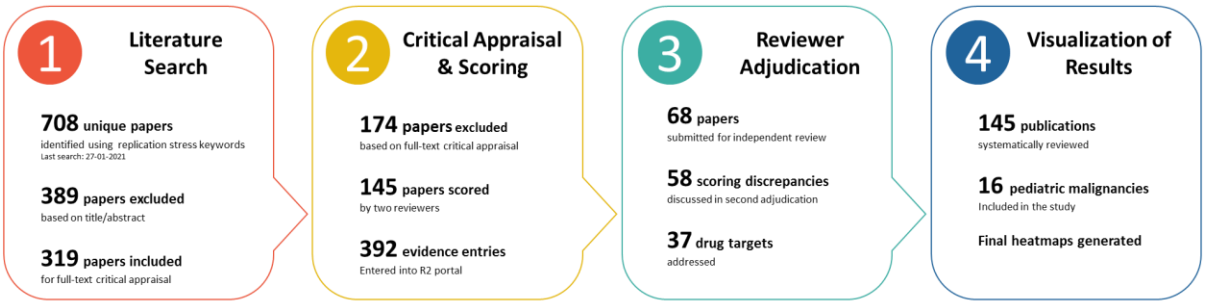

Figure 8: Overview of stepwise process with numbers of papers/evidence entries for the TAR [189].

The applied workflow consists of literature search, critical appraisal and scoring, reviewer adjudication and visualization of results. The papers were stepwise analyzed in more detail and scores and evidences were entered in the R2 portal (step 2). In a next step scoring discrepancies were evaluated and specific drug targets were identified (step 3). For easier understanding results were finally grouped into drug targets and results were visualized as heatmaps in the R2 portal (step 4).

The topic of the initial TAR study that was published by Schubert *et al*. was the drug target MDM2, which is a single drug target and well defined [188]. In contrast, "replication stress" as a target is a complex process comprising many potential targets and thereby increasing tremendously the amount of literature. In addition, the methodology was established for single targets and not for processes. To account for this, the methodology was slightly adapted and not only specific keywords as e.g. drug targets but also more general search terms related to replication stress were used (Table 1). For replication stress, DNA repair pathways as well as cell cycle control play a major role (Figure 9a). By choosing specific keywords, the six druggable targets ATM, ATR, CHK1, DNA-PK, PARP and WEE1, which are relevant for DNA repair and cell cycle control, were specifically addressed within the TAR. However, as replication stress is a very broad and complex process, also other general keywords were used and additional potential drug targets were identified (Figure 9b), which accounted for 127 (32%) of all evidence entries. Full and systematic evaluation of the additional potential targets was not included in this TAR, nevertheless it gives information about potential new targets of replication stress that can be further studied and explored by using the interactive heatmap on the TAR platform within the R2 portal (https://hgserver1.amc.nl/cgi-bin/r2/main.cgi?option=imi2_targetmap_v1).

a

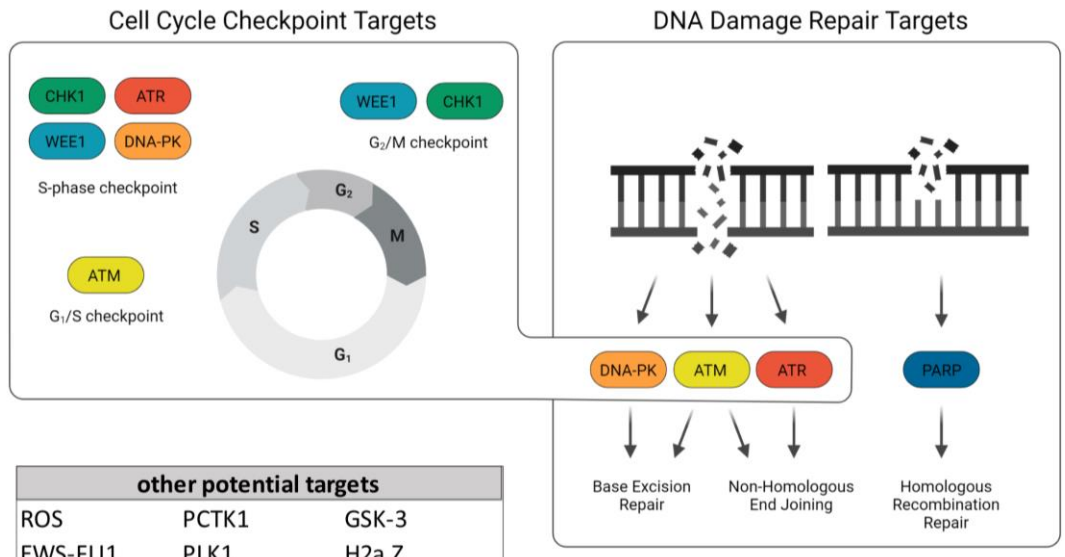

b

other potential targets		
ROS	PCTK1	GSK-3
EWS-FLI1	PLK1	H2a.Z
FACT/SSRP1	RB1	STAG
WIP1	RBBP4	ZBB38
CDK	TFAP4	tubulin
AKT	SIRT6	Notch
RAD51	PP2A	BRCA
EZH2	Cdc5L	ATRX
MRE11	MTH1	BET/BRD4
MRK	mTOR	Aurora kinase
HDAC		

Figure 9: Overview of specific targets (a) and alternative potential targets revealed by using general key words (b) within the TAR [189].

The six specific keywords are druggable targets and either involved in cell cycle, DNA damage repair or both (a). By using general keywords related to replication stress other potential targets of replication stress were identified (b).

Analysis of all results together showed that neuroblastoma (NBL), Ewing sarcoma (ES), osteosarcoma (OS) and medulloblastoma (MB) were the most comprehensively studied within the TAR (Figure 10a). They did not only have the most evidence entries (NBL = 79, ES = 71, OS = 71 and MB = 58), but they were also the only entities with evidence scores for all PoC modules, indicating a more robust analysis of replication stress as a target. In comparison, other entities could not be evaluated for all PoC modules or did not even have a single evidence entry like inflammatory myofibroblastic tumors (IMT) or extracranial germ cell tumors (GCT). Albeit all PoC modules are addressed for NBL, ES, OS and MB some scores for a module did only reflect one publication as e.g., module 1 (target/pathway activation) for ES, which has a negative overall score, but it also has only one evidence entry (Figure 10a). Overall, the PoC modules “target/pathway activation”, “predictive biomarkers” and “resistance”

were the least represented across all 16 tumor entities (Figure 11a), indicating a lack of data supporting stratification for replication stress as a target.

For the six specific drug targets (ATM, ATR, CHK1, DNA-PK, PARP and WEE1) that were included as keywords, the available data and related literature was also analyzed independently and visualized in separate heatmaps (Figure 10b-g). The most comprehensively studied target was PARP with 127 (32%) evidence entries and data for all nine PoC modules. PARP was studied in 10/16 malignancies, while it was not investigated in ATRT, MRT, IMT, GCT, RB and LGG (Figure 11b). Since evidence entries related to PARP encompassed the largest groups, as compared to the other specific targets, not only in numbers but also being the most comprehensive ones because they addressed all PoC modules, PARP is the most promising target. This is further supported by the promising results that were achieved by combining PARP-inhibitors with classic chemotherapy (Figure 10b; Figure 11c). Nevertheless, less data does not indicate less potential as a promising target. Even though the other specific targets were addressed by less papers and fewer evidence entries (ATM: n = 7, ATR: n = 35, CHK1: n = 50, DNA-PK: n = 18, WEE1: n = 29), scores were evaluated and indicated that these targets are still of interest and the TAR helps to highlight the status quo as well as gaps that need to be filled (Figure 10c-g).

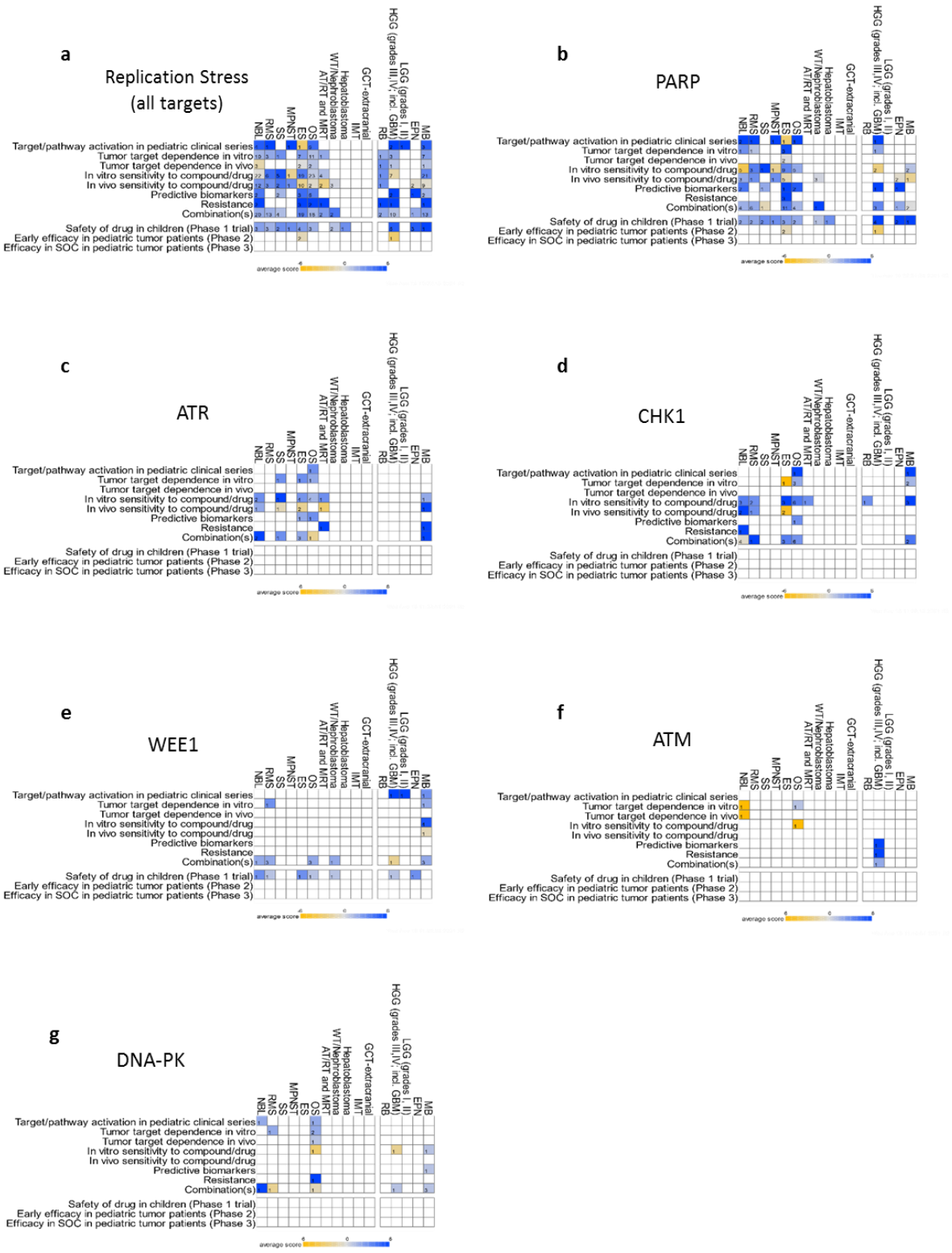

Figure 10: Summary of evidence scores for replication stress (a), PARP (b), ATR (c), CHK1 (d), WEE1 (e), ATM (f) and DNA-PK (g).

Each box shows the average of scores with yellow indicating a negative result and blue a positive result for every PoC module. The results can also be viewed using the R2 TAR platform (https://hgserver1.amc.nl/cgi-bin/r2/main.cgi?option=imi2_targetmap_v1).

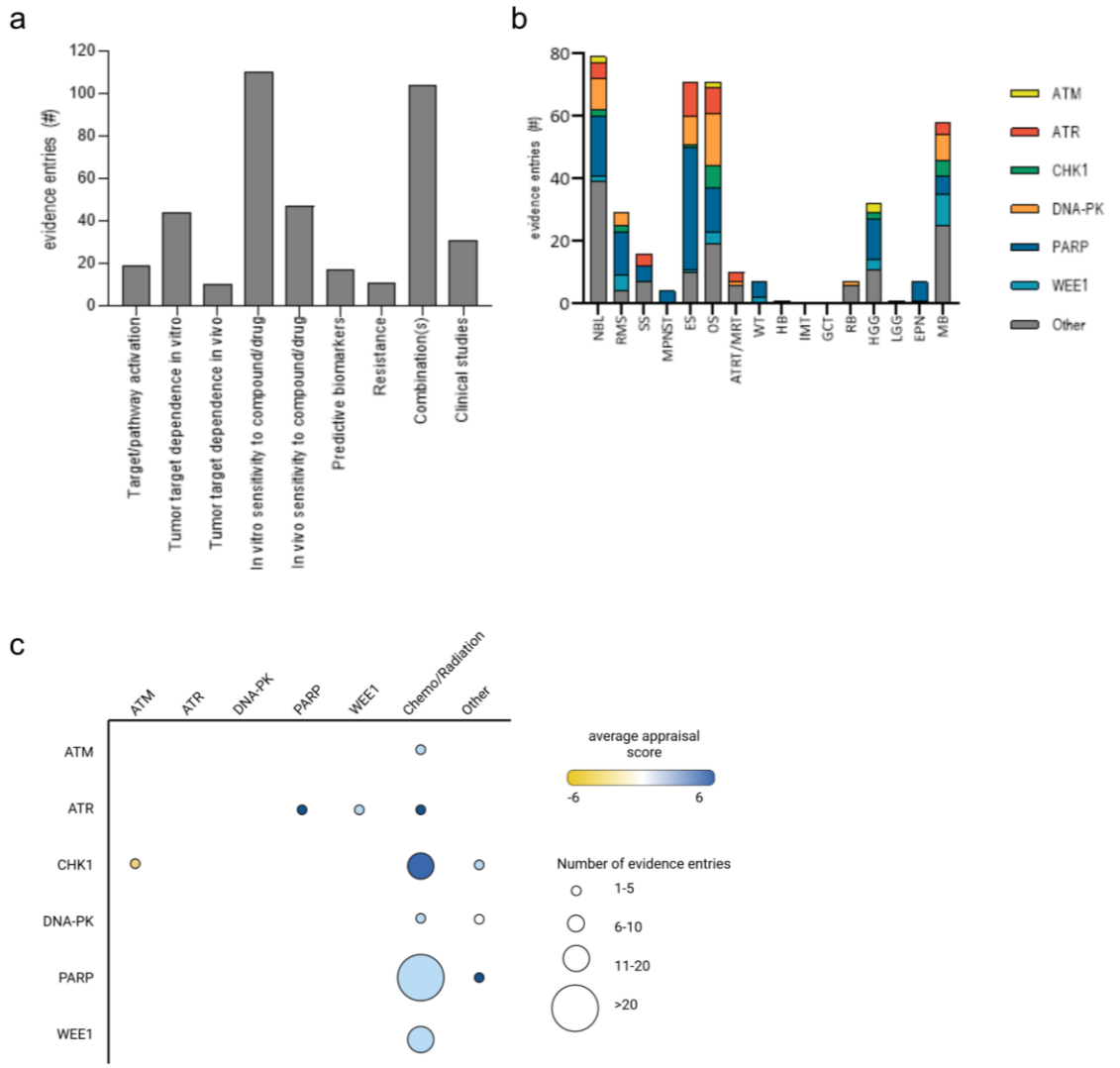

Figure 11: Overview of number of evidence entries per module (a), per entity divided by drug target (b), and details (number and type) of evaluated combination therapies (c) [189].

For c): The number of papers addressing the particular combination is reflected by the size of the dot and the average appraisal score of each combination is indicated by the color with yellow reflecting a negative score and blue a positive score.

One of the modules that was studied the most, and not only for PARP-inhibitors, was module 8 – combinations and especially combinations of an inhibitor with classic chemotherapy or radiation (Figure 11c). Even though PARP was represented by the most evidence entries in this module, entries for ATR and CHK1 revealed higher evidence scores indicating promising therapeutic options for these targets in combination with classic chemotherapeutics or radiation. In addition, scores for ATR and CHK1 were also positive for all other addressed modules in MB (Figure 10c, d). For example, ATR was studied as a target for MB for several modules (*in vitro/in vivo* sensitivity, resistance, combinations) and scored positive for all of them. Even though the scores were only based on one paper, it still points

out that ATR might be a promising target for MB [208]. Besides the positive results for ATR, evidence entries for MB with respect to CHK1 were also consistently positive for the assessed modules (target/pathway activation, tumor target dependence *in vitro*, *in vitro* sensitivity to compound, combinations) (Figure 10d). Overall, evidence scores for CHK1 were positive across all studied entities. The only malignancy that did not on average score positive for CHK1 is ES, which had positive results for two modules (*in vitro* sensitivity, combinations) but negative scores for the modules "tumor target dependence *in vitro*" and "*in vivo* sensitivity to compound" (Figure 10d). However, since the scores are only based on 2-3 included papers per module, more studies are necessary to comprehensively investigate CHK1 as a target in ES.

The target WEE1 achieved positive appraisal scores throughout all studied malignancies (Figure 10e), though only based on few evidence entries. However, the results indicate that combination of WEE1-inhibition and chemotherapy leads to better results than WEE1-inhibition as monotherapy (Figure 11e). This is supported by the results of a Phase I clinical trial that evaluates WEE1-inhibition in combination with Irinotecan and achieves positive scores for NBL, HGG, EPN, RMS, ES, OS and WT (Figure 10e) [209]. Even though data of a clinical trial was evaluated for WEE1, data for the modules "predictive biomarkers" and "resistance" is lacking and proposes that more research needs to be done to more comprehensively study WEE1 as a target in pediatric solid tumor entities.

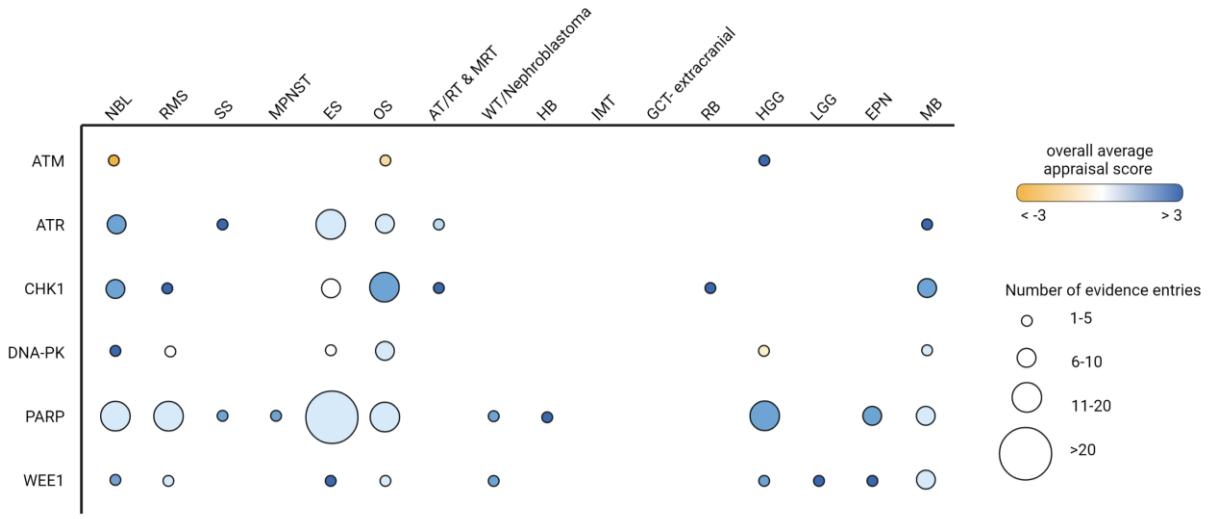

Figure 12: Summary of specific targets across all 16 pediatric solid entities [189].

The size of the dots represents the number of evidence entries and the color indicates the overall evidence score averaged by all PoC modules.

Out of the six specific targets, ATM and DNA-PK had the fewest data entries to evaluate and were often only annotated by a single publication. For ATM only seven scoring entries were included, which addressed six different modules in three different entities (Figure 10f). Even though only based on one evidence entry each, ATM as a target scored highly positive for HGG in three modules (predictive biomarker, resistance, combinations) [210,211]. These results suggest ATM as a promising target for therapy of HGG, even though further research needs to confirm this. Evaluation of DNA-PK as a target was more distributed among the PoC modules than evaluation of ATM. For DNA-PK evidence entries for all PoC modules except "*in vivo* tumor target dependence" across five tumor types (NBL, RMS, OS, HGG and MB) were identified (Figure 10g). Remarkable high scoring results of DNA-PK were noted for "combinations" in NBL[212] and "resistance" in OS [213]. For all the other scored models and tumor types the average appraisal score was not positive but also not negative (Figure 12). This emphasizes the need of additional research to confirm the published results and evaluate DNA-PK as a potential target for pediatric solid cancers.

4.3. Discussion

The TAR methodology was developed to systematically and objectively assess published literature and evaluate a specific target for pediatric solid tumors. Within the ITCCP4 consortium different specific topics as e.g. *MDM2* for TARs were defined, however in the TAR presented here the methodology was not only used to evaluate one specific target or pathway but the broader process "replication stress", which incorporates many proteins that can be targeted and also different pathways. To account for the many different pathways and proteins that play a role for replication stress, broad and more general keywords as "replication stress" or "genomic instability" were used but also six specific targets that are relevant for replication stress, namely PARP, ATR, ATM, CHK1, DNA-PK and WEE1, were added to the keywords. The use of the general keywords revealed 31 potential targets (Figure 9b) in the scope of targeting replication stress but to be able to comprehensively evaluate the targets further literature search for those specific targets would be necessary. More robust analysis was possible for the six specific targets that were used as keywords, however the adapted methodology also came along with additional challenges since more targets were combined within one TAR. To be able to compare the different targets, for each evaluated publication the main target was defined and the results were not only visualized in one combined heatmap but also separately for each of the six main targets (Figure 10). However, since each target was addressed by a different number of publications and the average overall score was different for each target (Figure 12), prioritization of the targets and recommendations for future (pre-)clinical studies were difficult. In addition, due to the broad

topic of replication stress, not all relevant targets could be included and a compromise between general keywords, specific targets, diversity of replication stress and conclusiveness had to be found. Besides these challenges linked to the evaluation of a process instead of a specific target or pathway, the TAR methodology itself has limitations as for example very specific and variable responses of patients within a clinical trial. To be able to compare outcomes they had to be generalized for scoring and details could only be mentioned within the evidence entries. In addition, it is difficult to compare results across entities since for some entities only very limited amount of literature could be included.

Even though the evaluation of a process instead of a specific target introduced some challenges, adaptations and limitations to the TAR methodology, replication stress is still a promising drug target for therapy of pediatric solid tumors. Since the process comprises many pathways and proteins, a vast number of therapeutic strategies and targets are possible and though the process of replication stress was evaluated systematically, the focus was on six specific druggable targets, namely ATM, ATR, CHK1, DNA-PK, PARP and WEE1. Of these targets, PARP was the most studied and evaluated target being addressed by the most literature. PARP as a target was not only scored and addressed in respect to all PoC modules but also evidence scores were positive for most of the modules. For 9/16 included entities, PARP had evidence entries for PoC module 8 – combinations, where it was synergistically combined with chemotherapeutics (Figure 10b). By combining two drugs for treatment, the replication stress process can be hit twice to increase the effect of the treatment and to inhibit possible alternative pathways to resolve replication stress. In addition, by adding a targeted drug to treatment with chemotherapeutics, doses of chemotherapeutics can be reduced and toxic side effects of high-dose chemotherapy can be limited. This strategy was also applied in the evaluated phase I clinical studies in which PARP-inhibitors were combined with radiotherapy or chemotherapy (Temozolomide and/or Irinotecan) [214-218]. The clinical studies that combined PARP-inhibitors and chemotherapeutics/radiotherapeutics revealed positive results across all studied tumor entities, which indicates that the combination treatment was well tolerated by the patients. Though results were positive, only for two malignancy types, ES and HGG, phase II clinical studies were published and scored (Figure 10b). Interestingly, the average appraisal scores were rather negative and indicated poor clinical efficacy. However, the evaluation was only based on two publications for HGG and one publication for ES and ranged from no clinical benefit to stable disease [214,218,219]. This discrepancy and limited amount of data emphasizes the need of additional research and especially clinical studies.

Combinatorial treatment strategies were not only performed with PARP-inhibitors, but also with inhibitors for all other specific targets addressed in the TAR. Nevertheless, the majority of combination treatments used a targeted inhibitor and chemotherapy or radiotherapy as combination partner. Most

of the combination studies were scored with slightly positive results indicating only a minor synergistic effect (Figure 11c). A combination that scored highly positive, and consequently implied a synergistic combination, was inhibition of CHK1 and use of chemotherapy in MB, ES, OS, NBL and RMS [220-222]. Besides the combinatorial studies that combined a targeted inhibitor with chemo- or radiotherapy, some publications reported about the use of two targeted inhibitors in combination as e.g. ATR-inhibitor and WEE1-inhibitor or PARP-inhibitor [223,224]. Investigation of a two-fold strategy to target replication stress can be advantageous since chemo- and radiotherapy is known to induce toxic side effects and unfavorable long-term adverse events [204]. Treatment of patients with metastatic melanoma or BRAF-mutant brain tumors by inhibition of BRAF and MEK, that are both part of the MAPK-signaling pathway, had shown good efficacy and supports the treatment strategy to target more proteins within the same pathway [152,225]. The same strategy also resulted in synergistic effects when applied to pathways relevant for replication stress, which can either be done as a "vertical blockade" by inhibiting two proteins within the same pathway or as a "lateral blockade" when proteins of different pathways, but still relevant for replication stress, were inhibited. Two studies that were investigated within the TAR presented here treated either ES cells with ATR- and WEE1-inhibitors, which can be seen as vertical blockade, or applied lateral blockade by using ATR- and PARP-inhibitors to NBL cells [223,224]. Both studies reported synergy for the combination treatments, which makes them promising treatment strategies. In general it can be beneficial to combine targeted inhibitors instead of adding chemo- or radiotherapy to prevent the toxic side effects. But no matter for which combination, more preclinical research needs to be performed across the different pediatric tumor types and the different targets to be able to verify the most promising combinations.

To identify encouraging treatment strategies not only more preclinical research for combinations is necessary, but it is important to plan and conduct meaningful preclinical studies in general. To do so, it is necessary to understand the underlying biological mechanisms of a treatment strategy and to choose models with suitable molecular backgrounds. In the TAR presented here, with less than 10% of all evidence entries, the PoC modules "biomarker" and "resistance" were within the modules with the least evidence entries, which demonstrates the lack of publications and preclinical studies that take the biological mechanism and understanding of a therapeutic strategy into account (Figure 11a). In addition, some tumor entities (e.g. IMT and extracranial GCT) were not addressed at all but in general the different molecular groups and subgroups of one entity were not addressed or not mentioned in a publication. Since sequencing and methylation analyses revealed highly relevant differences of groups and subgroups of one entity, adequate model selection is crucial. However, this also highlights that more molecular characterized models are needed as for some groups and subgroups only a few or no models are available (e.g. *in vitro* models for Group 4 MB). Only with

suitable model selection and identification of the molecular groups (and subgroups) of an entity, treatment strategies can be tested and applied reasonably. For example, the fusion gene EWS-FLI1, which is detected in ~85% of patients with ES, has been reported to lead to deficient DNA repair mechanisms, error-prone DNA transcription and higher replication stress in general [226,227]. These characteristics make therapies that target replication stress promising for this group, however, identification of the fusion gene is necessary and models have to be selected accordingly. ES tumors that do not have the EWS-FLI1 fusion gene might respond differently to therapies that target replication stress.

To perform successful preclinical research and clinical trials it is pivotal to understand the biological background of a treatment strategy and select suitable models, however the lack of literature taking into account the molecular groups and subgroups of an entity identifies drawbacks of research and should be addressed in future preclinical studies and clinical trials. In addition, results derived from *in vitro*, and also *in vivo* experiments, can often not directly be translated into clinical setting due to limited number of used models in preclinical studies compared to many more patients enrolled in a clinical trial and differences in the applied guidelines for interpretation of data.

5. Targeting replication stress *in vitro* and *in vivo*

5.1. Introduction

As highlighted before, DNA replication is a strongly regulated process that ensures duplication of DNA during each cell cycle and its accuracy is pivotal for cellular proliferation and genome stability. In case the replication fork is stalled or the process is being disturbed, the cell experiences replication stress and when this is maintained over time and accumulated DNA damage, genome instability and cell death occurs [200,201]. Characteristic for cancer cells and especially cells of aggressive entities are high levels of proliferation and increased DNA replication. Replication stress is therefore very common in these cells and can be a promising vulnerability for therapeutic intervention [228,229]. Replication stress can even be listed as a hallmark of cancer supported by the fact that escape from apoptosis and genome instability are a consequence of replication stress [206]. In healthy cells the DNA damage response, which is controlled by cell cycle checkpoints, activates the DNA repair system or induces senescence and apoptosis [230-233]. This mechanism works as a barrier to prevent malignant progression of the cell [234]. In contrast, in cancer cells constitutive growth signals and/or defective DNA damage response pathways lead to replication stress, which can even be targeted by therapies to overcome checkpoints and push the cell towards mitotic catastrophe [235]. Interestingly, the phenomenon of replication stress is known of cancer cells but is only barely seen in normal cells, even if they have high proliferation rates [236].

Physiologically, single-stranded DNA (ssDNA) activates ataxia telangiectasia and rad3 related- (ATR) signaling, which leads to phosphorylation of checkpoint kinase 1 (CHK1), the cell cycle checkpoint Rad17 and the H2A histone family member X (H2AX), but if a cell faces replication stress, replication forks are being stalled and single-stranded DNA (ssDNA) accumulates [201,236,237]. With increasing levels of ssDNA within a cell, stalled replication forks can collapse and lead to double-strand DNA (dsDNA) breaks [201,238]. If cells still enter mitosis, due to e.g., oncogene expression that activates G1/S-transition, dsDNA breaks and non-replicated chromosomes lead to mitotic catastrophe and cell death [238,239]. In brief, low levels of replication stress can induce genomic instability and support tumorigenesis but if a cell has high levels of replication stress, this leads to cell death (Figure 13) [236,237,240].

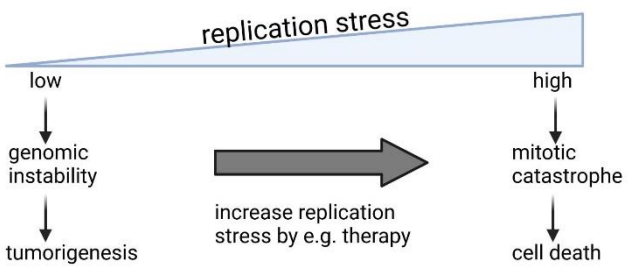

Figure 13: Level of replication stress has distinct effect on cells.

Low levels of replication stress leads to genomic instability and tumorigenesis; high level of replication stress can induce mitotic catastrophe and cell death; level of replication stress can be increased by e.g. therapy; Figure adapted from Zhang *et al*. 2016 [235]; created with BioRender.com.

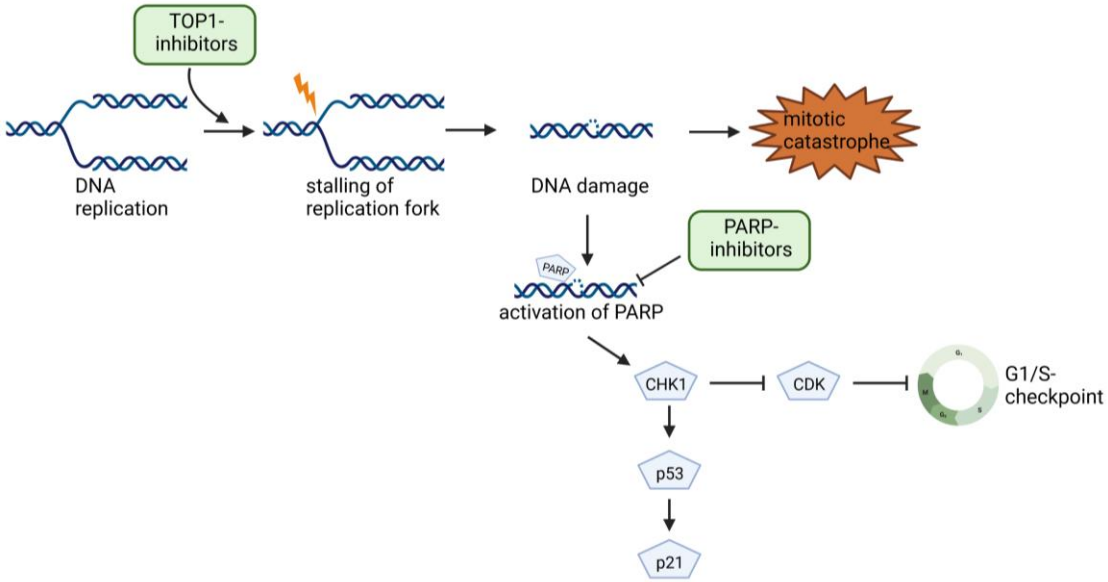

Figure 14: Schematic overview of induced replication stress leading to mitotic catastrophe.

By using topoisomerase-inhibitors replication forks are stalled and to resolve stalling DNA damage is induced; for repair of ssDNA breaks PARP is activated and translocated to the site of DNA break; activation of PARP consequently leads to activation of CHK1, p53 and p21; activated CHK1 inhibits CDK which then inhibits the cell cycle by affecting the G1/S-checkpoint; by inhibition of PARP DNA damage accumulates and can lead to mitotic catastrophe; Figure adapted from Zhang *et al*. 2016 [235]; created with BioRender.com.

MYC and MYCN are transcription factors that are also known as proto-oncogenes, which are physiologically expressed in rapidly dividing but not in quiescent tissue stem cells [241]. In about 30% of human cancers *MYC* is overexpressed and related to aggressive growth and poor clinical outcome [242]. Tumors with high expression or amplification of *MYC(N)* are usually characterized by genome instability with numerous chromosomal gains and deletions [243].

High expression of *MYC(N)* due to *MYC(N)*-amplification or overexpression can lead to increased transcription which, as a consequence, can be in conflict with DNA replication and promote replication stress. High levels of replication stress can lead to DNA:RNA-hybrids called R-loops. These structures are formed if replication catches up with transcription and prevents correct unwinding of DNA [244]. R-loops may also occur in normal cells but are usually resolved by the enzyme Topoisomerase I, which catalyzes cutting and re-annealing of one strand of dsDNA [245]. However, if transcription levels are high, R-loops accumulate and are associated with increased genomic instability [246].

Targeting MYC(N) remains a major challenge as it plays a central role not only in tumor but also in healthy cells and is characterized by low druggability. This leads to an urgent need for development of innovative strategies. Examples for tumors with high *MYC(N)*-expression for which current treatments are unsuccessful are MB SHH and Group 3 with *MYCN*- and *MYC*-amplification, respectively, glioblastoma with *MYCN*-amplification and ETMR with high *MYCN*-expression (Figure 15) [30,104,247]. Tumors with high levels of R-loops are e.g. ETMR, MB Group 3 and *ZFTA*-fusion positive EPN, whereas e.g. MB Group 4 tumors do not have accumulated R-loops (Figure 15) [108].

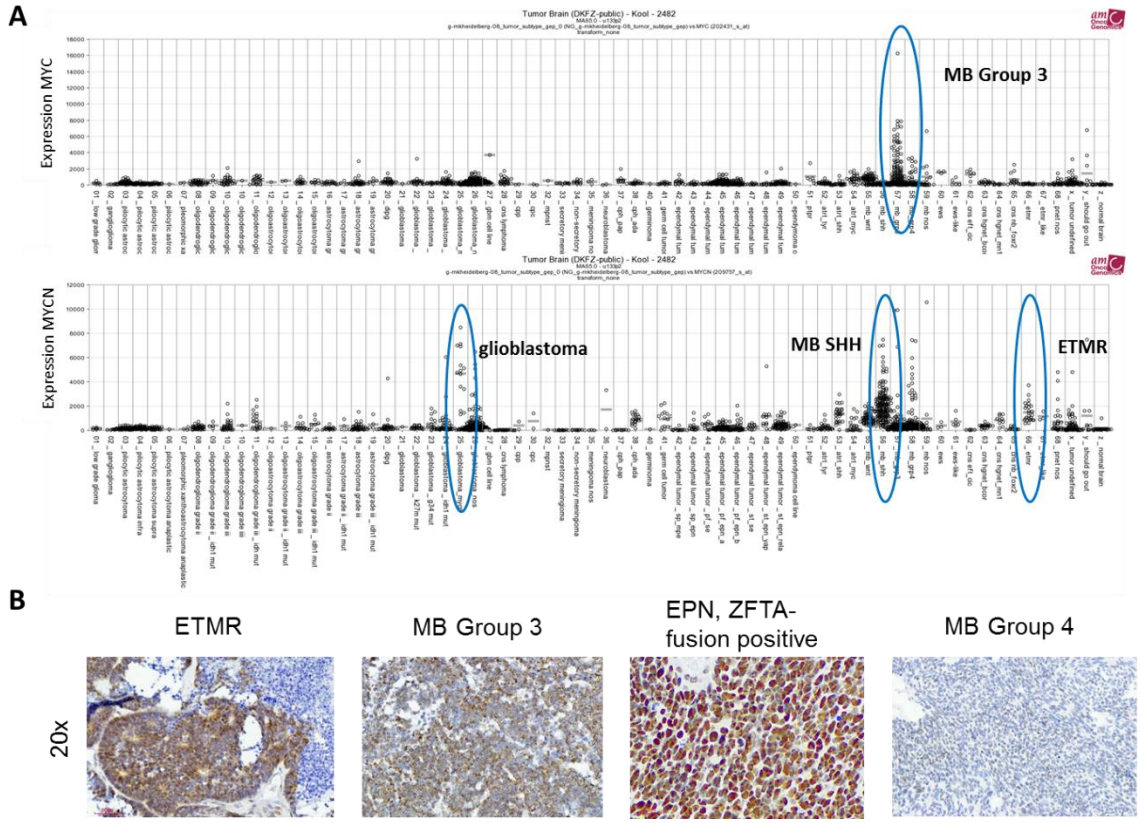

Figure 15: Expression level of MYC(N) and presence of R-loops in a series of pediatric brain tumors.

A) MB SHH and Group 3 have high expression levels of MYCN and MYC, respectively due to amplification; a subset of glioblastoma has amplification of MYCN; ETMR have high expression of MYCN but not due to amplification; B) IHC stains (20x) with the DNA:RNA-hybrid specific antibody S9.6 show that ETMR, MB Group 3 and *ZFTA*-fusion positive EPN have high levels of R-loops, MB Group 4 tumors do not; stains: unpublished data, performed by a collaboration partner (Bishop lab, San Antonio, Texas, USA).

Inhibition of Topoisomerase I increases replication stress as the inhibitor forms a complex with Topoisomerase I and when it is bound to the DNA the inhibitor prevents the re-start of stalled replication forks (Figure 14) [248,249]. Poly (ADP-ribose) polymerase (PARP) 1 and 2 are nuclear proteins that are activated by DNA breaks [250]. PARP1 protects DNA breaks and the chromatin structure by binding to stalled replication forks and guides proteins necessary for DNA repair and cell cycle checkpoints as e.g. CHK1 to the site of the DNA breakpoint [251-253]. Inhibition of PARP1 traps the polymerase on the DNA and prevents the access of DNA repair proteins [254].

Targeting replication stress by inhibiting Topoisomerase I in combination with inhibition of PARP was, as evaluated in the TAR, already intensively studied and shown to be synergistic in e.g. Ewing Sarcoma [187]. In addition, treatment of an ETMR cell line showed synergistic efficacy to treatment with the Topoisomerase I-inhibitor Topotecan and the PARP-inhibitors Veliparib or Pamiparib [108]. Characteristics of ETMR tumors are among others high levels of *MYCN* expression and presence of R-

loops [108,255]. For further exploration of the treatment strategy, the approach was extended to additional models and performed *in vitro* and *in vivo*. Instead of Topotecan as a Topoisomerase I-inhibitor, which was used in the published study with ETMR, Irinotecan was used since experiments previously performed in the department showed that Topotecan induced body weight loss in NSG mice. For the *in vitro* treatments the ETMR cell line Bt183 and the MB Group 3 cell line HD-MB03 were used. In addition, fetal Astrocytes were treated to investigate the effect of the treatment with non-cancerous cells. The *in vivo* treatments were performed with various PDX models that are either characterized by high *MYC(N)*-expression or –amplification, or high levels of R-loops.

5.2. Results

5.2.1. *In vitro* drug screens with SN-38

Irinotecan (IRN) is a pro-drug that needs to be transformed to SN-38, which is the active metabolite. For the conversion, which mainly takes place in the liver, the enzyme carboxylesterase is required [256]. However, to some degree also tumor cells can convert Irinotecan to SN-38 [257]. Nevertheless, for *in vitro* applications use of SN-38 is more reliably mimicking the *in vivo* situation and this was thus used to investigate the effect of Irinotecan *in vitro*.

To identify the best synergistic combination partner for SN-38, a drug screen with SN-38 in combination with a library of 76 drugs was performed in collaboration with the Translational Drug Screening Unit (TDSU) of the KiTZ, Heidelberg where the screens were performed under the supervision of Dr. Heike Peterziel. For the screens, the ETMR cell line Bt183 and the MB Group 3 cell line HD-MB03 were used and 1000 cells were seeded per well in a 384-well plate that was pre-printed with the drugs. First, a drug screen with SN-38 alone was performed to evaluate the dose-response curve and the IC20-concentration that was needed as partner for the combination drug screens. For Bt183 the IC20 was 0.4 nM and for HD-MB03 it was 1.5 nM (Figure 16A). In a second step, the cells were seeded onto plates that were pre-printed with the evaluated IC20-concentration of SN-38 combined with another drug in different concentrations. A drug library of 76 mostly approved but also investigational drugs was tested and each drug was tested in triplicates. After the read-out with CellTiterGlo®, the measured signal was normalized to the DMSO-control and the efficacy of the drugs alone versus the combination was determined. For evaluation of synergistic combinations, the drug sensitivity scores (DSS) of the combination and the single drugs was calculated as well as the difference of the scores (dDSS), which indicates whether a drug combination is synergistic, additive or anatgonistic [258]. For synergistic combinations a threshold of dDSS >5 was chosen and a drug combination with dDSS <-5 was called as being antagonistic. Analysis of the combination screens with

Bt183 and HD-MB03 revealed seven and three synergistic combination partners for SN-38 respectively (Figure 16B). The two top hits with the highest dDSS were for both cell lines the PARP-inhibitors Olaparib and Talazoparib, which also were the only PARP-inhibitors in the drug library (Figure 16B).

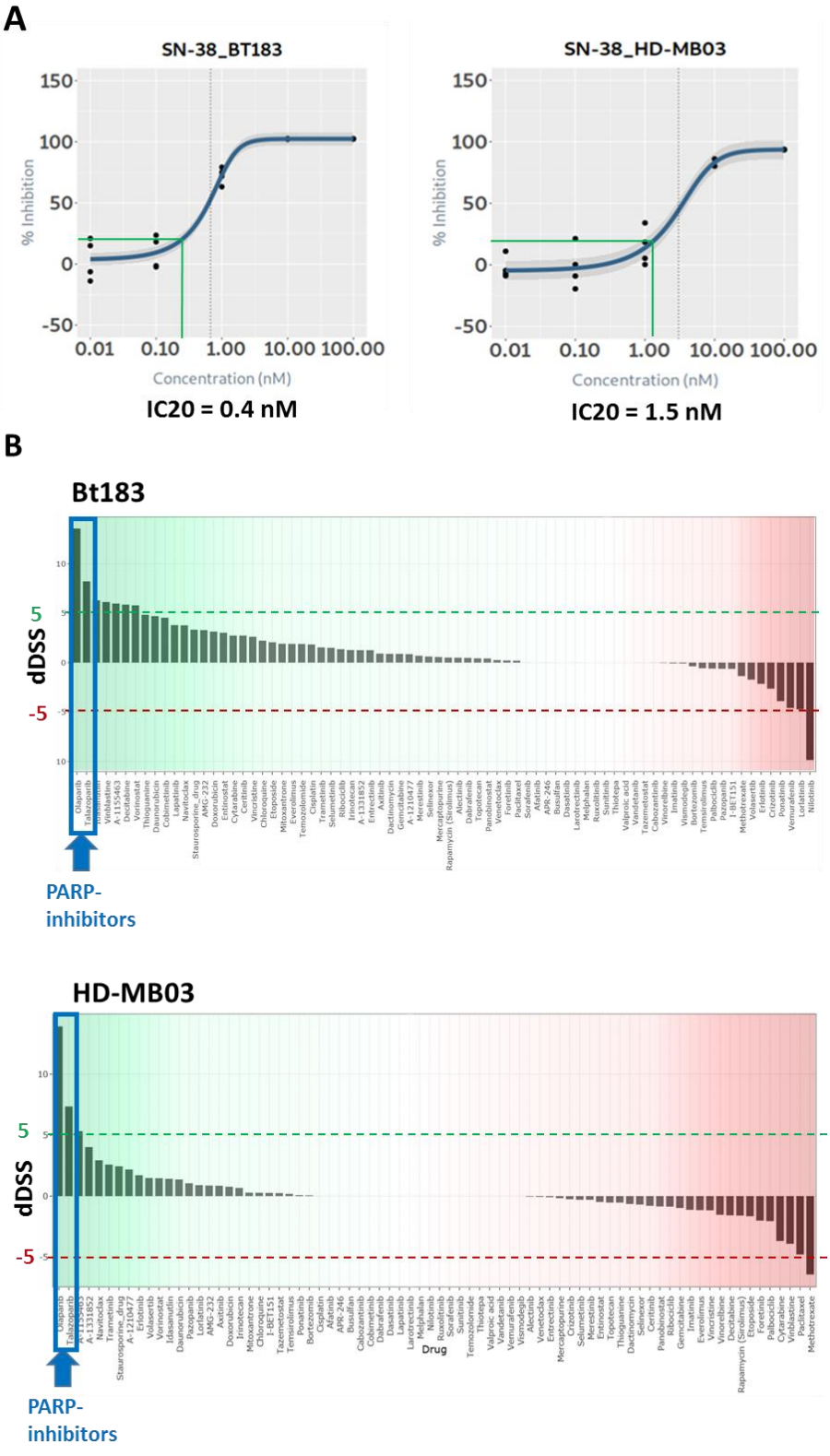

Figure 16: Results of the high-throughput drug screen with Bt183 and HD-MB03 cells.

A) Treatment with SN-38 alone showed good efficacy for both cell lines and an IC20-concentration of 0.4 nM (Bt183; left panel) and 1.5 nM (HD-MB03; right panel) was determined. B) Combination drug screens of Bt183 (upper panel) and HD-MB03 (lower panel) cells with SN-38 in combination with a drug library of 76 drugs shows that PARP-inhibitors are the top hits, being most synergistic (highlighted by blue arrows); experiment and analysis was performed by Dr. Heike Peterziel, KiTZ, Heidelberg.

Both PARP-inhibitors, Olaparib and Talazoparib, are well established and have been in clinical use for various indications as e.g., BRCA-deficient breast and ovarian cancer [259,260]. Besides these two PARP-inhibitors, also other PARP-inhibitors, namely Niraparib, Rucaparib and Veliparib are well-established. Even though they all inhibit PARP, they show differences in characteristics as PARP trapping or blood-brain-barrier (BBB) penetrance [261]. The PARP-inhibitor with the best PARP trapping efficacy is Talazoparib, however it only poorly enters the brain (Figure 17A). A PARP-inhibitor that enters the brain is Veliparib, however it does not show good PARP trapping efficacy. Though, very recently the PARP-inhibitor Pamiparib was developed and combines good PARP-trapping and BBB-penetrance (Figure 17A) [262,263]. Since the project described here is about targeting high-risk brain tumor entities, drugs that cross the BBB are pivotal and Pamiparib was chosen as the PARP-inhibitor of choice. To verify whether not only Olaparib and Talazoparib but also Pamiparib was a synergistic combination partner with SN-38, an *in vitro* drug test with Bt183 and HD-MB03 cells treated with various concentrations of SN-38 in combination with a fixed concentration of Pamiparib and tests with various concentrations of Pamiparib and a fixed concentration of SN-38 were performed. In addition, the treatment was applied to fetal Astrocytes to examine the effect of the treatment on non-cancerous brain cells. This time the cells were seeded in 96-well plates and eight concentrations of each drug were tested either alone or in combination with the IC20-concentration of the combination partner. For Astrocytes, SN-38 alone induced cell death up to about 40% for concentrations up to 320 nM (Figure 17C; left panel). Higher concentrations of SN-38 than 320 nM were not tested for Astrocytes since the clinical achievable concentration of SN-38 is reflected by using 33 nM SN-38 *in vitro*, which was well-covered in the applied treatment. Addition of 1.25 µM Pamiparib to the concentration range of SN-38 did result in lower viability ratios reflecting the added effect of 1.25 µM Pamiparib to SN-38, but no synergistic effect was observed. The same (no synergy) was observed, when Pamiparib was applied in various concentrations with or without the addition of 20 nM SN-38. In contrast, treatment of Bt183 cells with Pamiparib and SN-38 led to a synergistic reduction of viability as already seen for the combinations of Olaparib and Talazoparib with SN-38 (Figure 17C; middle panel). For HD-MB03 cells treatment with Pamiparib alone did not have an effect and viability could only be reduced to about 80% even with the highest concentration of 5 µM (Figure 17C; right panel). However, if a non-toxic concentration of SN-38 (reduction of viability to 90%) was added, viability of cells was reduced to a maximum of 40%, indicating again a synergistic effect of the drug combination.

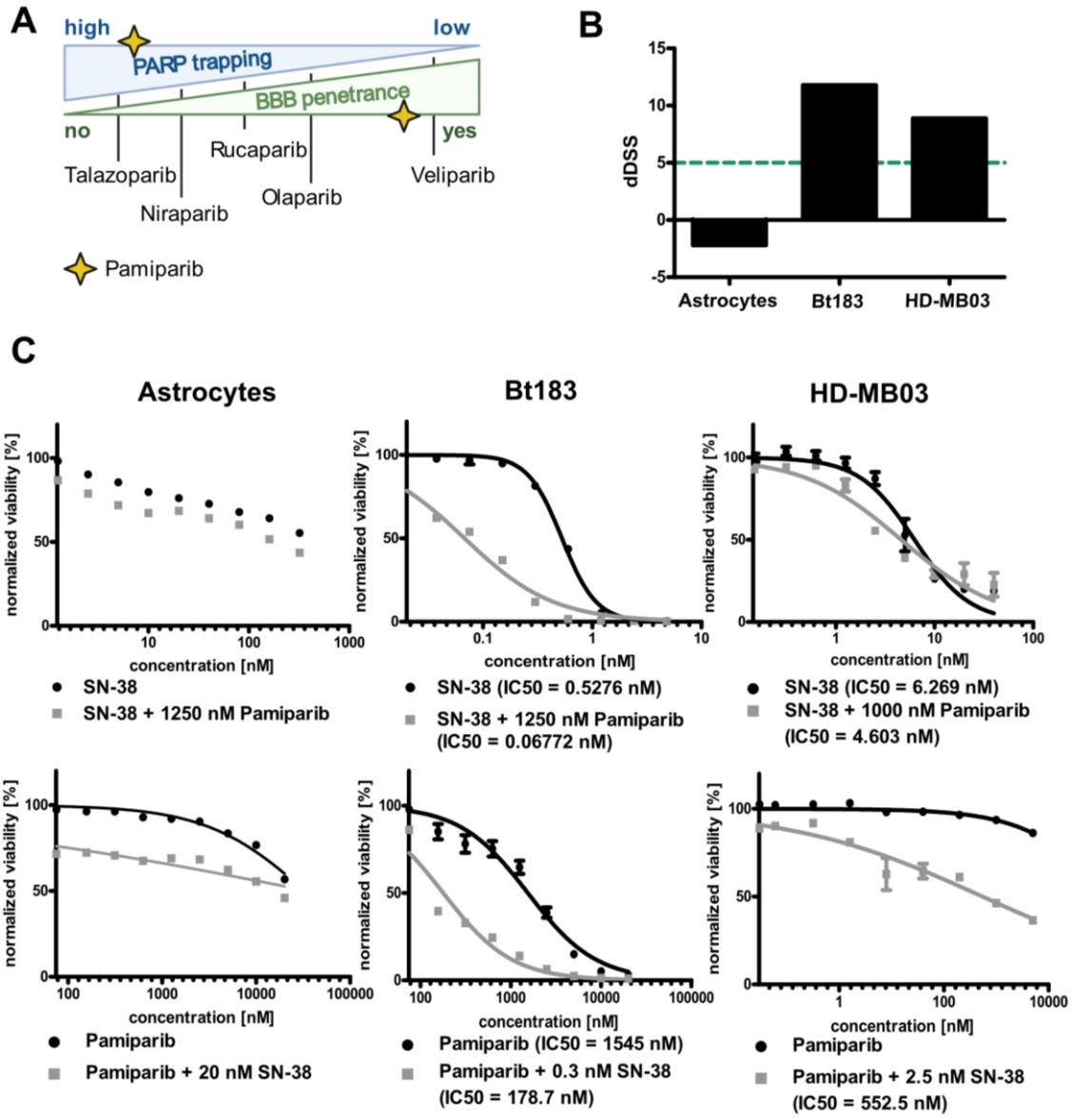

Figure 17: Pamiparib is a PARP-inhibitor that has good PARP trapping efficacy, enters the brain and is synergistic in combination with SN-38 for Bt183 and HD-MB03 cells.

A) Established PARP-inhibitors differ in their ability for trapping of PARP and crossing the blood-brain-barrier; B) evaluation of synergy of Pamiparib + IC20 of SN-38 was performed by calculation of the dDSS score and shows synergy (dDSS >5) for Bt183 and HD-MB03 cells but not for Astrocytes; green dashed line indicates threshold (dDSS >5) for synergy; C) *in vitro* combination treatment of Astrocytes, Bt183 and HD-MB03 cells with various concentrations of SN-38 ± IC20 of Pamiparib (upper row) or various concentrations of Pamiparib ± IC20 of SN-38 (lower row); normalized viability indicates mean ± SEM of triplicates.

For calculation of the synergy, again the dDSS-score was established by using the BREEZE-pipeline [198]. A combination was called synergistic if the difference of the drug sensitivity scores of the combination of Pamiparib + SN-38 and the treatment with Pamiparib alone was higher than 5, which was the case

for Bt183 cells (dDSS = 11.8) and HD-MB03 cells (dDSS = 8.9) but not for Astrocytes (dDSS = -2.2) (Figure 17B).

In vitro treatment of Astrocytes, Bt183 and HD-MB03 cells with combinations of SN-38 and Pamiparib showed that the combination is synergistically lethal in both tumor cell lines but not in healthy tissue cells. For further evaluation of the treatment and testing for efficacy, the combination was investigated *in vivo* using PDX models.

5.2.2. *In vivo* treatment with Irinotecan and Pamiparib

After analysis of the efficacy of SN-38 in combination with Pamiparib *in vitro*, the treatment was applied to various PDX models *in vivo*. The PARP-inhibitor Pamiparib was applied per oral gavage and due to the short half-live (about 3 hrs) in mice twice daily [264]. Instead of SN-38, as used *in vitro*, the pro-drug Irinotecan was administered via intraperitoneal injections. For the treatment study five different PDX models were used (Figure 18A). The models nch2194 (*MYC*-amplified MB Group 3), med-1712FH (*PTCH1*-mutated MB SHH), BT084 (*MYCN* amplified and *TP53* mutated MB SHH) and Bt165 (EPN-*ZFTA* fusion positive) were injected orthotopically into the cerebellum (MB models) or into the striatum (EPN model). Since the models were previously labelled with luciferase, intravital measurement of bioluminescence was possible after injection of luciferin. However, the model Bt183 (ETMR) was not labelled with luciferase and therefore injected subcutaneously. The preclinical study with Bt183 was performed at Charles River in Freiburg (Charles River Discovery Research Services Germany GmbH, Freiburg, Germany). All other preclinical studies were performed at the KiTZ in Heidelberg.

NMRI-nude mice were injected subcutaneously with Bt183 cells and treated either with either 2.5 mg/kg Irinotecan, 1.5 mg/kg Pamiparib or a combination of both drugs (Figure 18B). Tumor volumes were measured twice weekly by caliper and mice were treated for seven weeks. For the vehicle-treated and the Pamiparib-treated group the tumors constantly grew and Pamiparib did not influence tumor growth when compared to the vehicle group. Mice that were treated with Irinotecan or the combination of Irinotecan and Pamiparib showed tumor regression starting on Day 3 after start of treatment. About five weeks after treatment start, tumors of the Irinotecan-treated mice slowly started to regrow from about 17% of the initial tumor volume to roughly 60%. Interestingly, tumors of the combination-treated group completely disappeared and were not palpable anymore four weeks after the start of treatment.

For the intracranial orthotopic PDX models NSG mice were injected with the PDX model and tumor growth was tracked via bioluminescence measurement (starting four weeks after injections) once per week. As soon as the bioluminescence signal reached a threshold of $1x10^6$ p/s the respective mice were randomized into the different treatment groups (vehicle; 2.5 mg/kg Irinotecan; 1.5 mg/kg Pamiparib BID; 2.5 mg/kg Irinotecan + 1.5 mg/kg Pamparib BID). The treatment was applied in a 5 days on/2 days off schedule, the health status was checked daily and via body weight three times per week and the treatment was applied until the mice showed any tumor-related symptoms (e.g. tilted head, hydrocephalus) or lost 20% of their initial body weight.

Tumors of the MB SHH med-1712FH model grew constantly over the time of the treatment, independent of the applied drugs (Figure 18C). Mice that were treated with Irinotecan only showed slightly reduced tumor growth and the median survival was 12 days longer than the vehicle-treated animals, however, the difference was not significant. Mice of the combination group lived on average three weeks longer and the maximal survival was ten days longer than the mice of the vehicle-treated group, which accounted for a significant ($p = 0.03$) survival benefit for mice treated with Irinotecan and Pamiparib in combination when compared to the vehicle-treated group. Interestingly, treatment with Pamiparib led to a faster tumor growth and survival of the mice was shorter than for all the other groups (about eight weeks after treatment start). However, differences in tumor volume were only marginal.

For the MB SHH BT084 model the treatment with Irinotecan or the combination induced only a minor reduction of the tumor growth. The group treated with the combination was the only group that lived significantly longer ($p = 0.04$) than the vehicle-treated group (Figure 18C). As for the med-1712FH model, mice in the Pamiparib-group had to be euthanized first (median survival was 24 days). For the vehicle- and Irinotecan-group survival was not significantly different and mice had to be euthanized after a median survival time of 31 and 39 days, respectively with a maximal survival of 45 and 48 days respectively.

The *MYC*-amplified Group 3 MB model nch2194 showed hardly any difference in tumor volume and survival between the vehicle- and the Pamiparib-treated mice and mice had to be euthanized after a maximum of 43 and 46 days, respectively (Figure 18C). However, tumor growth was reduced when treated with Irinotecan or the combination and mice lived up to 14 and 8 weeks longer, respectively than the vehicle-treated mice, indicating a significant ($p = 0.0005$) survival benefit. Tumor volumes of mice treated with Irinotecan remained stable over the first four weeks of treatment and started to grow slowly afterwards. Furthermore, treatment with Irinotecan only induced the greatest survival

benefit with significantly longer survival than the vehicle group (p = 0.005) but also longer survival than the combination-treated group (median survival 116 days vs. 82 days).

Tumors of the supratentorial *ZFTA*-fusion positive ependymoma Bt165 model showed the same phenomenon as seen for the *MYC*-amplified Group 3 MB nch2194 model (Figure 18C). The IVIS signals and tumor volumes were identical between the vehicle- and the Pamiparib-group as well as between the group treated with Irinotecan only and the group treated with Irinotecan and Pamiparib. Even though tumor volumes steadily grew for the Irinotecan- and the combination-groups, growth rate was visibly reduced and tumors grew slower than for the two other groups (vehicle and Pamiparib only). Maximum survival was eight weeks for the vehicle- and 10.5 weeks for the Pamiparib-group. Treatment with Irinotecan or Irinotecan and Pamiparib in combination induced a significant survival benefit ($p < 0.0001$ and $p = 0.002$, respectively) compared to the survival of the mice in the vehicle-treated group. Even though the longest survival of mice treated with Irinotecan was greater than for the combination-treated group (226 vs. 158 days), median survival was comparable with 135 and 133 days, respectively, resulting in no significant difference in survival for these two groups.

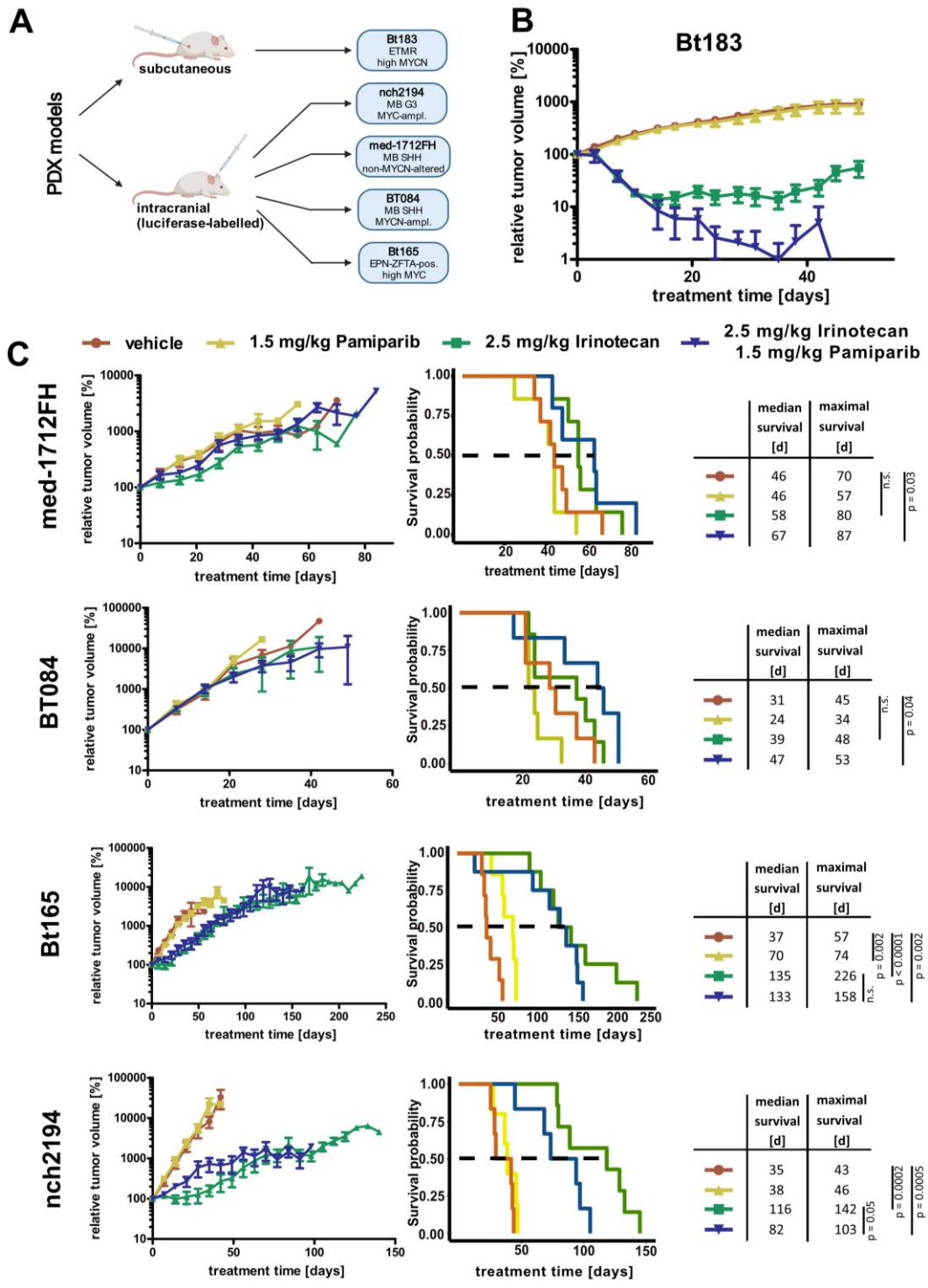

Figure 18: *In vivo* treatment of five PDX models with Irinotecan and/or Pamiparib.

A) Five models were used for *in vivo* treatments and injected either subcutaneously or orthotopically; B) Relative tumor volumes (s.c.) of mice injected with Bt183 cells displayed over time of treatment, (n = 4 per group); C) Volumes of intracranial tumors of the Med-1712FH (n= 7 per group), BT084 (n = 6 or 7), nch2194 (n = 5 or 6 or 7) and Bt165 (n = 7 or 8) models were determined by bioluminescent imaging and Kaplan-Meier plots indicate survival benefit for several groups, table shows median and maximal survival; treatment arms are the same for all treated models with vehicle (orange), combination of 2.5 mg/kg Irinotecan + 1.5 mg/kg Pamiparib (blue), 2.5 mg/kg Irinotecan (green) and 1.5 mg/kg Pamiparib (yellow); tumor volume indicates mean ± SEM, p-values were calculated with log-rank test.

5.2.3. Refinement of *in vivo* treatment with Irinotecan and Pamiparib

Treatment with Irinotecan or the combination of Irinotecan and Pamiparib did induce a significant survival benefit for mice injected with the *MYC*-amplified Group 3 MB nch2194 or the *ZFTA*-fusion positive ependymoma Bt165 model. However, differences between the groups treated with Irinotecan only or with the combination could not be detected and Pamiparib did not add any obvious additional value to the treatment. For the nch2194 model the Irinotecan-Pamiparib combination treatment even led to earlier euthanasia. In addition, further evaluation of the applied dose of Irinotecan, which was 2.5 mg/kg, revealed that the metabolism of the conversion from Irinotecan to the active compound SN-38 is more effective in mice than in humans [265,266]. To ensure reaching doses in mice that can also be achieved in humans the administered dose of Irinotecan was decreased to 0.83 mg/kg and 0.27 mg/kg for follow-up experiments. Besides adapting the dose of Irinotecan, the dose of Pamiparib was increased to 9 mg/kg BID since a synergistic effect of Irinotecan and Pamiparib was observed when applied to the subcutaneous ETMR model but no effect was detected when applied to intracranial tumors. The dose of Pamiparib was increased to the highest dose that is still clinically achievable (9 mg/kg BID) to ensure that the highest possible concentration of the PARP-inhibitor reaches the brain. Since the MB Group 3 model nch2194 responded well to the treatment, this model was chosen to test further adaptations of the treatment schedule. The model was again injected intracranially into the cerebellum of NSG mice and as soon as the threshold of $1x10^6$ p/s was reached, the mice were randomized into eight different treatment groups (vehicle; 9 mg/kg Pamiparib; 0.27 mg/kg IRN; 0.83 mg/kg IRN; 2.5 mg/kg IRN; and combinations of the three different concentrations of IRN with 9 mg/kg Pamiparib). The IVIS signal was measured once per week and treatment was again applied in a 5 days on/2 days off schedule. The tumor volume of the vehicle- and Pamiparib-treated group grew constantly and all mice had to be euthanized within six weeks (Figure 19A). Treatment with the various doses of IRN showed a dose-dependent effect on tumor volume and survival and mice survived about ten weeks (0.27 mg/kg IRN), 12.5 weeks (0.83 mg/kg IRN) and 16.5 weeks (2.5 mg/kg IRN) after start of the treatment indicating a significantly ($p < 0.001$) longer survival than the mice in the vehicle-treated group. However, for the combinations of Pamiparib with 0.27 mg/kg IRN or 0.83 mg/kg IRN no differences could be observed to their respective monotherapy of IRN and the mice lived equally long with no significant difference in survival. Nevertheless, the mice in the group treated with Pamiparib and 2.5 mg/kg IRN in combination showed a difference in survival compared to mice treated with 2.5 mg/kg IRN alone, but mice lived shorter and had to be euthanized already latest in week 14 after treatment start albeit the IVIS signal indicated similarly sized tumors. Analysis of the IVIS images confirmed that the tumor volume of the vehicle-treated group constantly increased (Figure 19B). The tumor volume of the group treated with 2.5 mg/kg IRN + 9 mg/kg

Pamiparib showed regression during weeks two to four after treatment start, but started to grow again slowly afterwards. Even though a dose-dependency of Irinotecan was observed, again no additional or synergistic effect of Pamiparib was detected. To confirm whether Pamiparib entered, as published, the brain and tumor tissue and inhibits PARP, a western blot analysis of PAR was performed. Since active PARP synthesizes a chain of PAR at the site of the ssDNA break and inhibition of PARP leads to reduction of PAR, levels of PAR can be used as a read-out of PARP activity. Tumor tissue of mice euthanized 2 hrs after the last dose was isolated and protein lysates were prepared. Comparison of the samples by western blot confirmed that levels of PAR were increased in samples treated with Irinotecan indicating higher levels of ssDNA breaks than in the vehicle-treated sample (Figure 19C). In contrast, for samples treated with Pamiparib, either alone or in combination with IRN, signal for PAR was clearly decreased with relative intensities below 20% of vehicle sample, and ensures target engagement of Pamiparib.

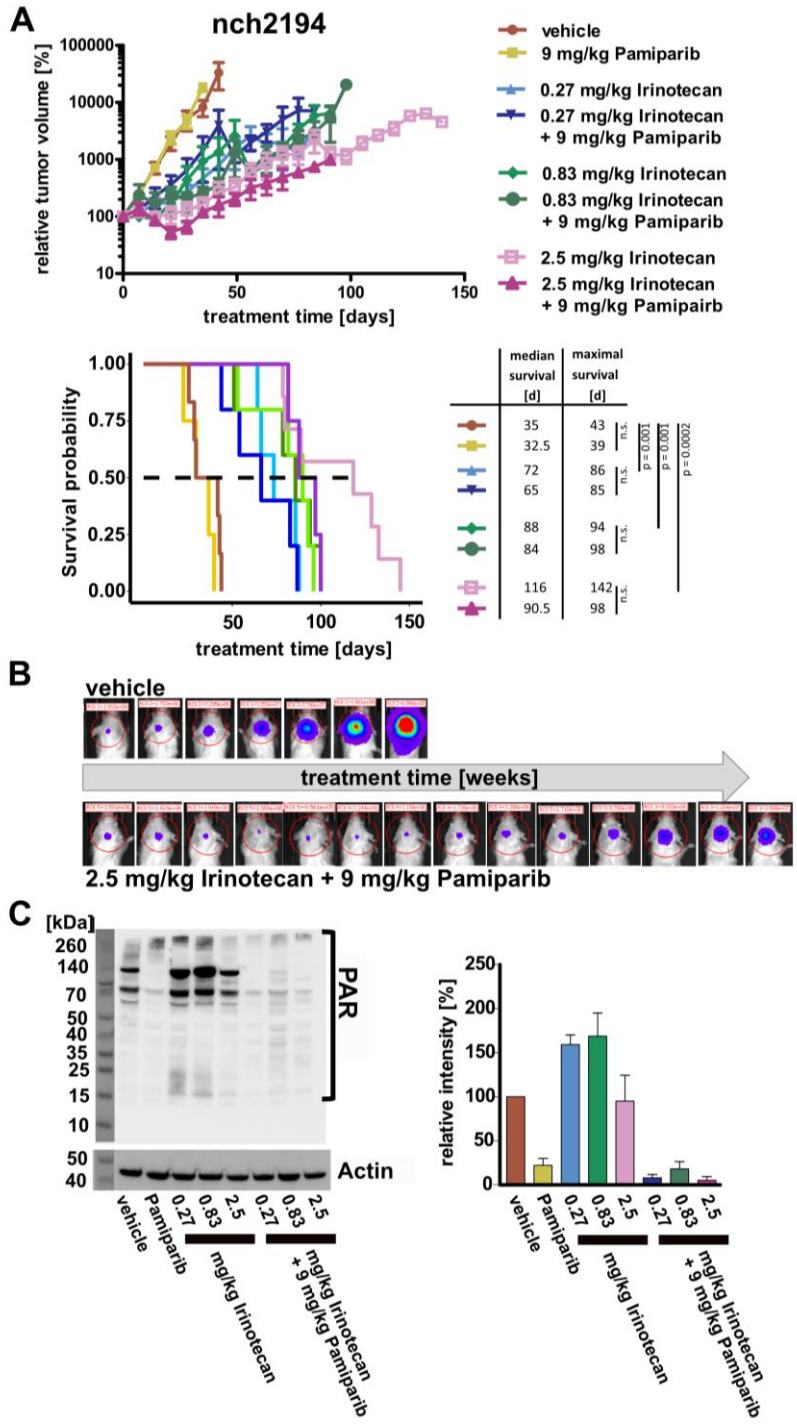

Figure 19: *In vivo* treatment of nch2194 (MB Group 3) with various doses of Irinotecan alone or in combination with Pamiparib.

A) IVIS signals were measured once per week and plotted over the time of the treatment (n = 5 per group) and the Kaplan-Meier plot indicates survival benefit for all groups treated with Irinotecan compared to vehicle- and Pamiparib-treated groups (red and yellow, respectively); the table shows median and maximal survival of each group; tumor volume indicates mean ± SEM, p-values were calculated with log-rank test; B) exemplary IVIS images of one animal of the vehicle-treated group and one mouse treated with 2.5 mg/kg IRN + 9 mg/kg Pamiparib showing tumor regression in the first weeks when treated with the combination and tumor growth after seven weeks of treatment; C) Western Blot analysis of treated samples for levels of PAR showing reduction for samples treated with Pamiparib alone or in combination, loading control was performed by detecting β actin; quantification of intensity was performed with ImageJ and normalized to vehicle-treated samples.

In conclusion, even though PARP was inhibited by more than 80% compared to vehicle-samples by the applied dose of Pamiparib and treatment with Irinotecan was associated with a survival benefit for the mice, no additive or synergistic effect of the combination treatment was observed as compared to treatments with Irinotecan only.

5.2.4. *In vivo* treatment with pegylated-SN-38

Even though treatment with Irinotecan was effective and induced growth inhibition and survival benefit, the treatment did not lead to partial or complete regression of the orthotopic tumors and the combination treatment of Irinotecan and Pamiparib did not induce synergistic effects albeit PARP was inhibited. To investigate whether the effect of Irinotecan or the combination can be intensified, a new formulation of SN-38, peg-SN-38, was tested. Peg-SN-38 is characterized by a better blood-brain-barrier penetrance than Irinotecan, a better accumulation in the tumor tissue and a longer half-life [267]. For peg-SN-38, four molecules of SN-38 are conjugated to macromolecular carriers, in this case poly-ethylene-glycol (PEG) [267,268]. The peg-linker slowly releases the drug and since SN-38 is used, conversion of Irinotecan to SN-38 by carboxylesterases is not necessary. In addition, peg-SN-38 accumulates in solid tumor tissue due to the pegylation, which supports the enhanced permeability and retention (EPR) effect that describes the phenomenon that macromolecules can accumulate in tumor tissue but not in healthy tissue since angiogenesis is highly stimulated by tumor growth and more prone to impaired transport dynamics than blood supply of healthy cells [269,270]. The higher BBB-penetrance, accumulation in the tumor and long half-life of SN-38 with slow release supports a high and constant drug exposure of SN-38 to the tumor cells. To test whether these changes may lead to a better and sustained effect of the treatment, again an *in vivo* treatment study with the nch2194 model was planned. However, since tolerated concentrations of peg-SN-38 alone or in combination with a PARP-inhibitor were not reported yet, a toxicity test with non-tumor bearing mice was performed first to define the maximum tolerated (MTD) dose. Mice were treated for a time period of eight weeks with various concentrations of peg-SN-38 (15, 30 or 60 µmol/kg) either alone or in combination with 9 mg/kg BID Pamiparib. As a read-out body weight was measured three times per week and mice were euthanized either after treatment end or when they showed health issues due to body weight loss. Treatment with 15 µmol/kg peg-SN-38 either alone (solid grey lines) or in combination with 9 mg/kg Pamiparib (dashed grey lines) did not show an effect on body weight of the mice and yielded similar weights as the vehicle control animals (black lines) (Figure 20A, left plot). Treatments with 30 mg/kg peg-SN-38 in combination with 9 mg/kg Pamiparib led to variations in body weight and even though mice only lost about 10% of the initial body weight (Figure 20A, middle plot), the concentration was

not selected for further treatment, since experiences with previous treatment studies showed that tumor-bearing mice are typically more sensitive to variations in body weight. Treatment with 60 µmol/kg peg-SN-38 + 9 mg/kg Pamiparib led to toxic side effects and mice had to be euthanized within three weeks of treatment due to body weight loss, however, treatment with 60 µmol/kg peg-SN-38 alone did not lead to toxicity (Figure 20A, right plot). For the following treatment study with tumor-bearing mice, the dose of 15 µmol/kg peg-SN-38 was chosen for the combination treatment with 9 mg/kg Pamiparib and a treatment group treated with 60 µmol/kg peg-SN-38 in monotherapy was included in the preclinical study since this dose was the MTD for monotherapy and reflects the clinical achievable concentration.

For the treatment study, the mice were intracranially injected with cells of the nch2194 model and, as soon as the IVIS signal reached $1x10^6$ p/s, were randomized into five different treatment groups: vehicle; 9 mg/kg Pamiparib; 15 µmol/kg peg-SN-38 $\pm$ 9 mg/kg Pamiparib; 60 µmol/kg peg-SN-38. Pamiparib was applied as described before (9 mg/kg BID, p.o., 5 days on/2 days off) and peg-SN-38 was applied by intraperitoneal injection once per week. Similar to the aforementioned experiments, tumor volumes for the vehicle- and Pamiparib-treated group did not show any differences, while the IVIS signals for the three groups that were treated with peg-SN-38 indicated that the tumors were stable and tumor growth was inhibited (Figure 20B, left plot). Moreover, tumors treated with the maximal dose of 60 µmol/kg peg-SN-38 regressed within the first weeks of treatment to about 60% of the initial tumor volume, but after three weeks they slowly started to regrow. Mice that were treated with the combination of 15 µmol/kg peg-SN-38 and 9 mg/kg Pamiparib had to be euthanized about 15 weeks after treatment start and with a median survival of 81 days, however mice that were treated with 15 µmol/kg peg-SN-38 alone lived two weeks longer and had a median survival time of 88 days (Figure 20B, right plot). Treatment with 60 µmol/kg peg-SN-38 resulted in the same survival benefit as treatment with 15 µmol/kg peg-SN-38 alone with median and maximal survival of 87 and 121 days, respectively. Survival of the mice in the three groups treated with peg-SN-38 (15 µmol/kg alone or in combination with Pamiparib and 60 µmol/kg) was significantly ($p = 0.002$) longer than survival of the mice of the vehicle-treated group. To confirm that Pamiparib inhibits PARP also when combined with peg-SN-38, protein lysates of the tumor samples were analyzed for PAR-levels by Western Blot. Levels of PAR were clearly reduced to less than 25% for the samples of the Pamiparib-treated group as well as for the sample of the combination-group (Figure 20C). In addition, levels of PAR were higher in the sample treated with 60 µmol/kg peg-SN-38 than in the sample treated with 15 µmol/kg peg-SN-38. This difference points towards higher levels of ssDNA breaks, when treated with higher dose of peg-SN-38.

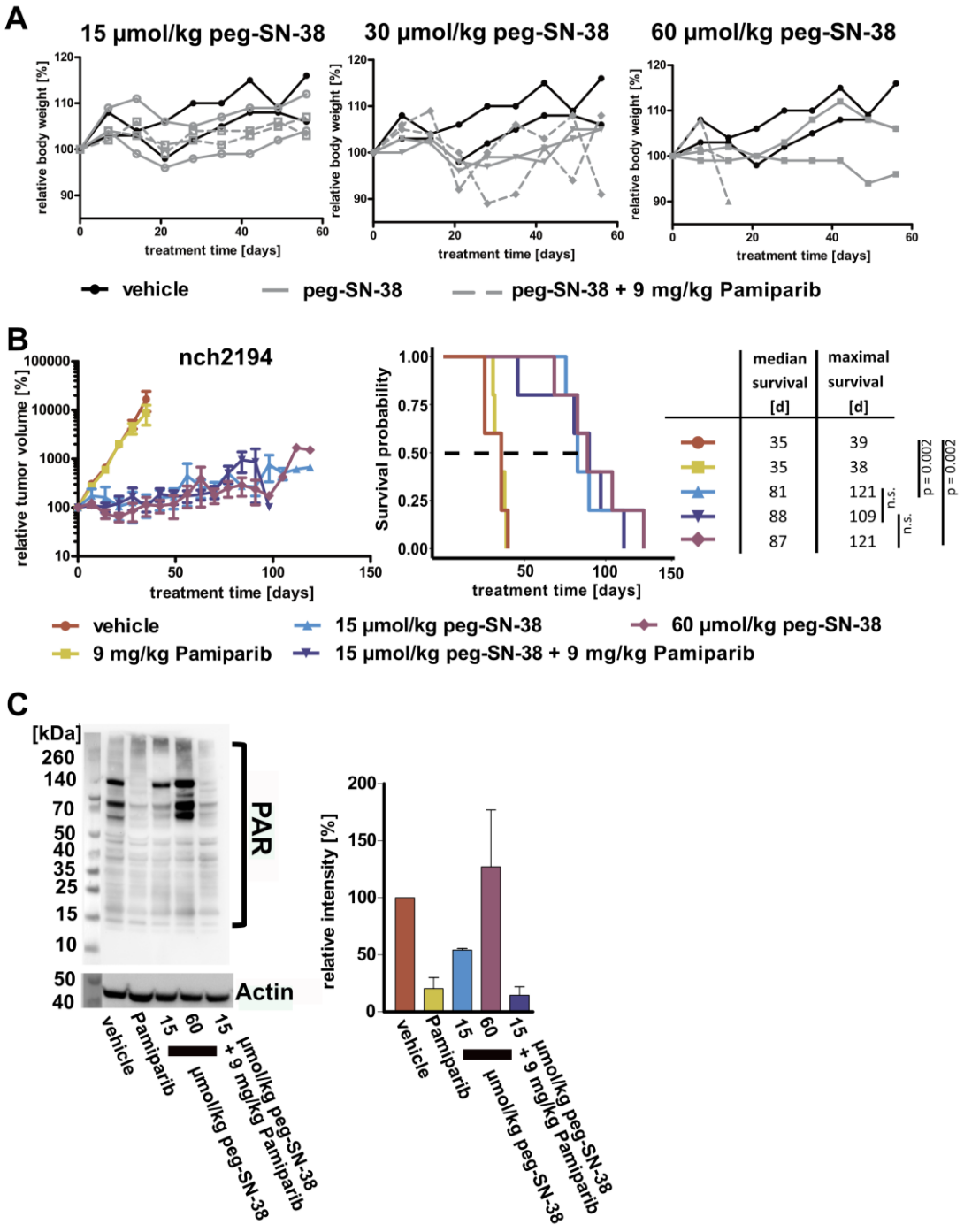

Figure 20: *In vivo* treatment of nch2194 (MB Group 3) with peg-SN-38 and Pamiparib.

A) Toxicity test shows stable body weight of NSG mice when treated with 15 µmol/kg peg-SN-38 in combination with 9 mg/kg Pamiparib (left plot) or with 60 µmol/kg peg-SN-38 alone (right plot) but combination led to variations in body weight for 30 µmol/kg peg-SN-38 (middle plot) or induced toxic body weight loss when treated with 60 µmol/kg peg-SN-38 + 9 mg/kg Pamiparib (right plot); vehicle treated mice shown in black, treatment with peg-SN-38 either alone (solid line) or in combination with 9 mg/kg Pamiparib (dashed line) shown in grey, one line indicates one mouse; B) mean IVIS signals of tumor-bearing mice (injected with the nch2194 model) treated with vehicle (orange), Pamiparib (yellow), 15 µmol/kg peg-SN-38 alone (light blue) or in combination with Pamiparib (dark blue), or with 60 µmol/kg peg-SN-38 (violet) (n = 5 per group); the Kaplan-Meier plot shows survival benefit for groups treated with peg-SN-38 but no synergistic effect when Pamiparib is added; the table shows median and maximal survival per group; tumor volume indicates mean ± SEM, p-values were calculated with log-rank test D) Western Blot analysis for levels of PAR shows PARP inhibition for samples treated with Pamiparib, loading control was performed by evaluation of β-actin, quantification of intensity was performed with ImageJ and normalized to vehicle-treated sample.

In summary, the treatment with peg-SN-38 led to tumor growth inhibition over several weeks. However, mice had to be euthanized at the latest 17 weeks after treatment start and no additive or synergistic effect of Pamiparib when combined with peg-SN-38 was observed. Mice of the combination group had to be euthanized slightly earlier and the maximal survival was 109 days compared to 121 days for groups treated with 15 and 60 µmol/kg peg-SN-38 alone. The survival benefit induced by the treatment with the highest clinically achievable dose of peg-SN-38, which is 60 µmol/kg, (median survival 87 days, maximal survival 121 days) was higher than the survival benefit of the highest clinically achievable dose of plain Irinotecan, which is 0.83 mg/kg, whereas the median survival was 88 days and the maximal survival was 94 days. For neither of the dosing regimens, addition of Pamiparib resulted in a significant survival difference.

5.3. Discussion

Combination treatment with PARP-inhibitors and topoisomerase-inhibitors was already studied extensively not only preclinically but also in clinical trials and showed good efficacy in e.g. Ewing sarcoma [187,217,271-273]. However, expanding the treatment to brain tumors remained challenging since the established PARP-inhibitors did either show good PARP-trapping abilities but were not BBB-penetrant or, if they were BBB-penetrant, ability to trap PARP was low [261,274]. Recently, the new PARP-inhibitor Pamiparib has been brought on the market, which combines good PARP-trapping efficacy and BBB-penetrance and is studied in many clinical trials for various cancer entities [263,275-277]. Inhibitors of topoisomerase have already been known for many years and a few years ago Topotecan was reported to be effective in ETMR tumors [278]. In this study of Schmidt *et al*. Bt183 ETMR tumor cells were treated *in vitro* and *in vivo* with Topotecan and a good response was demonstrated with a survival benefit for mice treated with Topotecan of 31 days [278]. Following up on these findings, it was also shown that treatment with Topotecan in combination with the PARP-inhibitors Veliparib or Pamiparib was synergistic in Bt183 cells [108]. In the project described here the effect of the treatment strategy to inhibit PARP and topoisomerases in combination was not only performed with Bt183 cells but expanded to more models both *in vitro* and *in vivo* to see whether other tumor types may also respond to this combination treatment and what the biomarker could be to predict such a response.

ETMR tumors are not only characterized by high expression of *MYCN* but also by the presence of high levels of R-loops. Other tumors that were stained positive for R-loops were MB Group 3 tumors for which the cell line HD-MB03 is a well-established model. In the project described here both the ETMR Bt183 and the HD-MB03 cell lines were used for *in vitro* screens. However, in contrast to the experiments mentioned above, Irinotecan or respectively SN-38 instead of Topotecan was used as

topoisomerase-inhibitor for the treatments. In an *in vivo* screen with a panel of 21 models derived from various adult and pediatric tumor entities including three pediatric brain tumor models (MB Group 3 and GBM), treatment with Irinotecan yielded better efficacy and resulted in complete regression for more tumors (2/3 vs. 1/3) than treatment with Topotecan. [279]. However, these results can only give an indication that Irinotecan might be more efficient than Topotecan since the study used cell lines including DAOY as Group 3 MB, which is now known to be an unreliable model for this entity. More relevant for the choice of Irinotecan instead of Topotecan for the experiments presented here was that experiments performed previously in the department showed that long-term treatment with Topotecan induced body weight loss in NSG mice after about six weeks of treatment. For reliable *in vitro* results it is important to use SN-38, which is about 1000-fold more active than Irinotecan [256,280]. The *in vitro* drug screens with Bt183 and HD-MB03 cells demonstrated synergy for SN-38 and Olaparib, Talazoparib and Pamiparib. In contrast, no synergistic effect was observed for fetal Astrocytes when treated with SN-38 $\pm$ Pamiparib, which indicates that the treatment strategy is not affecting all cells including normal cells.

After confirming synergy *in vitro*, the treatment was expanded to PDX models *in vivo* and various models were used. As the hypothesis for the treatment is based on high expression of *MYC(N)*, the *PTCH1*-mutated MB SHH PDX model med-1712FH that does not have a *MYC(N)*-amplification was included as a potential negative control. Indeed no effect of the treatment with Irinotecan, Pamiparib or the combination on the tumor volumes as compared to the vehicle treated animals was observed. However, still mice treated with the combination had a longer median survival than the control mice with 46 days for vehicle mice and 67 days for mice treated with the combination. For the other PDX models nch2194 and Bt165, a MB Group 3 model with *MYC*-amplification and a *ZFTA*-fusion positive ependymoma model with high *MYC* expression, respectively, treatment with Irinotecan and Pamiparib in combination induced both a significant tumor growth inhibition and a survival benefit. Similar as in the *in vitro* drug tests, *in vivo* treatment with Pamiparib alone had no effect on tumor growth or survival and mice lived equally long compared to the control group. Interestingly, mice treated with Irinotecan alone lived about 80 (for Bt165) or 50 (for nch2194) days longer than the mice treated with the combination. The better response of the monotherapy versus the combination therapy can potentially be explained by the fact that the mice of the combination group are more stressed due to treatment with Pamiparib since it is applied two times per day via oral gavage. Even though treatment was routinely performed and done by experienced personnel, every additional handling of the mice adds stress to them besides e.g. tumor growth and might have an influence when performed over longer time periods. Another model that was used for *in vivo* treatments was BT084, which is a MB SHH model with a *MYCN* amplification. Since MYC and MYCN are very closely related and show similar

properties, the hypothesis of the treatment strategy was formulated to be valid for both transcription factors [281]. Surprisingly, growth of tumors of the BT084 model did not show any difference, neither with the combination treatment, nor with any drug alone compared to tumor volumes of the vehicle-treated group. However, mice that were treated with the combination showed a median survival of 47 days, which is 16 days longer than the median survival of the mice of the control group and indicates a significant difference ($p = 0.04$). Nevertheless, the effect of the treatment was minor and can be called ineffective when compared to the treatment results observed in the Bt165 or the nch2194 models. Even though *MYC* and *MYCN* are of the same gene family and can to some extent compensate for each other, differences were still observed, e.g. expression of *MYCN* is more tissue specific and not as generalized as the expression of *MYC* and experiments knocking out either *MYC* or *MYCN* resulted in embryonic lethality and showed that the proteins cannot fully compensate for each other [282-285]. In addition, expression of *MYCN* but not *MYC* can be regulated by the SHH signaling pathway, which is known to be the driving force for MB tumors of the SHH group [286]. Besides the orthotopic injection of PDX models, cells of the Bt183 model were injected subcutaneously into mice and then treated. Also for the s.c. setting, treatment with Pamiparib did not induce any change to tumor growth. Treatment with Irinotecan alone induced regression of the tumors to 14% of the initial tumor volume followed by stable disease for three weeks. However, treatment with Pamiparib and Irinotecan in combination resulted in complete regression of the tumors. In contrast to the treatment studies with orthotopic brain tumors, the combination of Pamiparib and Irinotecan had synergistic effects on tumor growth and induced complete regression, which was not detected when the drugs were used in monotherapy. Similar results were observed in an *in vivo* study with s.c. Ewing Sarcoma tumors that were treated with Irinotecan and different PARP-inhibitors [187].

Since for the orthotopic models nch2194 and Bt165 an effect of Irinotecan but no additional effect of the combination could be observed the dosing schedule was adapted and the dose of Pamiparib was increased to the maximum clinical achievable concentration of 9 mg/kg and the dose of Irinotecan was decreased to 0.27 mg/kg and 0.83 mg/kg, since conversion of Irinotecan to SN-38 is much more effective in mice than in humans due to presence of carboxylesterases in the plasma [287]. Calculation of the clinical relevant dose of Irinotecan for preclinical experiments remains difficult and a diversely discussed topic [265,280]. In addition, treatment with 2.5 mg/kg Irinotecan induced a significant survival benefit for the nch2194 and the Bt165 model and might not have left room for synergy when combined with Pamiparib. When comparing tumor volumes of mice treated with various concentrations of Irinotecan a dose-dependency was observed with slower growing tumors for higher concentrations as well as greater survival benefit for mice treated with higher concentrations of Irinotecan. Nevertheless, no additional effect of Pamiparib could be detected even though PARP was

effectively inhibited (up to 80%) as reduced levels of PAR indicated. Mice treated with 0.27 mg/kg or with 0.83 mg/kg Irinotecan ± 9 mg/kg Pamiparib lived about 50 days longer than the control and Pamiparib-treated mice. Remarkably, mice treated with 2.5 mg/kg Irinotecan + 9 mg/kg Pamiparib showed reduction of the initial tumor volume during the first weeks of treatment, however mice treated with 2.5 mg/kg alone lived longer than all the other groups.

Reduced levels of PAR confirm target engagement of Pamiparib and the inhibition of tumor growth by Irinotecan shows that both drugs enter the brain and reach the tumor. However, still no synergy could be observed even though subcutaneous treatment of Bt183 tumors showed a synergistic effect for the combination treatment. Similar results were also reported in previously published studies that report, as mentioned above, synergy for s.c. ES tumors when treated with Irinotecan and PARP-inhibitors [187]. However, Norris *et al*. accounted that *in vivo* treatment of ES and NBL tumors with Topotecan and Cyclophosphamide in combination with Olaparib did not yield a synergistic effect even though PARP was fully inhibited, which might be due to the fact that Topotecan and Cyclophosphamide were already highly effective and did not leave room for an enhanced effect when Olaparib was added [288]. As seen in the experiments performed in the project described here, monotherapy with Olaparib did not have an effect. Nevertheless, by reducing the dose of Irinotecan as outlined above the effect of Irinotecan was lowered to ensure to leave room for the effect of the PARP-inhibitor, which was not detectable regardless of the concentration of Irinotecan.

Recent publications and clinical trials test and apply not plain Irinotecan but a pegylated version of SN-38 (peg-SN-38), which is characterized by tumor accumulation and longer half-lives than Irinotecan [267]. In addition, the effect of peg-SN-38 is independent of the presence of carboxylesterases and can subsequently more easily be translated from mice to humans [268]. In a study with murine mammary tumors it was shown that use of peg-SN-38 led to a prolonged and maintained effect compared to therapy with Topotecan or Irinotecan [289]. For the MB Group 3 model nch2194 that was used here tumor growth was inhibited when peg-SN-38 was applied, however tumor volumes did not show major differences when treated with 15 µmol/kg peg-SN-38 ± Pamiparib or 60 µmol/kg peg-SN-38. Mice of the group treated with 60 µmol/kg peg-SN-38 lived slightly longer than mice treated with 15 µmol/kg peg-SN-38, however the difference was not significant. Again, adding Pamiparib to the treatment did not affect tumor growth or survival of the mice. When comparing the effect of peg-SN-38 to plain Irinotecan the effect of 0.83 mg/kg Irinotecan needs to be compared to 60 µmol/kg peg-SN-38 since these concentrations represent the highest clinically achievable concentrations. For mice treated with 60 µmol/kg peg-SN-38 the median survival was 87 days compared to 88 days when treated with 0.83 mg/kg Irinotecan and comparison of the survival curves did show no significant

difference (p = 0.4). However, tumor volumes remained smaller when treated with 60 µmol/kg peg-SN-38 than with 0.83 mg/kg Irinotecan, but why treatment with peg-SN-38 did not result in longer survival is not clear.

In this part of the project, replication stress was targeted *in vitro* and *in vivo*. Even though the combination of SN-38 and PARP-inhibitors was highly synergistic *in vitro* and the most synergistic combination among a panel of 76 drugs, combination of Irinotecan and the BBB-penetrant PARP-inhibitor Pamiparib did not yield synergistic effects *in vivo* when tumors were injected orthotopically into the brain. Further refinements of the dosing schedule as adaptation of the dose of the drugs or applying a pegylated version of SN-38 did also not show synergy. However, for an ETMR model that was injected subcutaneously, a synergistic effect was detectable for the combination of 2.5 mg/kg with 1.5 mg/kg Pamiparib. To better understand why the drugs are leading to synergy for the subcutaneous tumor but not for the different orthotopic tumors even though PARP is inhibited, the models that were used in the brain can be injected subcutaneous and then treated. Another, and more clinically relevant, possibility is to inject the ETMR tumor model orthotopically and compare the results of the treatment. The initial plan of the project was to also use the ETMR model orthotopically, however different approaches to label the model with luciferase failed and up to now bioluminescence and subsequently the tumor volume cannot be determined when the cells are injected into the brain. Moreover, another reason that synergy was not detectable in orthotopic brain tumors can be that the PARP trapping efficiency and BBB-penetrance of Pamiparib, the used PARP-inhibitor, are not sufficient. Even though demonstrating reduced levels of PAR by Western Blot for samples taken 2 hrs after the last dosing, trapping of PARP can be only for e.g. short time and not long enough or the ratio of inhibited PARP is not high enough to induce accumulation of DNA damage in the cell and PAR levels need to be further reduced than by about 80%. To overcome the BBB, approaches as focused ultrasound or treatment with a just recently published pegylated version of Talazoparib, which is characterized by significantly longer half-life *in vivo* (1 day vs. 3 hrs for Pamiparib), high exposure of released Talazoparib and accumulation in the tumor, can be used [290,291]. In addition, Talazoparib has a better PARP trapping efficiency than Pamiparib. In following treatment studies the new formulation can be tested in combination with Irinotecan or pegylated SN-38 to study whether synergy can then be detected.

6. Generation and molecular characterization of SMO-inhibitor resistant SHH MB PDX models

The third subproject of my PhD thesis was about the generation and molecular characterization of SHH medulloblastoma PDX models that became resistant to treatment with a SMO-inhibitor. The project was initiated by Sebastian Brabetz, a former PhD student in the group, and the generation of the models is described in his thesis [292]. My part of the project was the molecular characterization of the resistant models and testing treatment strategies for these.

The project has been submitted for publication to *Neuro-Oncology* (in revision) and the figures in this chapter are taken from the manuscript.

6.1. Introduction

The first analysis of the Hedgehog (HH) signaling pathway was in fruit flies and it is a highly preserved and well-studied signaling pathway that transmits signals from the membrane to the nucleus [293-295]. It is pivotal for embryonic development but also development of many tissues and organs [296]. In adult tissues the pathway is mostly inactive but still relevant for maintenance of somatic stem cells as well as pluripotent cells and it is necessary for tissue repair of e.g. epithelial cells [297,298]. Moreover, the HH signaling pathway plays a role for transmitting mechanical, chemical or thermal signals in primary cilia [299]. The pathway can be activated by different ligands, namely Sonic HH (SHH), Indian HH (IHH) or Desert HH (DHH), which affect polarity of organisms [296].

In the inactive state, the transmembrane protein patched 1 (PTCH1) inhibits Smoothened (SMO), which is also located in the transmembrane, and Suppressor of fused (SUFU) is bound to glioma-associated oncogene (GLI) in the cytoplasm (Figure 21, left panel).

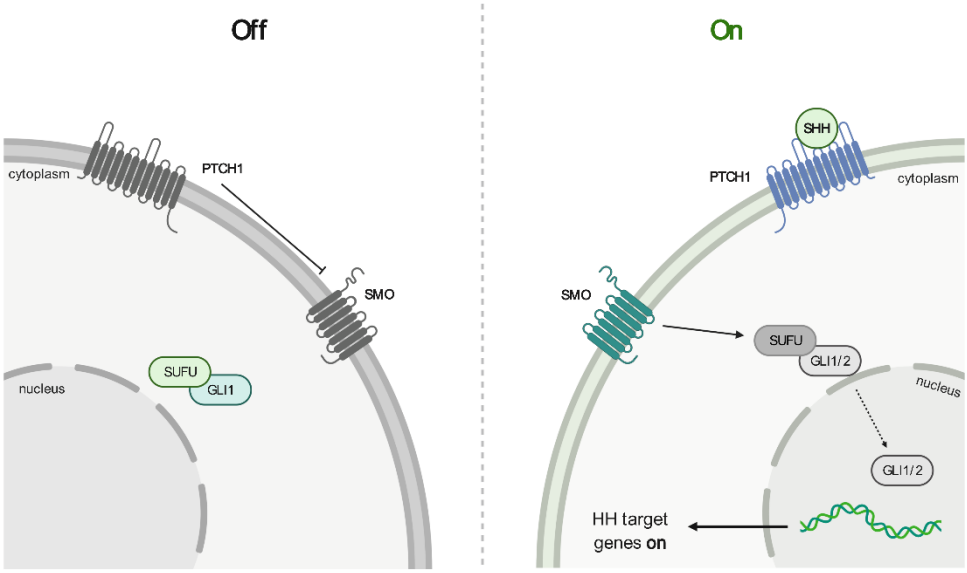

Figure 21: The HH signaling pathway in inactive (left) and active (right) state.

Left panel: if the HH signaling pathway is inactive, PTCH1 inhibits SMO and SUFU is bound to GLI1, GLI2 or GLI3 in the cytoplasm; right panel: when the pathway is activated, SHH is bound to PTCH1, SMO gets activated and GLI1/2/3 is released of SUFU and transferred to the nucleus; retrieved and adapted from https://app.biorender.com/biorender-templates.

The pathway gets activated if one of the ligands, SHH, IHH or DHH, binds to PTCH1, which is then internalized and degraded. Subsequently, PTCH1 does not inhibit SMO anymore and is in its active form translocated to the primary cilia. Following that, GLI detaches from SUFU and enters the nucleus where it acts as a transcription factor (Figure 21, right panel). Located in the nucleus, GLI promotes the expression of HH target genes in a feed-forward loop as e.g. *GLI1/2* and *MYCN* but also negative regulators of the pathway as *PTCH1* [300].

Even though the HH pathway is normally inactive after embryonic development, it can be constitutively activated by e.g., mutations in *PTCH1* or *SUFU*, which result in developmental problems as seen in patients with the Gorlin-syndrome [301,302]. Activation of the HH pathway by mutations has also been detected in many different tumor types, including basal cell carcinoma (BCC), rhabdomyosarcoma (RMS), and brain tumors such as SHH-activated medulloblastoma and high-grade glioma [303-309].

Due to its tumorigenic role across various entities, targeting the HH pathway as a therapeutic approach is promising and especially SMO as a therapeutic target has been studied intensively leading to the approval of different drugs targeting this gene [310,311]. The inhibitors were used for preclinical and clinical studies and showed promising activity in BCC and MB SHH patients with mutations upstream of *SMO* as in *PTCH1*, but not in tumors with mutations in *SMO* itself or downstream of *SMO*, such as in *SUFU* or with amplification *of MYCN/GLI2* [58,312-315]. Treatment with SMO-inhibitors is also ineffective

for most tumors harboring a mutation in *SMO* since the mutation leads to structural changes that prevent binding of the inhibitor [315]. Most likely, SMO-inhibitors are also ineffective in tumors that show increased HH signaling but without the obvious mutations that activate the pathway, such as in ATRT-SHH tumors or *ZFTA*-fusion positive ependymomas, as in these tumors the HH pathway gets activated more at a transcriptional level but also downstream of *SMO* [316-318].

Despite being potentially promising for therapy, treatment with SMO-inhibitors induced side effects as premature closure of growth plates in young children and limits the treatment to adult patients only [313]. Another drawback that was frequently observed in the clinic is that patients often acquire resistance to the treatment. Patients with BCCs or a metastatic MB that were treated with Vismodegib frequently developed resistance to SMO-inhibition with 50% of resistant cases harboring mutations in *SMO* but also mutations downstream of *SMO* [315,319].

Since resistance to treatment with SMO-inhibitors is observed frequently, studies on how to prevent resistance or how to overcome resistance are needed and new therapeutic approaches need to be established. However, to mimic the clinical situation and to further investigate the biology of resistance and to test new treatment strategies, good and reliable preclinical models are needed. First studies used mouse MB models with *Ptch1* and *Tp53* mutations, treated the murine tumors with either Sonidegib or Vismodegib and reported that the tumors acquired resistance quickly [320,321]. Some models developed resistance within 16 days, which is likely also due to the *p53*-mutated background of the mice since the mutation promotes genomic rearrangements and amplifications [321]. Analysis of the resulting resistant tumors showed amplification of *Gli2* in 50% of the models as cause of the resistance and out of 135 resistant tumors, only 7 (~5%) acquired resistance due to inactivating mutations in *Smo* [321]. Albeit giving first insights into the mechanisms of resistance, the models do not reflect the situation observed in patients, since their mutations in *SMO* were mostly the cause of resistance [315,322]. Moreover, another difference of the resistant murine models is the *Tp53* mutations since *TP53*- and *PTCH1*-mutations almost never co-occur in patients. Mutated *TP53* in SHH MB is mostly observed in older children in conjunction with Li-Fraumeni-syndrome (i.e., germline mutation of *TP53*). In addition, those tumors mostly harbor a *MYCN* and/or *GLI2* amplification, which makes them resistant to treatment with SMO-inhibitors [314]. To closely mimic the human situation and be able to study the mechanisms of resistance seen in patients, better and more faithful models are necessary. In the project described here the first Sonidegib-resistant SHH MB PDX models were generated and molecularly characterized.

6.2. Results

6.2.1. Generation of SMO-inhibitor resistant PDX models

For generation of SMO-inhibitor resistant SHH MB PDX models, the model med-1712FH was chosen. The model was established from a 4.9 year old male patient with a medulloblastoma. DNA methylation profiling and TSNE dimensionality reduction using a published reference cohort of Cavalli *et al*. 2017 classified the model as MB SHH and more specifically as subgroup MB-SHH-3 (Figure 22A) [46]. The copy number profile derived from the methylation data shows that the model harbors a heterozygous loss of chromosome 9q and amplification of *YAP1* (Figure 22B). In addition, DNA sequencing showed that the model has missense mutations in *PTCH1*, *ELP1* and *CREBBP*. The inactivating mutation in *PTCH1* makes the model sensitive to treatment with SMO-inhibitors. The SMO-inhibitor sensitive, established and luciferase-labelled model was injected intracranially into the cerebellum of NSG mice and bioluminescence signal was determined once per week. As soon as a threshold of a bioluminescence signal of $2x10^6$ p/s was reached, mice were randomized into a vehicle or treatment group and they were treated in cycles with 20 mg/kg Sonidegib (Figure 22C). Whenever the bioluminescence signal decreased to $<1x10^6$ p/s, treatment was stopped and mice were put off treatment allowing the tumor to re-grow as long as the signal increased to $>2x10^6$ p/s again. The intermitted treatment schedule was applied until the tumor volume, as indicated by the IVIS signal, increased under treatment indicating that the tumors did not respond to the treatment anymore thereby becoming resistant to Sonidegib. By applying an intermitted treatment schedule, it was possible to induce resistance over time and conduct treatments based on tumor burden of each mouse individually, which resulted in the generation of nine resistant models. Resistance to Sonidegib was developed after 3-6 treatment cycles, spanning from 30-51 weeks in total (Figure 22D). Control mice, treated with vehicle compound, had to be euthanized 4-10 weeks after treatment start. Mice that were treated with Sonidegib lived significantly ($p < 0.0001$) longer than the mice in the vehicle-treated group and the median survival was 267 days for the group treated with Sonidegib compared to 50 days for the vehicle-treated group (Figure 22E). As soon as the mice showed any termination criteria, they were euthanized and tumor material was preserved (fresh frozen, FFPE or cryopreserved as single cell suspension) for sequencing analysis, stains for proliferation and apoptosis analysis or further *in vivo* experiments.

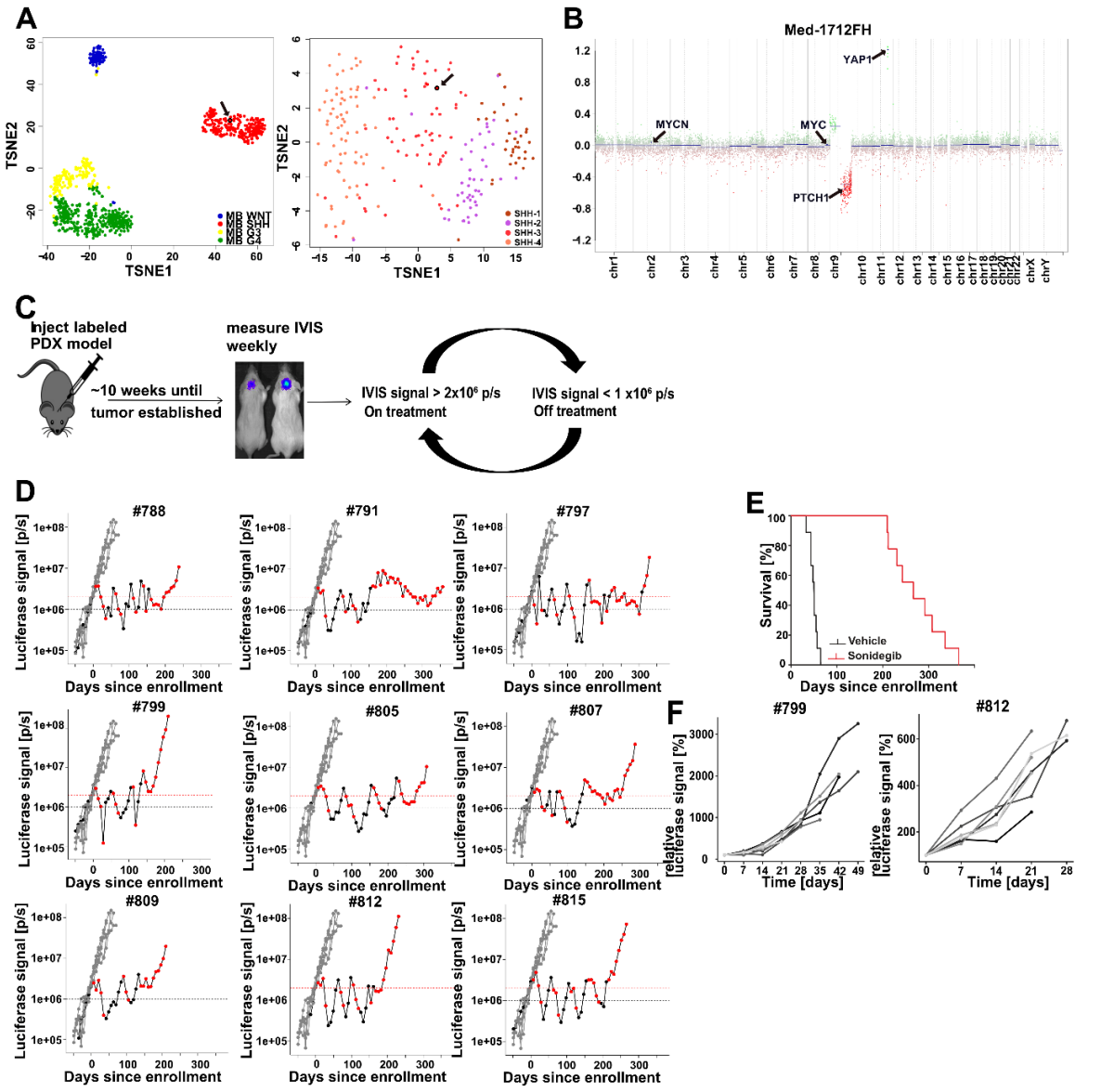

Figure 22: Characterization of the med-1712FH model and induction of resistance to Sonidegib by intermitted treatment schedule.

A) TSNE clustering of a MB reference cohort of Cavalli et al. 2017 [46] shows the different groups of MB (n = 764; left panel) and the subgroups of MB SHH (n = 224; right panel); the used med-1712FH model clusters as MB SHH and SHH-3 (indicated by black arrow); B) Copy number analysis of med-1712FH demonstrates loss of chromosome 9q with *PTCH1* and amplification of 11q with *YAP1*; C) Cells of the luciferase-labelled PDX model med-1712FH were injected intracranially, after about 10 weeks of tumor establishment, IVIS signal was determined weekly and treatment was started when IVIS signal reached $2x10^6$ p/s and stopped when the signal was lower than $1x10^6$ p/s; D) each plot shows the IVIS signals of vehicle-treated animals (grey; n=8) and of one Sonidegib-treated mouse; red dots: IVIS signals during time of treatment, black dots: IVIS signals during time off treatment; thresholds for on/off treatment: $2x10^6$ p/s (dashed red line) and $1x10^6$ p/s (dashed black line); E) mice treated with Sonidegib (n=9; red) lived significantly ($p < 0.0001$) longer than mice of the vehicle-group (n = 8; black); F) resistant models #799 and #812 were re-injected after cryopreservation and treated with Sonidegib (starting signal: $1x10^6$ p/s) to ensure resistance after freezing/thawing; D)+E) based on data and adapted from [292].

In a next step, cryo-preserved aliquots of two resistant models (med-1712FH_#812 and med-1712FH_#799) were thawed and re-injected into ten NSG mice each to verify that models keep the resistance also after freezing and thawing. Again, bioluminescence signal was measured once per week and treatment for the mice was started when the signal of $1x10^6$ p/s was reached. For all mice included in the study tumor volume increased constantly even though they were treated with 20 mg/kg Sonidegib daily (5 days on/2 days off) (Figure 22F). Since the tumors grew under treatment, Sonidegib-resistance could be confirmed even after cryo-preservation of the cells.

6.2.2. Genomic analyses of the resistant models

The nine resistant lines were subjected to whole genome sequencing (WGS) to receive more information about the underlying mechanism(s) of resistance. In addition, DNA methylation analysis was performed and the TSNE clustering showed that the three vehicle samples and the nine resistant samples formed a very tight cluster with the original med-1712FH sample (Figure 23A+B). The cluster did not appear within the other samples of the TSNE since the methylation profiles of the vehicle, resistant and original med-1712FH models are highly similar and were therefore slightly separated from the other clusters. Nevertheless, and as the original med-1712FH model alone clustered directly within the MB SHH and the SHH-3 cluster, the vehicle-treated and resistant models were all characterized as MB-SHH-3 tumors. In addition, the brain tumor classifier (v12) clearly called them all as MB-SHH-3 with prediction scores between 0.96 and 1 (Figure 23C). Immunohistochemical analyses for proliferation (Ki67-staining), apoptosis (cleaved Caspase-3 staining), and a HE staining of the resistant models and the original, treatment-naïve model did not reveal any differences indicating that the tumor growth related characteristics were still very similar (Figure 23D).

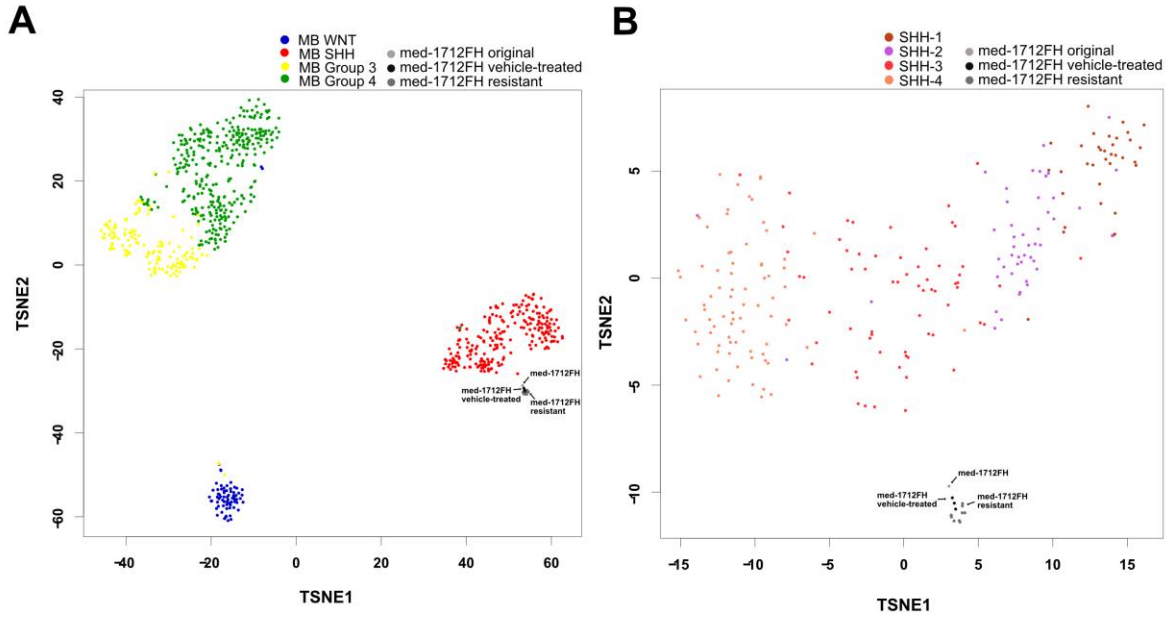

C

Sample ID	prediction	classifier score
med-1712FH	MB-SHH-3	1
788	MB-SHH-3	0.96
790	MB-SHH-3	0.99
791	MB-SHH-3	0.99
795	MB-SHH-3	1
797	MB-SHH-3	0.96
799	MB-SHH-3	0.98
805	MB-SHH-3	0.99
806	MB-SHH-3	1
807	MB-SHH-3	0.99
809	MB-SHH-3	0.99
812	MB-SHH-3	0.99
815	MB-SHH-3	0.99

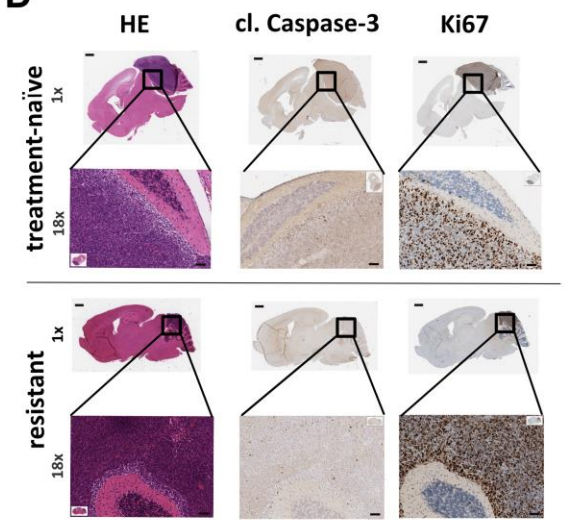

Figure 23: Methylation analysis and histological evaluation of the resistant samples in comparison to the treatment-naïve med-1712FH sample.

TSNE dimensionality reduction of a published cohort of Cavalli *et al*. 2017 [46] and the three vehicle samples, nine resistant samples and the original med-1712FH sample shows that the generated samples cluster very close with the original med-1712FH sample in proximity to the MB SHH cluster (n = 776) (A) and to the SHH-3 subgroup (n = 236) (B); C) the brain tumor classifier (v12) predicts all resistant and vehicle-treated samples as MB-SHH-3 (classifier scores: 0.96 – 1); D) histology sections (1x and 18x) of a treatment-naïve and a resistant sample stained against HE, cleaved Caspase 3 and Ki67 did not show differences, scale bars indicate 1 mm (for magnitude 1x) and 50 µm (for magnitude 18x).

The WGS data of the resistant samples was compared to the sequencing data of the original, treatment - naïve med-1712-FH model (med-1712-FH_#140) that was used as starting material. Eight of the nine resistant models harbored missense mutations in *SMO* and all acquired mutations occurred only once with one mutation per resistant model (Figure 24A+B). The SMO protein spans over 787

amino acids and contains different functional domains such as a cysteine-rich domain and a frizzled heptahelical membrane region. The mutations were all located within the frizzled membrane region of the protein, which expands from amino acid 221 to amino acid 558 (Figure 24A) [323]. Other published studies that applied treatment with SMO-inhibitors reported resistance and 20 different acquired mutations in *SMO* of which five were in MB GEMMs that were treated with Sonidegib [321]. More clinically relevant, the remaining 15 mutations were detected in tumor samples of MB and BCC patients that were treated with SMO-inhibitors and became resistant [315,320,322,324,325]. Of the eight resistant PDX MB models that were generated within the project described here, 5/8 mutations (63%) overlapped with mutations that were reported in the studies mentioned above (Figure 24B). One of the acquired mutations (S387N) was also reported in the study with MB GEMMs [321] and four mutations (T241M, V321M, I408V, D473Y) were also detected in Vismodegib-resistant BCC samples [315,322,324,325]. Interestingly, one location where an acquired mutation was found (D473) was not only reported for a Vismodegib-resistant BCC sample but also detected in a MB tumor sample that became resistant to Vismodegib-treatment [320]. Besides the acquired mutations in *SMO* in eight models, the remaining model gained an inactivating, loss-of-function mutation (S1358X) in *multiple epidermal growth factor-like domains protein 8* (*MEGF8*), which is a single-pass type I transmembrane protein that was characterized as a negative regulator of HH signaling [326]. Expression analysis confirmed significantly reduced expression of MEGF8 in the mutated sample compared to the other resistant and vehicle samples (Figure 24C). The physiological MEGF8-protein is involved in regulation of HH signaling and relevant for degradation of SMO. Mutated, inactive MEGF8 leads to accumulation of SMO and consequently HH signaling is increased [327]. Moreover, except the mutations in SMO and MEGF8, analysis of WGS did not reveal many other mutations and alterations in the resistant samples and copy number profiles were identical for the original and the resistant samples. For each newly generated resistant sample maximally one to five SNVs and/or one to two InDels were detected (Figure 24D).

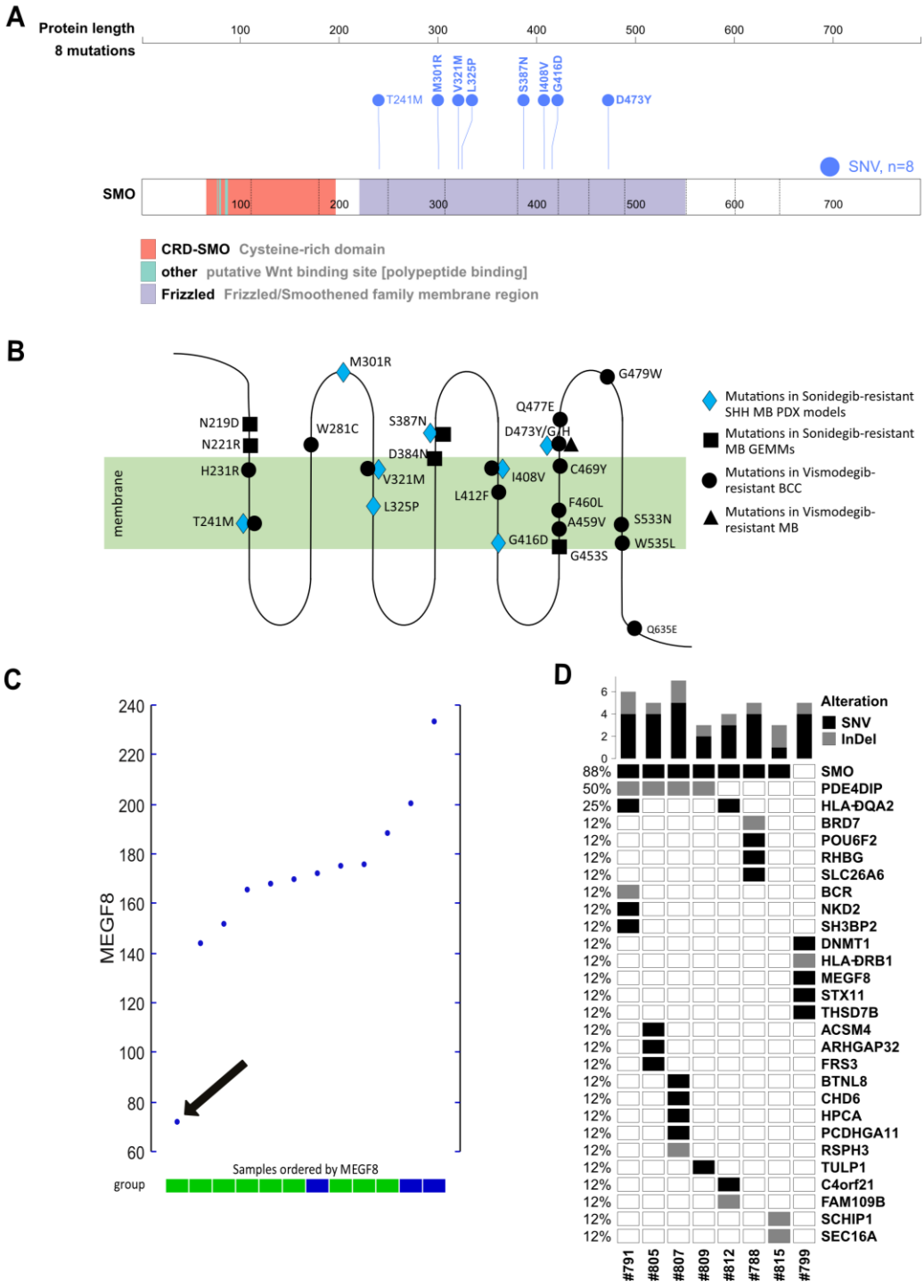

Figure 24: WGS data analysis unveils mutations in *SMO* for eight resistant samples and one model with a mutation in *MEGF8*.

A) the SMO-protein consists of different regions and the eight detected mutations in the resistant lines are all within the frizzled region (visualized by ProteinPaint; https://proteinpaint.stjude.org/ [328]); B) illustrated structure of SMO with extra- and intracellular as well as transmembrane regions and the analyzed mutations of the resistant MB SHH PDX models (depicted in blue) partly overlap with previously published detected mutations of MB GEMMs (black square)[321], BCC (black circle)[315,322,324,325] or MB (black triangle)[320] samples; C) *MEGF8*-expression of the nine resistant lines (green) and three vehicle samples (blue); the resistant sample with mutation in *MEGF8* shows the lowest expression (highlighted by black arrow); D) besides the mutations related to HH signaling few other SNVs and InDels were, compared to a treatment-naïve med-1712FH sample, analyzed as shown in the oncoplot.

Besides WGS, RNA sequencing of three vehicle-treated and the nine resistant samples was performed to assess whether the acquired resistance caused any transcriptional changes besides the constitutive activation of HH signaling. The analysis of sequencing data showed that 283 genes were significantly (p-value <0.05) down- and 240 genes upregulated in the resistant samples compared to the vehicle samples (Figure 25A). Other than that, expression levels of *GLI1/2* were analyzed and not significantly altered between the two groups (Figure 25B+C). This confirmed that *GLI1/2* is still expressed in the resistant samples and suggested active HH signaling. Moreover, no changes could be detected in expression levels of *MYCN* and *SUFU* (Figure 25D+E). In addition, Ingenuity Pathway Analysis (IPA) comparing resistant and vehicle-treated lines was performed and highlighted three upregulated pathways (activation z-score >2) and five downregulated pathways (activation z-score <-2) (Figure 25F). However, none of the eight annotated pathways seem to be relevant for HH signaling, growth of (cancer) cells or tumorigenesis.

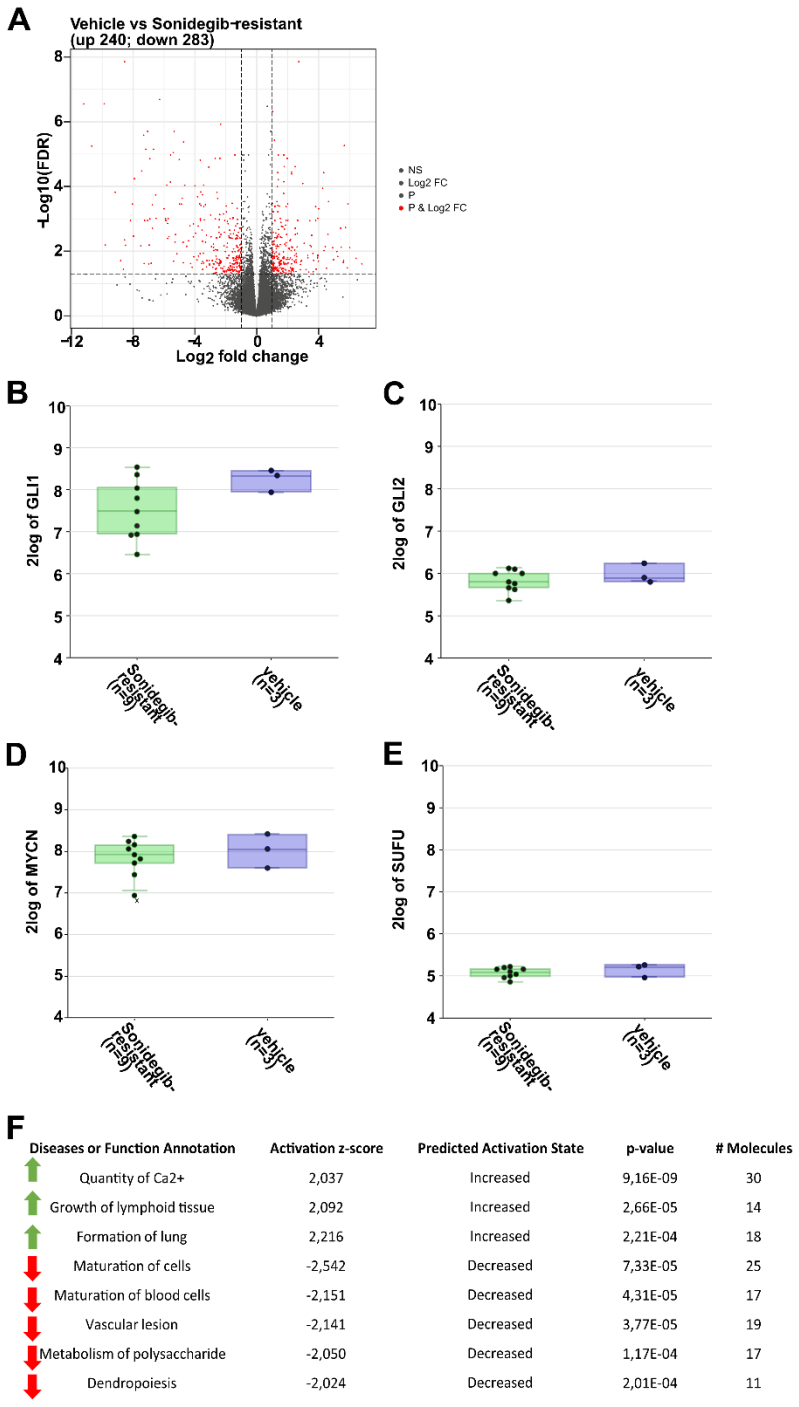

F

Diseases or Function Annotation	Activation z-score	Predicted Activation State	p-value	# Molecules
Quantity of Ca2+	2,037	Increased	9,16E-09	30
Growth of lymphoid tissue	2,092	Increased	2,66E-05	14
Formation of lung	2,216	Increased	2,21E-04	18
Maturation of cells	-2,542	Decreased	7,33E-05	25
Maturation of blood cells	-2,151	Decreased	4,31E-05	17
Vascular lesion	-2,141	Decreased	3,77E-05	19
Metabolism of polysaccharide	-2,050	Decreased	1,17E-04	17
Dendropoiesis	-2,024	Decreased	2,01E-04	11

Figure 25: Expression analysis of vehicle and resistant samples and Ingenuity Pathway Analysis.

A) RNA-sequencing revealed 240 up- and 283 downregulated genes in the resistant versus vehicle-treated samples ($p < 0.05$); Expression levels of *GLI1* (B), *GLI2* (C), *MYCN* (D) and *SUFU* (E) did not show differences between the resistant (n = 9; green) and the vehicle-treated (n = 3; blue) samples; F) IPA result of annotated diseases or functions that are up- or downregulated in the resistant samples compared to vehicle-treated samples; no pathways related to tumor growth or proliferation/apoptosis of (cancer) cells in general.

6.2.3. Target engagement of Sonidegib in PDX models on treatment

When treatment of med-1712FH tumor-bearing mice was started and before tumors developed resistance, the tumors responded nicely to the treatment and tumor volume regressed on treatment. To further understand and assess the initial response of the models to treatment with Sonidegib, three initially vehicle-treated mice that started to show tumor-related symptoms but no termination criteria yet, were treated on two consecutive days with Sonidegib and euthanized four hours later. Tumors were removed and tumor cell pellets were subjected to RNA-sequencing. Analysis of RNA-sequencing data revealed 17 up- and 105 downregulated genes ($p < 0.05$) in the short-time treated samples compared to the vehicle-treated samples (Figure 26A). Analysis of expression levels unveiled that expression of *GLI1* and *MYCN* were significantly downregulated ($p = 9.51e-4$ and $p = 0.019$, respectively) in the short-time treated samples when compared to the vehicle samples (Figure 26C+E). Expression levels of *GLI2* and *SUFU* were not affected by the short-time treatment (Figure 26D+F). Upregulation of the KEGG HH signaling pathway in the vehicle and resistant samples compared to the short-time treated samples was confirmed by Gene Set Enrichment Analysis (GSEA) (Figure 26B). In addition, IPA revealed that in short-time treated samples pathways or functions linked to organismal death and growth failure were upregulated (activation z-score >2). Conversely, the MAPKKK cascade and pathways relevant for body size were downregulated (activation z-score <-2) in the short-time treated samples, which points towards decreased cell proliferation and cell division (Figure 26G).

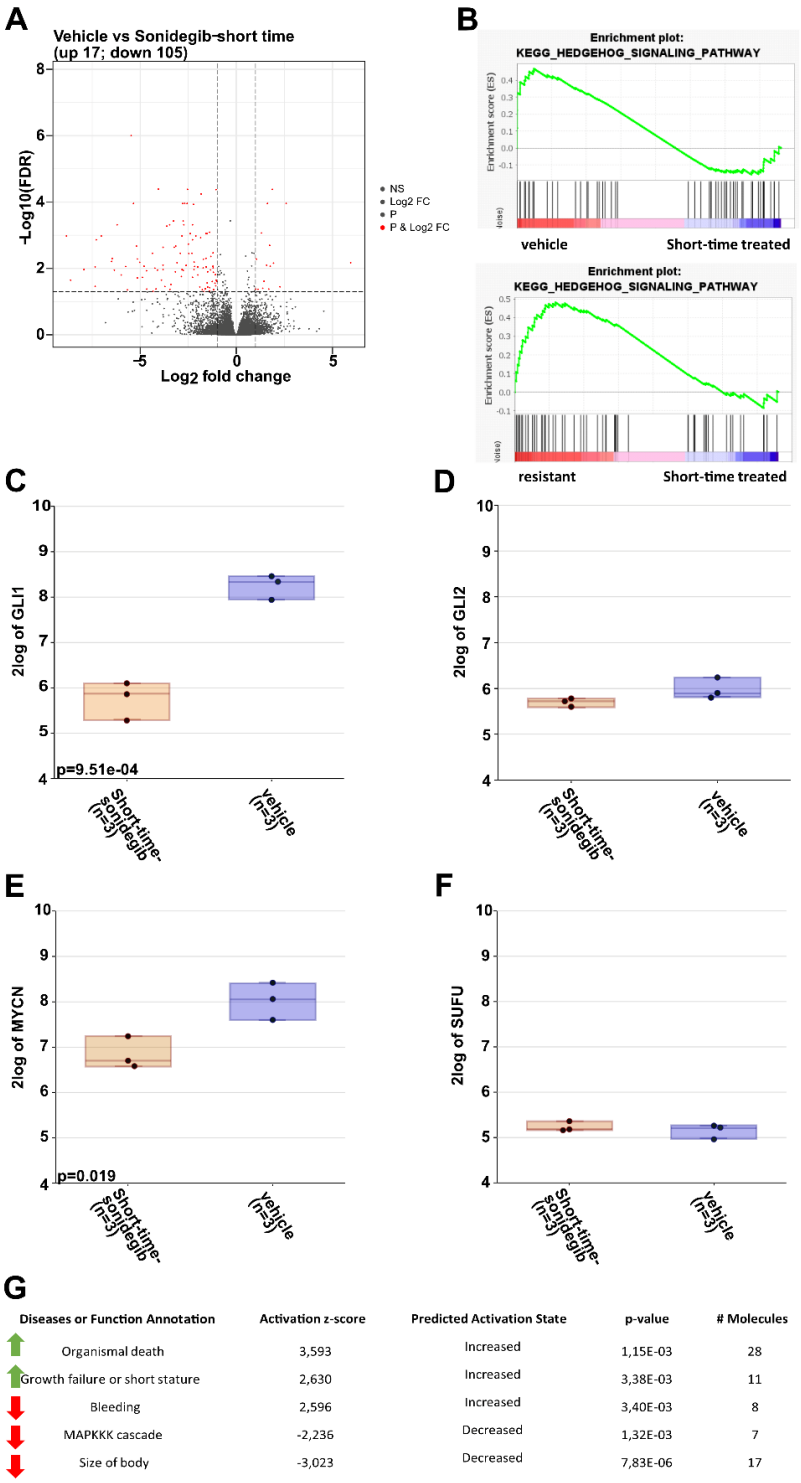

Diseases or Function Annotation	Activation z-score	Predicted Activation State	p-value	# Molecules
Organismal death	3,593	Increased	1,15E-03	28
Growth failure or short stature	2,630	Increased	3,38E-03	11
Bleeding	2,596	Increased	3,40E-03	8
MAPKKK cascade	-2,236	Decreased	1,32E-03	7
Size of body	-3,023	Decreased	7,83E-06	17

Figure 26: Expression analysis of short-time treated samples and pathway analysis comparing short-time treated samples to vehicle-treated and resistant samples.

A) RNA-sequencing revealed 17 up- and 105 downregulated genes in short-time treated samples compared to vehicle-treated samples ($p < 0.05$); B) Gene set enrichment analysis of short-time treated samples compared to vehicle-treated (upper panel) or resistant (lower panel) samples confirmed upregulation of the HH pathway in vehicle-treated and resistant samples; expression of *GLI1* (C) and *MYCN* (E) was significantly downregulated in the short-time treated samples, expression of *GLI2* (D) and *SUFU* (F) was not altered; G) IPA of short-time treated versus vehicle-treated samples shows upregulation of pathways related to organismal death and growth failure and downregulation of the MAPKKK cascade.

6.2.4. *In vitro* and *in vivo* treatment with XPO1-inhibitor Selinexor

To improve therapy for patients, the resistant models can be used to study new treatment strategies to overcome resistance. For this purpose, a high-throughput drug screen with a library of 76 drugs, including mostly approved but also some investigational drugs, was performed in collaboration with Dr. Ina Oehme and Dr. Heike Peterziel of the Translational Drug Screening Unit (TDSU) at the KiTZ, Heidelberg. Cells of the sensitive, treatment-naïve med-1712FH model and a SMO-mutated resistant model (#791) were used for the screen. The cells were seeded (1000 cells/well) on 384-well plates pre-printed with the compounds and the read-out was done 72 hrs later using CellTiterGlo®. One of the most potent drugs that was effective in the sensitive (IC50 = 86.1 nM) as well as in the resistant (IC50 = 65.6 nM) model was Selinexor (Figure 27A+B). Selinexor is an FDA-approved XPO1-inhibitor that inhibits nuclear export of tumor suppressor proteins as e.g. p53 [329] and is in clinical use for treatment of multiple myeloma [330]. In addition, Selinexor can cross the blood-brain-barrier and was already effectively applied as treatment of a MB model with *SUFU* mutation [331].

For confirmation of efficacy *in vivo* one vehicle-treated (#806), one *SMO*-mutated (#812) and the *MEGF8*-mutated (#799) model were selected. Cells of the respective models were injected intracranially into NSG mice and treatment with 5 mg/kg Selinexor or solvent control (p.o., 5 days on/2 days off) was started as soon as bioluminescence signal reached a threshold of $1x10^6$ p/s. Treatment and tumor volume determination via bioluminescent imaging was performed until mice showed termination criteria. For the analysis, tumor volumes as well as survival of the groups was compared. Tumor volumes of the sensitive model did not show huge differences between the two groups, but nevertheless mice in the Selinexor-treated group lived at maximum 85 days longer (Figure 27C, left panels). For the two resistant models, treatment with Selinexor induced tumor growth inhibition and stable disease for several weeks as well as a significant survival benefit ($p = 0.0027$ for both resistant models) (Figure 27C). Tumors of mice injected with cells of the *SMO*-mutated model (#812) grew during the first weeks after start of treatment with Selinexor, however the tumor volumes remained stable for five weeks and even regressed during weeks six to eight (Figure 27C, middle panel). Thereafter, the tumors slowly grew back for five weeks followed by faster growth behavior until euthanasia of the animal. Tumors of the *MEGF8*-mutated model (#799) responded well to the treatment with Selinexor, which resulted in 13 weeks of stable disease with only minimal tumor growth (Figure 27C, right panel). After this time point the tumors started to grow faster, possibly due to resistance to the treatment, until mice had to be euthanized. Nevertheless, for both mutated, resistant models Kaplan-Meier analysis demonstrated a significant survival benefit with maximal survival of 88 days (for #812) and 101 days (for #799) longer than the respective vehicle-treated mice but no long-term regression of the tumors.

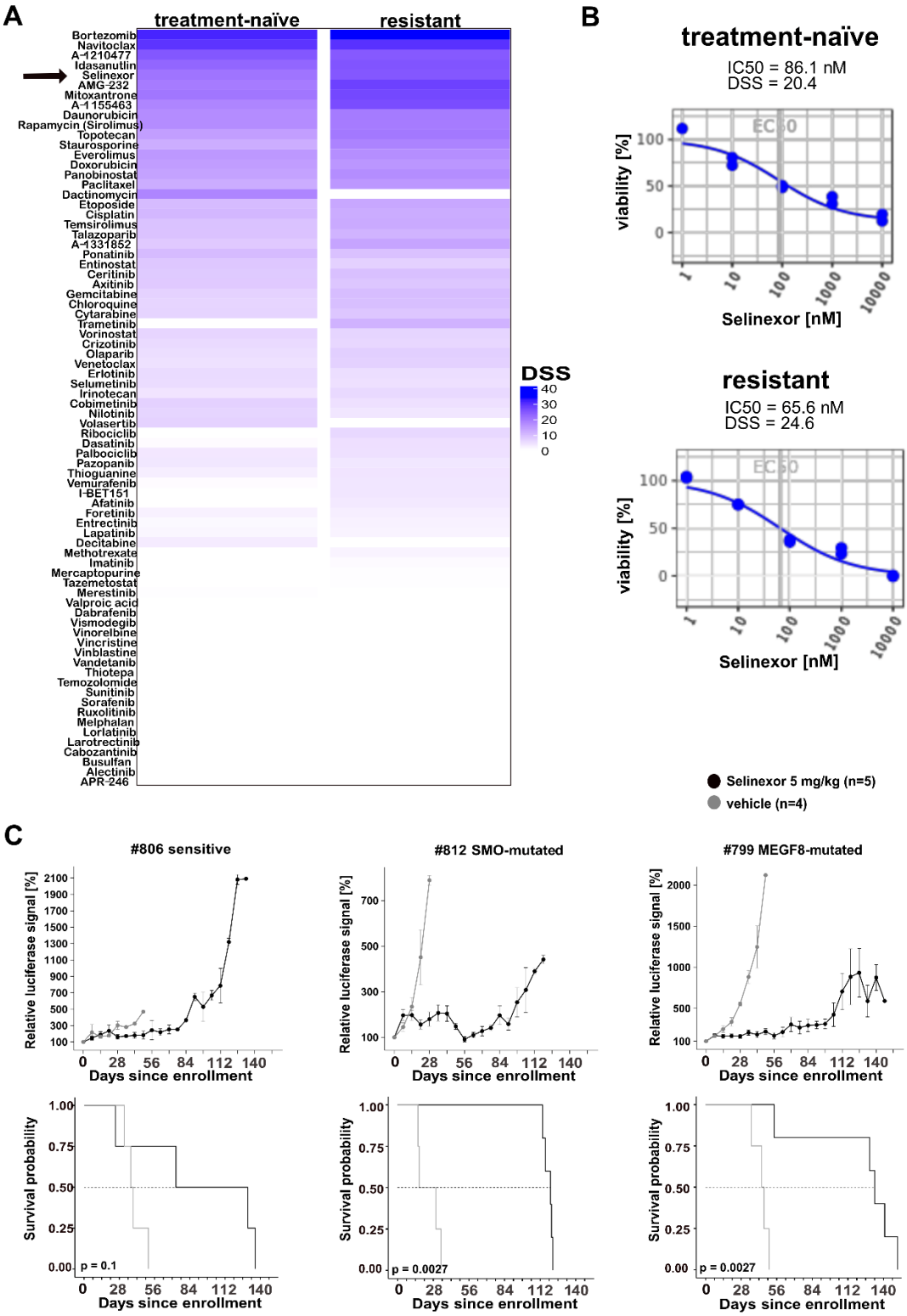

Figure 27: Treatment of original, treatment-naive med-1712FH cells and resistant med-1712FH cells *in vitro* and *in vivo*.

A) overview of the DSS scores of the *in vitro* drug screen using treatment-naïve and resistant (#791) med-1712FH cells with Selinexor as one of the top hits; B) IC50-values and dose-response curves of treatment-naïve (IC50 = 86.1 nM) and resistant (IC50 = 65.6 nM) med-1712FH cells; C) treatment of sensitive (#806), SMO-mutated (#812) and MEGF8-mutated (#799) med-1712FH tumors with Selinexor *in vivo* showed survival benefit for all groups treated with Selinexor and tumor growth inhibition for the two resistant models; vehicle group (n = 4) is shown in grey and Selinexor-treated group (n = 5) in black.

6.3. Discussion

For the treatment of MB and BCC tumors with aberrant activation of the HH pathway, SMO-inhibitors have been used quite effectively [315,319,320]. Nevertheless, only tumors with mutations and aberrations upstream of *SMO* will respond and tumors with mutations downstream of *SMO* or in *SMO* itself will be initially resistant (primary resistance) [58,313,314]. However, also initially responding tumors can acquire mutations in *SMO* or other genes downstream of *SMO* and become resistant to the treatment (secondary or acquired resistance) [315,319,320]. For overcoming resistance and evaluating new treatment strategies, either monotherapies or combination therapies, it is important to have faithful models that reflect the patients' situation as best as possible.

Mice with tumors of the MB SHH PDX model med-1712FH, which harbors a *PTCH1*-mutation, were treated with 20 mg/kg Sonidegib and initially responded well to the treatment. However, by applying the treatment in cycles and always giving the tumors time to re-grow, nine resistant tumors were generated that didn't respond to treatment with Sonidegib anymore. Analysis of WGS data of the resistant tumors showed that one of the generated resistant models acquired a mutation in *MEGF8*, which is a negative regulator of HH signaling [326]. The other eight (89%) resistant tumors gained a missense mutation in *SMO*, which led to aberrant activation of the HH signaling pathway. Interestingly, five of the eight (63%) mutations overlap with mutations that were reported previously either in BCC tumors treated with Vismodegib or in murine MB tumors treated with Sonidegib [315,321,322,325]. The other detected mutations in *SMO* were not reported yet. Most worthwhile mentioning is the detected mutation at position D473, which overlaps with a mutation detected in a biopsy of a patient with a MB tumor who was treated with Vismodegib and became resistant quickly after treatment start [319]. Detecting the same mutation as seen in patients supports clinical relevance of the generated resistant models and promotes them as reliable models for further treatment studies about resistant MB tumors.

That most of the resistant tumors acquired a mutation in *SMO* (8/9) and only one model acquired a mutation in *MEGF8* is in contrast to earlier findings that account mutations in *SUFU* or amplification of *GLI1/2* [315,321]. For BCC tumor samples of patients that developed resistance to Vismodegib mutations in *SMO* were reported as well as amplifications more downstream in the HH pathway [315]. For murine Sonidegib-resistant MB models only few mutations in *SMO* were detected and 50% of the models became resistant due to *Gli2*-amplification [321]. Remarkably, the tumors of the mouse model developed resistance already after 16 days of treatment, whereas the resistant human PDX models generated in the project described here, treated in cycles, took more than 100 days and treated in cycles. One possible explanation for this difference is the homozygous loss of *p53* in the murine

tumors, which promotes genomic instability and rearrangements of the genome, and thereby possibly facilitating a faster development of resistance.

Analysis of RNA-sequencing data of the resistant models confirms that the HH signaling pathway is active since expression levels of *GLI1/2* and *MYCN* were not different between the nine resistant and the three vehicle-treated models. However, when non-resistant mice were only treated for two days, the expression levels of *GLI1* and *MYCN* were decreased and indicate inhibition of the HH pathway and target engagement of Sonidegib. In addition, GSEA analysis revealed upregulation of the HH pathway in the resistant as well as in the vehicle-treated tumors relative to the short-time treated tumors. Pathway analysis with IPA showed that pathways related to organismal death were upregulated in the short-time treated samples in comparison to the resistant or vehicle-treated samples, and pathways related to proliferation were downregulated, which supports that treatment with Sonidegib, even if only for two days, induces apoptosis. When performing pathway analysis for the resistant samples in comparison to the vehicle-treated samples, no pathways related to proliferation or growth of cells, either cancer or healthy cells, were retrieved, which endorses that the metabolisms of resistant and vehicle-treated models are similar.

To take the resistant models one step further and verify possibilities to overcome resistance, the models were used for an *in vitro* drug screen and an *in vivo* treatment study. A drug screen was performed, which highlighted Selinexor as one of the top hits with low IC50-values (<100 nM) for treatment-naïve and resistant med-1712FH cells. Selinexor is a XPO1-inhibitor and already showed good efficacy as treatment for a MB model with *SUFU* mutations [331]. If *SUFU* is mutated, *GLI* cannot bind anymore and is not hindered to enter the nucleus, which results in aberrant activation of the HH signaling pathway. In addition, the model with mutation in *SUFU* is most likely primary resistant to SMO-inhibitors since *SUFU* acts downstream of *SMO*. *In vivo* treatment of one sensitive, vehicle-treated and two resistant models with Selinexor showed that for all models a survival benefit was induced for the groups treated with Selinexor, which indicates that inhibition of XPO1 prolongs survival independent of the HH pathway. However, when evaluating the bioluminescence signals that were measured weekly, significant tumor growth inhibition was only observed for the two SMO-inhibitor resistant models.

The models presented here are the first Sonidegib-resistant orthotopic MB SHH models that were generated of a PDX model, which can function as a base for more experiments to evaluate new treatment approaches for patients with tumors that are resistant to SMO-inhibitors. One possibility might be the use of inhibitors that target the HH pathway more downstream of *SMO* as for example *GLI* but so far no specific and BBB-penetrant GLI-inhibitors are on the market. Another possibility, and

more likely, is the combination of drugs as e.g. described in Hau *et al*. 2021 to prevent development of resistance and to test the combination treatment with a SMO-inhibitor and Selinexor upfront to prevent resistance [332].

7. General Discussion and Outlook

Treating high-risk pediatric brain tumor patients remains challenging and despite advances in neurosurgical procedures and the development and evaluation of new protocols for radio- and chemotherapy, a subset of tumors still forecasts poor outcome for the patients. Over the past years routine diagnostics of pediatric tumors has changed and not only a histological evaluation is important, but molecular analyses have now been added to the diagnosis determination criteria and included into the most recent WHO guidelines for classification of CNS tumors published in 2021 [8]. For almost all brain tumor entities, groups and subgroups are mainly based on molecular characteristics. With the analysis of more and more samples and collection of more data, more details about their underlying (epi-)genetic and molecular alterations is being revealed and for most of the pediatric entities even further molecular grouping or subgrouping is possible and often helpful. By specifying these groups and subgroups of tumor entities even further, more concrete details about driver events, prognosis and treatment strategies can be derived. This is also reflected in the advance of treatment strategies. Even though standard-of-care treatments still comprise surgery, followed by radiation and/or chemotherapy, more clinical trials are performed now that include mechanism-of-action based approaches and that use targeted inhibitors, sometimes in combination with either another targeted inhibitor or chemotherapeutics.

Further evaluation of new treatment strategies is pivotal to improve patients' outcome, however, it is also important to streamline efforts, since some tumor entities are only diagnosed very rarely and consequently clinical data and tumor tissue is precious. For preclinical testing of new treatment strategies, more and well-characterized models are needed, representing all the different entities and their respective groups and subgroups. To generate reliable and meaningful patient-derived tumor models, tissue samples of a biopsy or surgery are necessary for instance to inject into mice to establish PDX models that can be expanded and used for preclinical testing of new treatment strategies. An intensively studied vulnerability for new therapies is for instance replication stress, which is a common feature in cancer cells. In addition, it is a highly regulated process that combines different pathways and offers different targets for treatment strategies. However, it is important to prioritize the most promising strategy for the different entities and ensure that the applied strategies were thoroughly studied and evaluated. By performing a systematic literature research all literature that evaluated the therapeutic role of replication stress in pediatric solid tumor entities was investigated and scored for different proof-of-concept modules. The analysis gives a comprehensive and structured overview of published preclinical research findings and results of clinical trials, which can be interactively explored

by using the publicly available heatmaps on the R2 TAR platform (https://hgserver1.amc.nl/cgi-bin/r2/main.cgi?option=imi2_targetmap_v1). The systematic evaluation of the publications revealed 31 alternative potential new drug targets and six specific targets were added to the search terms in order to be analyzed in more detail. Out of these six specific drug targets, PARP was covered by most of the literature and evaluated most comprehensively. The results suggest combination treatments of PARP as promising treatment strategies in pediatric cancers. As combination partner not only chemotherapeutics, which was the most studied combination, but also other targeted inhibitors as ATR or CHK1 inhibitors are promising. Besides PARP, only treatment approaches targeting WEE1 have already been tested in clinical trials, even though preclinical evaluation was also promising and resulted in positive scores for inhibition of ATR or CHK1. Similar as seen for PARP, also WEE1, ATR and CHK1 inhibitors were frequently combined with other drugs and together suggest to combine targeted inhibitors for replication stress with other drugs as chemotherapeutics or other targeted inhibitors. However, since tumor entities are classified more specifically and knowledge about molecular groups and subgroups increases, biomarker evaluation to predict efficient treatment and responses also plays a major role. Interestingly, the module "predictive biomarkers" was within the least studied modules in the TAR. Even though scores and evidence entries were noted for 5/6 specific targets, numbers of papers for each target were very low and for robust evaluation more experiments and studies are necessary.

Identification of biomarkers for treatment strategies is explicitly important for applying mechanism-of-action based therapies. Treatment strategies with chemotherapeutics were identified because they kill rapidly dividing cells systematically and follow the "one-size-fits-all" solution. However, MoA based therapies are designed to interact with the target specifically and to be able to thoroughly predict which strategy fits best to a patient, biomarkers need to be evaluated and established. Even for chemotherapeutics it is important to take into account the underlying biology to predict which chemotherapeutic strategy might work best. Irinotecan as a chemotherapeutic agent was detected already in the 1960s, however at this time classification of tumor entities was by far not as detailed as now and the underlying biology of tumor entities was not known [333]. An overview paper published in 2000 summarized the results of clinical trials using Irinotecan as monotherapy for various tumor entities such as gastric cancer, colorectal cancer, breast cancer, small-cell lung cancer and cervical cancer with response rates varying between 0% and 17% [334]. A phase II study published in 2002 enrolled children with high-risk malignant brain tumors for treatment with Irinotecan, however the diagnosed tumor entities were only referred to as glioblastoma, anaplastic astrocytoma, diffuse pontine glioma, ependymoma or medulloblastoma/primitive neuroectodermal tumor and no further classification as molecular groups or any other characteristic was taken into account [335]. The reported

best response varied between complete response and progressive disease. Another clinical trial published in 1999 evaluated the effect of Irinotecan as therapy for adult malignant glioma and enrolled 60 patients of which 15% showed partial response and 55% stable disease when treated with Irinotecan [336]. To account for the different subgroups of glioma and to specify the efficacy of Irinotecan, the tumor samples were classified by histology and grouped into three different groups, which differed in response rates for stable disease (50%-60% of cases) as well as for partial response (0%-17% of cases). Even though differences in histology were taken into account to classify the tumors, classification was not as advanced as it is nowadays with molecular characteristics and identified molecular groups and subgroups for almost all entities.

Even though Irinotecan inhibits topoisomerase in general and not only in tumor cells, the observed effect on normal astrocytes *in vitro* (when testing the active metabolite SN-38) or on two MB SHH models *in vivo* was minimal indicating a distinct method of action. To be able to design experiments and preclinical studies to yield the best and most meaningful results, biomarker identification for the use of Irinotecan is needed. The hypothesis for the treatment strategy shown here was: high expression or amplification of *MYC(N)* leads to high proliferation and the presence of R-loops. By inhibiting Topoisomerase I the R-loops cannot be resolved and ssDNA breaks will occur, which need active PARP to be repaired. To prove the hypothesis *in vivo*, a MB SHH model with a *PTCH1*-mutation as driver event and without amplification of *MYCN* was tested and did indeed show no response to treatment with Irinotecan. In addition, the hypothesis for the treatment was supported by the significant survival benefit and tumor growth inhibition of the ETMR, MB Group3 and *ZFTA*-fusion positive EPN models when treated with Irinotecan. However, contradicting to the hypothesis was that the treatment with Irinotecan was also not effective for BT084, the included MB SHH model with *MYCN*-amplification. It is therefore clear that more models of the respective entities studied here need to be tested. But also models of other entities like high-grade glioma for instance and extracranial entities like neuroblastoma or sarcomas need to be tested to evaluate which other entities or subgroups of these entities may respond to these treatments and what the possible biomarkers are to predict the response to Irinotecan alone or in combination with PARP-inhibitors. Additional entities and models will be tested within the BRCAddict-project. The BRCAddict-project comprises *in vivo* treatments of 60 different PDX models distributed over six pediatric solid entities in a single-mouse-trial, meaning only one mouse per model gets tested for a specific treatment. As ten different models per entity will be included, which are all fully characterized molecularly, results can be directly compared. In a first round of treatments five different treatment arms (solvent control; Irinotecan + Temozolomide; Irinotecan + Talazoparib; peg-SN-38 + Talazoparib; Olaparib + AZD6738) will be tested subcutaneously. The best combination will then be tested orthotopically for the brain tumor models

(medulloblastoma and high-grade glioma). Since all used models are fully molecularly characterized, common characteristics of responders and non-responders can be evaluated and biomarkers can be defined, which can be validated in additional PDX models of these and other entities that are available through the ITCC-P4 consortium.

However, to improve treatment strategies for pediatric high-risk tumors it is not only necessary to test new hypothesis-driven treatment approaches but also to use reliable and genetically defined models that mimic the patients' tumor. In many publications cell lines are used that are in culture for a very long time already and for which the metabolism has adapted to the growth *in vitro*. It is known that research results can be error-prone and misleading not only due to cross-contaminations of cell lines with other cell lines but also due to over-culturing and consequently expression of altered key functions and genetic drifts [337]. Therefore, not only models for *in vitro* treatments need to be chosen wisely, also the use of the best matching *in vivo* models will support an easier translation of research findings to clinical use. PDX models are already known to be authentic to the host tumor, maintain heterogeneity and mimic tumor progression and the tendency to metastasize [175-177,338,339]. Nevertheless, further characteristics that reflect not only the original tumor but also considerations to prior anti-cancer treatments, relapses or resistance need to be taken into account. Especially for the evaluation of MoA based treatment approaches it is necessary to keep in mind the situation of the patient. So far, patients are mostly treated with chemotherapy or radiation first before MoA based treatment is applied but this is hardly reflected in preclinical studies. Furthermore, since tumor cells acquire resistance to MoA based treatment strategies frequently, the mechanisms of resistance and their influence on the metabolism of the tumor cells need to be analyzed. By treating the treatment-naïve *PTCH1*-mutated MB SHH PDX model med-1712FH with Sonidegib and applying an intermitted treatment schedule it was possible to generate nine resistant sub-lines with each harboring a different mutation that is responsible for the resistance to Sonidegib. The acquired mutations result in constitutive activation of the HH pathway, confirmed by expression and pathway analysis, that can no longer be inhibited by SMO-inhibitors. The majority of the identified mutations overlap not only with mutations found in resistant BCC and MB tumor models but also with a mutation that was recognized in a patient with a MB that became resistant to treatment with Vismodegib [319]. With the use of resistant models that reflect the mechanisms of resistance observed in patients, effective drugs can be tested and verified. In addition, different treatment strategies and schedules can be tested, for example follow-up treatment of tumors that became resistant with another drug that still shows efficacy or combination treatment approaches that prevent resistance.

Targeting high-risk pediatric brain tumors remains challenging and new treatment strategies can only be developed by collaborative work and streamlining efforts. Many findings and ideas for treatment approaches were published already, however translation into clinical use and investigation of efficacy in clinical trials was only performed and published for few of them. Efficient and successful translation of findings of preclinical research into clinical use needs to be improved by meaningful hypothesis-driven preclinical studies that support the analysis of biomarkers as well as a reasonable selection of model systems and a more rigorous analysis and interpretation of preclinical studies with the same guidelines for efficacy as applied for clinical trials.

8. References

1. Kaatsch P. Epidemiology of childhood cancer. *Cancer treatment reviews.* 2010; 36(4):277-285.

2. Mueller S, Chang S. Pediatric brain tumors: current treatment strategies and future therapeutic approaches. *Neurotherapeutics.* 2009; 6(3):570-586.

3. Ostrom QT, de Blank PM, Kruchko C, et al. Alex's Lemonade Stand Foundation infant and childhood primary brain and central nervous system tumors diagnosed in the United States in 2007–2011. *Neuro-oncology.* 2015; 16(suppl_10):x1-x36.

4. Johnson KJ, Cullen J, Barnholtz-Sloan JS, et al. Childhood brain tumor epidemiology: a brain tumor epidemiology consortium review. *Cancer Epidemiology and Prevention Biomarkers.* 2014; 23(12):2716-2736.

5. Gröbner SN, Worst BC, Weischenfeldt J, et al. The landscape of genomic alterations across childhood cancers. *Nature.* 2018; 555:321.

6. Pfister SM, Capper D, Jones DT. Modern Principles of CNS Tumor Classification. *Brain Tumors in Children*: Springer; 2018:117-129.

7. Northcott PA, Pfister SM, Jones DT. Next-generation (epi) genetic drivers of childhood brain tumours and the outlook for targeted therapies. *The Lancet Oncology.* 2015; 16(6):e293-e302.

8. Louis DN, Perry A, Wesseling P, et al. The 2021 WHO classification of tumors of the central nervous system: a summary. *Neuro-oncology.* 2021; 23(8):1231-1251.

9. Ostrom QT, Gittleman H, Farah P, et al. CBTRUS statistical report: Primary brain and central nervous system tumors diagnosed in the United States in 2006-2010. *Neuro-oncology.* 2013; 15(suppl_2):ii1-ii56.

10. Louis DN, Ohgaki H, Wiestler OD, et al. The 2007 WHO classification of tumours of the central nervous system. *Acta neuropathologica.* 2007; 114(2):97-109.

11. Miller KD, Ostrom QT, Kruchko C, et al. Brain and other central nervous system tumor statistics, 2021. *CA: a cancer journal for clinicians.* 2021; 71(5):381-406.

12. Louis DN, Perry A, Reifenberger G, et al. The 2016 World Health Organization classification of tumors of the central nervous system: a summary. *Acta neuropathologica.* 2016; 131(6):803-820.

13. Smoll NR, Drummond KJ. The incidence of medulloblastomas and primitive neurectodermal tumours in adults and children. *Journal of Clinical Neuroscience.* 2012; 19(11):1541-1544.

14. Northcott PA, Buchhalter I, Morrissy AS, et al. The whole-genome landscape of medulloblastoma subtypes. *Nature.* 2017; 547(7663):311.

15. Eberhart CG, Kepner JL, Goldthwaite PT, et al. Histopathologic grading of medulloblastomas: a Pediatric Oncology Group study. *Cancer.* 2002; 94(2):552-560.

16. Perry A. Medulloblastomas With Favorable Versus Unfavorable Histology: How Many Small Blue Cell Tumor Types are There in the Brain?: On: Histopathologic grading of medulloblastomas. A pediatric oncology group study. Eberhart CG, Kepner JL, Goldthwaite PT, et al. Cancer 200294: 552–560. *Advances in anatomic pathology.* 2002; 9(6):345-350.

17. Khatua S, Song A, Sridhar DC, Mack SC. Childhood medulloblastoma: current therapies, emerging molecular landscape and newer therapeutic insights. *Current neuropharmacology.* 2018; 16(7):1045-1058.

18. Kool M, Korshunov A, Remke M, et al. Molecular subgroups of medulloblastoma: an international meta-analysis of transcriptome, genetic aberrations, and clinical data of WNT, SHH, Group 3, and Group 4 medulloblastomas. *Acta neuropathologica.* 2012; 123(4):473-484.

19. Rutkowski S, Bode U, Deinlein F, et al. Treatment of early childhood medulloblastoma by postoperative chemotherapy alone. *New England Journal of Medicine.* 2005; 352(10):978-986.

20. Chi SN, Gardner SL, Levy AS, et al. Feasibility and response to induction chemotherapy intensified with high-dose methotrexate for young children with newly diagnosed high-risk disseminated medulloblastoma. *Journal of clinical oncology.* 2004; 22(24):4881-4887.

21. Ashley DM, Merchant TE, Strother D, et al. Induction chemotherapy and conformal radiation therapy for very young children with nonmetastatic medulloblastoma: Children's Oncology Group study P9934. *Journal of clinical oncology.* 2012; 30(26):3181.

22. Gottardo NG, Gajjar A. Current therapy for medulloblastoma. *Current treatment options in neurology.* 2006; 8(4):319-334.

23. Mabbott DJ, Penkman L, Witol A, Strother D, Bouffet E. Core neurocognitive functions in children treated for posterior fossa tumors. *Neuropsychology.* 2008; 22(2):159.

24. Gudrunardottir T, Lannering B, Remke M, et al. Treatment developments and the unfolding of the quality of life discussion in childhood medulloblastoma: a review. *Child's Nervous System.* 2014; 30(6):979-990.

25. Juraschka K, Taylor MD. Medulloblastoma in the age of molecular subgroups: a review: JNSPG 75th Anniversary Invited Review Article. *Journal of Neurosurgery: Pediatrics.* 2019; 24(4):353-363.

26. Cho Y-J, Tsherniak A, Tamayo P, et al. Integrative genomic analysis of medulloblastoma identifies a molecular subgroup that drives poor clinical outcome. *Journal of Clinical Oncology.* 2011; 29(11):1424.

27. Northcott PA, Korshunov A, Witt H, et al. Medulloblastoma comprises four distinct molecular variants. *Journal of clinical oncology.* 2011; 29(11):1408.

28. Kool M, Koster J, Bunt J, et al. Integrated genomics identifies five medulloblastoma subtypes with distinct genetic profiles, pathway signatures and clinicopathological features. *PloS one.* 2008; 3(8):e3088.

29. Thompson MC, Fuller C, Hogg TL, et al. Genomics identifies medulloblastoma subgroups that are enriched for specific genetic alterations. *Journal of clinical oncology.* 2006; 24(12):1924-1931.

30. Taylor MD, Northcott PA, Korshunov A, et al. Molecular subgroups of medulloblastoma: the current consensus. *Acta neuropathologica.* 2012; 123(4):465-472.

31. Faria CC, Smith CA, Rutka JT. New Molecular Targets and Treatments for Pediatric Brain Tumors. *Evolution of the Molecular Biology of Brain Tumors and the Therapeutic Implications*: IntechOpen; 2013.

32. Northcott PA, Jones DT, Kool M, et al. Medulloblastomics: the end of the beginning. *Nature Reviews Cancer.* 2012; 12(12):818-834.

33. Forget A, Martignetti L, Puget S, et al. Aberrant ERBB4-SRC signaling as a hallmark of group 4 medulloblastoma revealed by integrative phosphoproteomic profiling. *Cancer cell.* 2018; 34(3):379-395. e377.

34. Northcott PA, Shih DJ, Peacock J, et al. Subgroup-specific structural variation across 1,000 medulloblastoma genomes. *Nature.* 2012; 488(7409):49-56.

35. Garcia-Lopez J, Kumar R, Smith KS, Northcott PA. Deconstructing sonic hedgehog medulloblastoma: molecular subtypes, drivers, and beyond. *Trends in Genetics.* 2020.

36. Hovestadt V, Ayrault O, Swartling FJ, Robinson GW, Pfister SM, Northcott PA. Medulloblastomics revisited: biological and clinical insights from thousands of patients. *Nature Reviews Cancer.* 2020; 20(1):42-56.

37. Kumar R, Liu AP, Northcott PA. Medulloblastoma genomics in the modern molecular era. *Brain Pathology.* 2020; 30(3):679-690.

38. Hamilton SR, Liu B, Parsons RE, et al. The molecular basis of Turcot's syndrome. *New England Journal of Medicine.* 1995; 332(13):839-847.

39. Zurawel RH, Chiappa SA, Allen C, Raffel C. Sporadic medulloblastomas contain oncogenic β-catenin mutations. *Cancer research.* 1998; 58(5):896-899.

40. Waszak SM, Northcott PA, Buchhalter I, et al. Spectrum and prevalence of genetic predisposition in medulloblastoma: a retrospective genetic study and prospective validation in a clinical trial cohort. *The Lancet Oncology.* 2018; 19(6):785-798.

41. Zhan T, Rindtorff N, Boutros M. Wnt signaling in cancer. *Oncogene.* 2017; 36(11):1461-1473.

42. Eberhart CG, Tihan T, Burger PC. Nuclear localization and mutation of β-catenin in medulloblastomas. *Journal of Neuropathology & Experimental Neurology.* 2000; 59(4):333-337.

43. Zhukova N, Ramaswamy V, Remke M, et al. Subgroup-specific prognostic implications of TP53 mutation in medulloblastoma. *Journal of Clinical Oncology.* 2013; 31(23):2927.

44. Phoenix TN, Patmore DM, Boop S, et al. Medulloblastoma genotype dictates blood brain barrier phenotype. *Cancer cell.* 2016; 29(4):508-522.

45. Cattelino A, Liebner S, Gallini R, et al. The conditional inactivation of the β-catenin gene in endothelial cells causes a defective vascular pattern and increased vascular fragility. *The Journal of cell biology.* 2003; 162(6):1111-1122.

46. Cavalli FM, Remke M, Rampasek L, et al. Intertumoral heterogeneity within medulloblastoma subgroups. *Cancer cell.* 2017; 31(6):737-754. e736.

47. Bale SJ, Falk RT, Rogers GR. Patching together the genetics of Gorlin syndrome. *Journal of cutaneous medicine and surgery.* 1998; 3(1):31-34.

48. Taylor MD, Mainprize TG, Rutka JT. Molecular insight into medulloblastoma and central nervous system primitive neuroectodermal tumor biology from hereditary syndromes: a review. *Neurosurgery.* 2000; 47(4):888-901.

49. Brugières L, Pierron G, Chompret A, et al. Incomplete penetrance of the predisposition to medulloblastoma associated with germ-line SUFU mutations. *Journal of medical genetics.* 2010; 47(2):142-144.

50. Pastorino L, Ghiorzo P, Nasti S, et al. Identification of a SUFU germline mutation in a family with Gorlin syndrome. *American journal of medical genetics Part A.* 2009; 149(7):1539-1543.

51. Slade I, Murray A, Hanks S, et al. Heterogeneity of familial medulloblastoma and contribution of germline PTCH1 and SUFU mutations to sporadic medulloblastoma. *Familial cancer.* 2011; 10(2):337-342.

52. Taylor MD, Liu L, Raffel C, et al. Mutations in SUFU predispose to medulloblastoma. *Nature genetics.* 2002; 31(3):306-310.

53. Twigg SR, Hufnagel RB, Miller KA, et al. A recurrent mosaic mutation in SMO, encoding the hedgehog signal transducer smoothened, is the major cause of Curry-Jones syndrome. *The American Journal of Human Genetics.* 2016; 98(6):1256-1265.

54. Waszak SM, Giles W, Gudenas BL, et al. Germline elongator mutations in sonic hedgehog medulloblastoma. *Nature.* 2020; 580(7803):396-401.

55. Begemann M, Waszak SM, Robinson GW, et al. Germline GPR161 mutations predispose to pediatric medulloblastoma. *Journal of Clinical Oncology.* 2020; 38(1):43.

56. Northcott PA, Hielscher T, Dubuc A, et al. Pediatric and adult sonic hedgehog medulloblastomas are clinically and molecularly distinct. *Acta neuropathologica.* 2011; 122(2):231-240.

57. Northcott PA, Nakahara Y, Wu X, et al. Multiple recurrent genetic events converge on control of histone lysine methylation in medulloblastoma. *Nature genetics.* 2009; 41(4):465-472.

58. Kool M, Jones DT, Jäger N, et al. Genome sequencing of SHH medulloblastoma predicts genotype-related response to smoothened inhibition. *Cancer cell.* 2014; 25(3):393-405.

59. Skowron P, Farooq H, Cavalli FM, et al. The transcriptional landscape of Shh medulloblastoma. *Nature communications.* 2021; 12(1):1-17.

60. Killela PJ, Reitman ZJ, Jiao Y, et al. TERT promoter mutations occur frequently in gliomas and a subset of tumors derived from cells with low rates of self-renewal. *Proceedings of the National Academy of Sciences.* 2013; 110(15):6021-6026.

61. Remke M, Ramaswamy V, Peacock J, et al. TERT promoter mutations are highly recurrent in SHH subgroup medulloblastoma. *Acta neuropathologica.* 2013; 126(6):917-929.

62. Szalontay L, Khakoo Y. Medulloblastoma: an old diagnosis with new promises. *Current Oncology Reports.* 2020; 22(9):1-13.

63. Adamson DC, Shi Q, Wortham M, et al. OTX2 is critical for the maintenance and progression of Shh-independent medulloblastomas. *Cancer research.* 2010; 70(1):181-191.

64. de Haas T, Oussoren E, Grajkowska W, et al. OTX1 and OTX2 expression correlates with the clinicopathologic classification of medulloblastomas. *Journal of Neuropathology & Experimental Neurology.* 2006; 65(2):176-186.

65. Schwalbe EC, Lindsey JC, Nakjang S, et al. Novel molecular subgroups for clinical classification and outcome prediction in childhood medulloblastoma: a cohort study. *The Lancet Oncology.* 2017; 18(7):958-971.

66. Sharma T, Schwalbe EC, Williamson D, et al. Second-generation molecular subgrouping of medulloblastoma: an international meta-analysis of Group 3 and Group 4 subtypes. *Acta neuropathologica.* 2019; 138(2):309-326.

67. Möröy T, Vassen L, Wilkes B, Khandanpour C. From cytopenia to leukemia: the role of Gfi1 and Gfi1b in blood formation. *Blood, The Journal of the American Society of Hematology.* 2015; 126(24):2561-2569.

68. Northcott PA, Buchhalter I, Morrissy AS, et al. The whole-genome landscape of medulloblastoma subtypes. *Nature.* 2017; 547:311.

69. Northcott PA, Lee C, Zichner T, et al. Enhancer hijacking activates GFI1 family oncogenes in medulloblastoma. *Nature.* 2014; 511(7510):428-434.

70. Wang X, Xu J, Zhang B, et al. Genome-wide detection of enhancer-hijacking events from chromatin interaction data in rearranged genomes. *Nature Methods.* 2021; 18(6):661-668.

71. Zimmerman MW, Liu Y, He S, et al. MYC drives a subset of high-risk pediatric neuroblastomas and is activated through mechanisms including enhancer hijacking and focal enhancer amplification. *Cancer discovery.* 2018; 8(3):320-335.

72. Korshunov A, Witt H, Hielscher T, et al. Molecular staging of intracranial ependymoma in children and adults. *Journal of Clinical Oncology.* 2010; 28(19):3182-3190.

73. Purdy E, Johnston DL, Bartels U, et al. Ependymoma in children under the age of 3 years: a report from the Canadian Pediatric Brain Tumour Consortium. *Journal of neuro-oncology.* 2014; 117(2):359-364.

74. Villano J, Parker C, Dolecek T. Descriptive epidemiology of ependymal tumours in the United States. *British journal of cancer.* 2013; 108(11):2367-2371.

75. Kilday J-P, Rahman R, Dyer S, et al. Pediatric ependymoma: biological perspectives. *Molecular Cancer Research.* 2009; 7(6):765-786.

76. Vera-Bolanos E, Aldape K, Yuan Y, et al. Clinical course and progression-free survival of adult intracranial and spinal ependymoma patients. *Neuro-oncology.* 2015; 17(3):440-447.

77. Gajjar A, Pfister SM, Taylor MD, Gilbertson RJ. Molecular insights into pediatric brain tumors have the potential to transform therapy. *Clin Cancer Res.* 2014; 20(22):5630-5640.

78. Ostrum Q, Gittleman H, Liao P, et al. CBTRUS statistical report: primary brain and central nervous system tumors diagnosed in the United States in 2007–2011. *Neuro Oncol.* 2014; 16(S4)):iv1-iv63.

79. Merchant TE, Li C, Xiong X, Kun LE, Boop FA, Sanford RA. Conformal radiotherapy after surgery for paediatric ependymoma: a prospective study. *The lancet oncology.* 2009; 10(3):258-266.

80. Gerstner ER, Pajtler KW. Ependymoma. Paper presented at: Seminars in neurology2018.

81. Ellison DW, Kocak M, Figarella-Branger D, et al. Histopathological grading of pediatric ependymoma: reproducibility and clinical relevance in European trial cohorts. *Journal of negative results in biomedicine.* 2011; 10(1):1-13.

82. Tihan T, Zhou T, Holmes E, Burger PC, Ozuysal S, Rushing EJ. The prognostic value of histological grading of posterior fossa ependymomas in children: a Children's Oncology Group study and a review of prognostic factors. *Modern pathology.* 2008; 21(2):165-177.

83. Godfraind C. Classification and controversies in pathology of ependymomas. *Child's nervous system.* 2009; 25(10):1185.

84. Pajtler KW, Witt H, Sill M, et al. Molecular classification of ependymal tumors across all CNS compartments, histopathological grades, and age groups. *Cancer cell.* 2015; 27(5):728-743.

85. Wani K, Armstrong TS, Vera-Bolanos E, et al. A prognostic gene expression signature in infratentorial ependymoma. *Acta neuropathologica.* 2012; 123(5):727-738.

86. Witt H, Mack SC, Ryzhova M, et al. Delineation of two clinically and molecularly distinct subgroups of posterior fossa ependymoma. *Cancer cell.* 2011; 20(2):143-157.

87. Mack SC, Witt H, Piro R, et al. Epigenomic alterations define lethal CIMP-positive ependymomas of infancy. *Nature.* 2014; 506(7489):445-450.

88. Zacharoulis S, Ashley S, Moreno L, Gentet J-C, Massimino M, Frappaz D. Treatment and outcome of children with relapsed ependymoma: a multi-institutional retrospective analysis. *Child's nervous system.* 2010; 26(7):905-911.

89. Hübner J-M, Müller T, Papageorgiou DN, et al. EZHIP/CXorf67 mimics K27M mutated oncohistones and functions as an intrinsic inhibitor of PRC2 function in aggressive posterior fossa ependymoma. *Neuro-oncology.* 2019; 21(7):878-889.

90. Panwalkar P, Clark J, Ramaswamy V, et al. Immunohistochemical analysis of H3K27me3 demonstrates global reduction in group-A childhood posterior fossa ependymoma and is a powerful predictor of outcome. *Acta Neuropathologica.* 2017:1-10.

91. Gessi M, Capper D, Sahm F, et al. Evidence of H3 K27M mutations in posterior fossa ependymomas. *Acta neuropathologica.* 2016; 132(4):635-637.

92. Ryall S, Guzman M, Elbabaa SK, et al. H3 K27M mutations are extremely rare in posterior fossa group A ependymoma. *Child's Nervous System.* 2017; 33(7):1047-1051.

93. Toescu SM, Aquilina K. Current and emerging methods of management of ependymoma. *Current oncology reports.* 2019; 21(9):1-9.

94. Parker M, Mohankumar KM, Punchihewa C, et al. C11orf95–RELA fusions drive oncogenic NF-κB signalling in ependymoma. *Nature.* 2014; 506(7489):451-455.

95. Wu J, Armstrong TS, Gilbert MR. Biology and management of ependymomas. *Neuro-oncology.* 2016; 18(7):902-913.

96. Ellison DW, Aldape KD, Capper D, et al. cIMPACT-NOW update 7: Advancing the molecular classification of ependymal tumors. *Brain Pathology.* 2020; 30(5):863-866.

97. Ghasemi DR, Sill M, Okonechnikov K, et al. MYCN amplification drives an aggressive form of spinal ependymoma. *Acta neuropathologica.* 2019; 138(6):1075-1089.

98. Tamai S, Nakano Y, Kinoshita M, et al. Ependymoma with C11orf95-MAML2 fusion: presenting with granular cell and ganglion cell features. *Brain Tumor Pathology.* 2021; 38(1):64-70.

99. Guttridge DC, Albanese C, Reuther JY, Pestell RG, Baldwin Jr AS. NF-κB controls cell growth and differentiation through transcriptional regulation of cyclin D1. *Molecular and cellular biology.* 1999; 19(8):5785-5799.

100. Hinz M, Krappmann D, Eichten A, Heder A, Scheidereit C, Strauss M. NF-κB function in growth control: regulation of cyclin D1 expression and G0/G1-to-S-phase transition. *Molecular and cellular biology.* 1999; 19(4):2690-2698.

101. Kiefel H, Pfeifer M, Bondong S, Hazin J, Altevogt P. Linking L1CAM-mediated signaling to NF-κB activation. *Trends in molecular medicine.* 2011; 17(4):178-187.

102. Kiefel H, Bondong S, Pfeifer M, et al. EMT-associated up-regulation of L1CAM provides insights into L1CAM-mediated integrin signalling and NF-κB activation. *Carcinogenesis.* 2012; 33(10):1919-1929.

103. Hübner J-M, Kool M, Pfister SM, Pajtler KW. Epidemiology, molecular classification and WHO grading of ependymoma. *Journal of neurosurgical sciences.* 2017; 62(1):46-50.

104. Korshunov A, Sturm D, Ryzhova M, et al. Embryonal tumor with abundant neuropil and true rosettes (ETANTR), ependymoblastoma, and medulloepithelioma share molecular similarity and comprise a single clinicopathological entity. *Acta neuropathologica.* 2014; 128(2):279-289.

105. Spence T, Sin-Chan P, Picard D, et al. CNS-PNETs with C19MC amplification and/or LIN28 expression comprise a distinct histogenetic diagnostic and therapeutic entity. *Acta neuropathologica.* 2014; 128(2):291-303.

106. Lambo S, von Hoff K, Korshunov A, Pfister SM, Kool M. ETMR: a tumor entity in its infancy. *Acta Neuropathologica.* 2020:1-18.

107. Juhnke B-O, Gessi M, Gerber NU, et al. Treatment of Embryonal Tumours with Multilayered Rosettes with Carboplatin/Etoposide Induction and High-dose Chemotherapy within the Prospective P-HIT Trial. *Neuro-oncology.* 2021.

108. Lambo S, Gröbner SN, Rausch T, et al. The molecular landscape of ETMR at diagnosis and relapse. *Nature.* 2019; 576(7786):274-280.

109. Horwitz M, Dufour C, Leblond P, et al. Embryonal tumors with multilayered rosettes in children: the SFCE experience. *Child's nervous system.* 2016; 32(2):299-305.

110. Gessi M, Giangaspero F, Lauriola L, et al. Embryonal tumors with abundant neuropil and true rosettes: a distinctive CNS primitive neuroectodermal tumor. *The American journal of surgical pathology.* 2009; 33(2):211.

111. Eberhart CG, Brat DJ, Cohen KJ, Burger PC. Pediatric neuroblastic brain tumors containing abundant neuropil and true rosettes. *Pediatric and Developmental Pathology.* 2000; 3(4):346-352.

112. Korshunov A, Remke M, Gessi M, et al. Focal genomic amplification at 19q13. 42 comprises a powerful diagnostic marker for embryonal tumors with ependymoblastic rosettes. *Acta neuropathologica.* 2010; 120(2):253-260.

113. Li M, Lee KF, Lu Y, et al. Frequent amplification of a chr19q13. 41 microRNA polycistron in aggressive primitive neuroectodermal brain tumors. *Cancer cell.* 2009; 16(6):533-546.

114. Pfister S, Remke M, Castoldi M, et al. Novel genomic amplification targeting the microRNA cluster at 19q13. 42 in a pediatric embryonal tumor with abundant neuropil and true rosettes. *Acta neuropathologica.* 2009; 117(4):457-464.

115. von Hoff K, Haberler C, Schmitt-Hoffner F, et al. Therapeutic Implications of Improved Molecular Diagnostics for Rare CNS-Embryonal Tumor Entities: Results of an International, Retrospective, Observational Study. 2021.

116. Kleinman CL, Gerges N, Papillon-Cavanagh S, et al. Fusion of TTYH1 with the C19MC microRNA cluster drives expression of a brain-specific DNMT3B isoform in the embryonal brain tumor ETMR. *Nature genetics.* 2014; 46(1):39-44.

117. Korshunov A, Ryzhova M, Jones DT, et al. LIN28A immunoreactivity is a potent diagnostic marker of embryonal tumor with multilayered rosettes (ETMR). *Acta neuropathologica.* 2012; 124(6):875-881.

118. Shah AH, Khatib Z, Niazi T. Extracranial extra-CNS spread of embryonal tumor with multilayered rosettes (ETMR): case series and systematic review. *Child's Nervous System.* 2018; 34(4):649-654.

119. Khan S, Solano-Paez P, Suwal T, et al. Clinical phenotypes and prognostic features of embryonal tumours with multi-layered rosettes: a Rare Brain Tumor Registry study. *The Lancet Child & Adolescent Health.* 2021.

120. Jaramillo S, Grosshans DR, Philip N, et al. Radiation for ETMR: Literature review and case series of patients treated with proton therapy. *Clinical and translational radiation oncology.* 2019; 15:31-37.

121. Adamson PC. Improving the outcome for children with cancer: Development of targeted new agents. *CA: a cancer journal for clinicians.* 2015; 65(3):212-220.

122. Siegel Rebecca L, Miller Kimberly D. Jemal Ahmedin. Cancer statistics, 2019. *CA: a cancer journal for clinicians.* 2019; 69(1):7-34.

123. Girardi F, Allemani C, Coleman MP. Worldwide trends in survival from common childhood brain tumors: a systematic review. *Journal of global oncology.* 2019; 5:1-25.

124. McGregor LM, Metzger ML, Sanders R, Santana VM. Pediatric cancers in the new millennium: dramatic progress, new challenges. *Oncology.* 2007; 21(7):809.

125. van Tilburg CM, Pfaff E, Pajtler KW, et al. The pediatric precision oncology study INFORM: Clinical outcome and benefit for molecular subgroups: American Society of Clinical Oncology; 2020.

126. Duke ES, Packer RJ. Update on Pediatric Brain Tumors: the Molecular Era and Neuro-immunologic Beginnings. *Current neurology and neuroscience reports.* 2020; 20:1-8.

127. Pollack IF, Agnihotri S, Broniscer A. Childhood brain tumors: current management, biological insights, and future directions: JNSPG 75th anniversary invited review article. *Journal of Neurosurgery: Pediatrics.* 2019; 23(3):261-273.

128. Karajannis M, Allen JC, Newcomb EW. Treatment of pediatric brain tumors. *Journal of cellular physiology.* 2008; 217(3):584-589.

129. Bhatia S, Landier W. Evaluating survivors of pediatric cancer. *The Cancer Journal.* 2005; 11(4):340-354.

130. Mazor T, Pankov A, Johnson BE, et al. DNA methylation and somatic mutations converge on the cell cycle and define similar evolutionary histories in brain tumors. *Cancer cell.* 2015; 28(3):307-317.

131. Hovestadt V, Remke M, Kool M, et al. Robust molecular subgrouping and copy-number profiling of medulloblastoma from small amounts of archival tumour material using high-density DNA methylation arrays. *Acta neuropathologica.* 2013; 125(6):913-916.

132. Sturm D, Orr BA, Toprak UH, et al. New brain tumor entities emerge from molecular classification of CNS-PNETs. *Cell.* 2016; 164(5):1060-1072.

133. DeWitt JC, Mock A, Louis DN. The 2016 WHO classification of central nervous system tumors: what neurologists need to know. *Current opinion in neurology.* 2017; 30(6):643-649.

134. Komori T. The 2016 WHO classification of tumours of the central nervous system: the major points of revision. *Neurologia medico-chirurgica.* 2017; 57(7):301-311.

135. Hirose T. 2016 WHO Classification of Tumors of CNS: A Paradigm Shift from Histologic to Molecular Classification. *Brain and nerve= Shinkei kenkyu no shinpo.* 2018; 70(5):543-550.

136. Sawyers C. Targeted cancer therapy. *Nature.* 2004; 432(7015):294-297.

137. Institute NIoH-NC. Targeted Therapy to Treat Cancer 2020; https://www.cancer.gov/about-cancer/treatment/types/targeted-therapies. Accessed November 16th, 2021.

138. Abou-Jawde R, Choueiri T, Alemany C, Mekhail T. An overview of targeted treatments in cancer. *Clinical therapeutics.* 2003; 25(8):2121-2137.

139. Slamon DJ, Leyland-Jones B, Shak S, et al. Use of chemotherapy plus a monoclonal antibody against HER2 for metastatic breast cancer that overexpresses HER2. *New England journal of medicine.* 2001; 344(11):783-792.

140. Emole J, Talabi T, Pinilla-Ibarz J. Update on the management of Philadelphia chromosome positive chronic myelogenous leukemia: role of nilotinib. *Biologics: targets & therapy.* 2016; 10:23.

141. Kang Z-J, Liu Y-F, Xu L-Z, et al. The Philadelphia chromosome in leukemogenesis. *Chinese journal of cancer.* 2016; 35(1):1-15.

142. Druker BJ, Sawyers CL, Kantarjian H, et al. Activity of a specific inhibitor of the BCR-ABL tyrosine kinase in the blast crisis of chronic myeloid leukemia and acute lymphoblastic leukemia with the Philadelphia chromosome. *New England Journal of Medicine.* 2001; 344(14):1038-1042.

143. Druker BJ, Talpaz M, Resta DJ, et al. Efficacy and safety of a specific inhibitor of the BCR-ABL tyrosine kinase in chronic myeloid leukemia. *New England Journal of Medicine.* 2001; 344(14):1031-1037.

144. Goldman JM, Melo JV. Targeting the BCR-ABL tyrosine kinase in chronic myeloid leukemia: Mass Medical Soc; 2001.

145. Schindler G, Capper D, Meyer J, et al. Analysis of BRAF V600E mutation in 1,320 nervous system tumors reveals high mutation frequencies in pleomorphic xanthoastrocytoma, ganglioglioma and extra-cerebellar pilocytic astrocytoma. *Acta neuropathologica.* 2011; 121(3):397-405.

146. Davies H, Bignell GR, Cox C, et al. Mutations of the BRAF gene in human cancer. *Nature.* 2002; 417(6892):949-954.

147. Montagut C, Settleman J. Targeting the RAF–MEK–ERK pathway in cancer therapy. *Cancer letters.* 2009; 283(2):125-134.

148. Del Bufalo F, Ceglie G, Cacchione A, et al. BRAF V600E inhibitor (Vemurafenib) for BRAF V600E mutated low grade gliomas. *Frontiers in oncology.* 2018; 8:526.

149. Neel DS, Bivona TG. Resistance is futile: overcoming resistance to targeted therapies in lung adenocarcinoma. *NPJ precision oncology.* 2017; 1(1):1-6.

150. Ko B, He T, Gadgeel S, Halmos B. MET/HGF pathway activation as a paradigm of resistance to targeted therapies. *Annals of translational medicine.* 2017; 5(1).

151. Flaherty KT, Infante JR, Daud A, et al. Combined BRAF and MEK inhibition in melanoma with BRAF V600 mutations. *New England Journal of Medicine.* 2012; 367(18):1694-1703.

152. Wen PY, Stein A, van den Bent M, et al. Dabrafenib plus trametinib in patients with BRAFV600E-mutant low-grade and high-grade glioma (ROAR): a multicentre, open-label, single-arm, phase 2, basket trial. *The Lancet Oncology.* 2021.

153. Rubinstein L, Shoemaker R, Paull K, et al. Comparison of in vitro anticancer-drug-screening data generated with a tetrazolium assay versus a protein assay against a diverse panel of human tumor cell lines. *JNCI: Journal of the National Cancer Institute.* 1990; 82(13):1113-1117.

154. Katt ME, Placone AL, Wong AD, Xu ZS, Searson PC. In vitro tumor models: advantages, disadvantages, variables, and selecting the right platform. *Frontiers in bioengineering and biotechnology.* 2016; 4:12.

155. Workman P, Aboagye E, Balkwill F, et al. Guidelines for the welfare and use of animals in cancer research. *British journal of cancer.* 2010; 102(11):1555-1577.

156. Lilienblum W, Dekant W, Foth H, et al. Alternative methods to safety studies in experimental animals: role in the risk assessment of chemicals under the new European Chemicals Legislation (REACH). *Archives of toxicology.* 2008; 82(4):211-236.

157. Zellmer S, Schmidt-Heck W, Godoy P, et al. Transcription factors ETF, E2F, and SP-1 are involved in cytokine-independent proliferation of murine hepatocytes. *Hepatology.* 2010; 52(6):2127-2136.

158. Ghallab A. In vitro test systems and their limitations. *EXCLI journal.* 2013; 12:1024.

159. Tice RR, Austin CP, Kavlock RJ, Bucher JR. Improving the human hazard characterization of chemicals: a Tox21 update. *Environmental health perspectives.* 2013; 121(7):756-765.

160. Hausser H-J, Brenner RE. Phenotypic instability of Saos-2 cells in long-term culture. *Biochemical and biophysical research communications.* 2005; 333(1):216-222.

161. Gillet J-P, Calcagno AM, Varma S, et al. Redefining the relevance of established cancer cell lines to the study of mechanisms of clinical anti-cancer drug resistance. *Proceedings of the National Academy of Sciences.* 2011; 108(46):18708-18713.

162. Johnson J, Decker S, Zaharevitz D, et al. Relationships between drug activity in NCI preclinical in vitro and in vivo models and early clinical trials. *British journal of cancer.* 2001; 84(10):1424-1431.

163. Perlman RL. Mouse models of human diseaseAn evolutionary perspective. *Evolution, medicine, and public health.* 2016; 2016(1):170-176.

164. Monaco G, van Dam S, Ribeiro JLCN, Larbi A, de Magalhães JP. A comparison of human and mouse gene co-expression networks reveals conservation and divergence at the tissue, pathway and disease levels. *BMC evolutionary biology.* 2015; 15(1):1-14.

165. Waterston RH, Pachter L. Initial sequencing and comparative analysis of the mouse genome. *Nature.* 2002; 420(6915):520-562.

166. Liao B-Y, Zhang J. Evolutionary conservation of expression profiles between human and mouse orthologous genes. *Molecular biology and evolution.* 2006; 23(3):530-540.

167. Tacutu R, Budovsky A, Yanai H, Fraifeld VE. Molecular links between cellular senescence, longevity and age-related diseases–a systems biology perspective. *Aging (Albany NY).* 2011; 3(12):1178.

168. De Magalhães JP, Church GM. Analyses of human–chimpanzee orthologous gene pairs to explore evolutionary hypotheses of aging. *Mechanisms of ageing and development.* 2007; 128(5-6):355-364.

169. Chan ET, Quon GT, Chua G, et al. Conservation of core gene expression in vertebrate tissues. *Journal of biology.* 2009; 8(3):1-17.

170. Miller JA, Horvath S, Geschwind DH. Divergence of human and mouse brain transcriptome highlights Alzheimer disease pathways. *Proceedings of the National Academy of Sciences.* 2010; 107(28):12698-12703.

171. Sharpless NE, DePinho RA. The mighty mouse: genetically engineered mouse models in cancer drug development. *Nature reviews Drug discovery.* 2006; 5(9):741-754.

172. Vandamme TF. Use of rodents as models of human diseases. *Journal of pharmacy & bioallied sciences.* 2014; 6(1):2.

173. Lampreht Tratar U, Horvat S, Cemazar M. Transgenic mouse models in cancer research. *Frontiers in oncology.* 2018; 8:268.

174. Lwin TM, Hoffman RM, Bouvet M. Advantages of patient-derived orthotopic mouse models and genetic reporters for developing fluorescence-guided surgery. *Journal of surgical oncology.* 2018; 118(2):253-264.

175. Tentler JJ, Tan AC, Weekes CD, et al. Patient-derived tumour xenografts as models for oncology drug development. *Nature reviews Clinical oncology.* 2012; 9(6):338-350.

176. Hidalgo M, Amant F, Biankin AV, et al. Patient-derived xenograft models: an emerging platform for translational cancer research. *Cancer discovery.* 2014; 4(9):998-1013.

177. Brabetz S, Leary SE, Gröbner SN, et al. A biobank of patient-derived pediatric brain tumor models. *Nature medicine.* 2018; 24(11):1752-1761.

178. Calles A, Rubio-Viqueira B, Hidalgo M. Primary Human Non-Small Cell Lung and Pancreatic Tumorgraft Models—Utility and Applications in Drug Discovery and Tumor Biology. *Current protocols in pharmacology.* 2013; 61(1):14.26. 11-14.26. 21.

179. Siolas D, Hannon GJ. Patient-derived tumor xenografts: transforming clinical samples into mouse models. *Cancer research.* 2013; 73(17):5315-5319.

180. Hutchinson L, Kirk R. High drug attrition rates—where are we going wrong? *Nature reviews Clinical oncology.* 2011; 8(4):189-190.

181. Rubin EH, Gilliland DG. Drug development and clinical trials—the path to an approved cancer drug. *Nature reviews Clinical oncology.* 2012; 9(4):215-222.

182. Begley CG, Ellis LM. Raise standards for preclinical cancer research. *Nature.* 2012; 483(7391):531-533.

183. Francia G, Kerbel RS. Raising the bar for cancer therapy models. *Nature biotechnology.* 2010; 28(6):561-562.

184. Boyd MR. The NCI in vitro anticancer drug discovery screen. *Anticancer drug development guide*: Springer; 1997:23-42.

185. Venditti JM, Wesley RA, Plowman J. Current NCI preclinical antitumor screening in vivo: results of tumor panel screening, 1976–1982, and future directions. *Advances in Pharmacology.* 1984; 20:1-20.

186. Houghton PJ, Adamson PC, Blaney S, et al. Testing of new agents in childhood cancer preclinical models: meeting summary. *Clinical cancer research.* 2002; 8(12):3646-3657.

187. Stewart E, Goshorn R, Bradley C, et al. Targeting the DNA repair pathway in Ewing sarcoma. *Cell reports.* 2014; 9(3):829-840.

188. Schubert NA, Lowery CD, Bergthold G, et al. Systematic target actionability reviews of preclinical proof-of-concept papers to match targeted drugs to paediatric cancers. *European Journal of Cancer.* 2020; 130:168-181.

189. Kaylee M. Keller *, Sonja Krausert *, Apurva Gopisetty *, Dan Luedtke, Jan Koster, Nil A. Schubert, Ana Rodríguez, Sander R. van Hooff, Damian Stichel, M. Emmy M. Dolman, Gilles Vassal, Stefan M. Pfister, Hubert N. Caron, Louis F. Stancato, Jan J. Molenaar**, Natalie Jäger**, and Marcel Kool**. Target Actionability Review: a systematic evaluation of replication stress as a therapeutic target for pediatric solid malignancies. *European Journal of Cancer.* 2021; accepted; in press.

190. Kovalchik S. RISmed: download content from NCBI databases. *R package version.* 2015; 2(5).

191. Wang K, Li M, Hakonarson H. ANNOVAR: functional annotation of genetic variants from high-throughput sequencing data. *Nucleic acids research.* 2010; 38(16):e164-e164.

192. Dobin A, Davis CA, Schlesinger F, et al. STAR: ultrafast universal RNA-seq aligner. *Bioinformatics.* 2013; 29(1):15-21.

193. Li H, Durbin R. Fast and accurate short read alignment with Burrows–Wheeler transform. *bioinformatics.* 2009; 25(14):1754-1760.

194. Subramanian A, Tamayo P, Mootha VK, et al. Gene set enrichment analysis: a knowledge-based approach for interpreting genome-wide expression profiles. *Proceedings of the National Academy of Sciences.* 2005; 102(43):15545-15550.

195. Liberzon A, Subramanian A, Pinchback R, Thorvaldsdóttir H, Tamayo P, Mesirov JP. Molecular signatures database (MSigDB) 3.0. *Bioinformatics.* 2011; 27(12):1739-1740.

196. Capper D, Jones DT, Sill M, et al. DNA methylation-based classification of central nervous system tumours. *Nature.* 2018; 555(7697):469-474.

197. Lin GL, Monje M. A protocol for rapid post-mortem cell culture of diffuse intrinsic pontine glioma (DIPG). *Journal of visualized experiments: JoVE.* 2017(121).

198. Potdar S, Ianevski A, Mpindi J-P, et al. Breeze: an integrated quality control and data analysis application for high-throughput drug screening. *Bioinformatics.* 2020; 36(11):3602-3604.

199. Zwaan CM, Kearns P, Caron H, et al. The role of the 'innovative therapies for children with cancer'(ITCC) European consortium. *Cancer treatment reviews.* 2010; 36(4):328-334.

200. Desany BA, Alcasabas AA, Bachant JB, Elledge SJ. Recovery from DNA replicational stress is the essential function of the S-phase checkpoint pathway. *Genes & development.* 1998; 12(18):2956-2970.

201. Zeman MK, Cimprich KA. Causes and consequences of replication stress. *Nature cell biology.* 2014; 16(1):2-9.

202. Yao Y, Dai W. Genomic instability and cancer. *Journal of carcinogenesis & mutagenesis.* 2014; 5.

203. Ubhi T, Brown GW. Exploiting DNA replication stress for cancer treatment. *Cancer research.* 2019; 79(8):1730-1739.

204. Kopp LM, Gupta P, Pelayo-Katsanis L, Wittman B, Katsanis E. Late effects in adult survivors of pediatric cancer: a guide for the primary care physician. *The American journal of medicine.* 2012; 125(7):636-641.

205. Osborn AJ, Elledge SJ, Zou L. Checking on the fork: the DNA-replication stress-response pathway. *Trends in cell biology.* 2002; 12(11):509-516.

206. Macheret M, Halazonetis TD. DNA replication stress as a hallmark of cancer. *Annual Review of Pathology: Mechanisms of Disease.* 2015; 10:425-448.

207. Halazonetis TD, Gorgoulis VG, Bartek J. An oncogene-induced DNA damage model for cancer development. *science.* 2008; 319(5868):1352-1355.

208. Henssen AG, Reed C, Jiang E, et al. Therapeutic targeting of PGBD5-induced DNA repair dependency in pediatric solid tumors. *Science translational medicine.* 2017; 9(414).

209. Cole KA, Pal S, Kudgus RA, et al. Phase I clinical trial of the Wee1 inhibitor adavosertib (AZD1775) with irinotecan in children with relapsed solid tumors: a COG phase I consortium report (ADVL1312). *Clinical Cancer Research.* 2020; 26(6):1213-1219.

210. Deland K, Starr BF, Mercer JS, et al. Tumor genotype dictates radiosensitization after Atm deletion in primary brainstem glioma models. *The Journal of clinical investigation.* 2021; 131(1).

211. Agnihotri S, Burrell K, Buczkowicz P, et al. ATM regulates 3-methylpurine-DNA glycosylase and promotes therapeutic resistance to alkylating agents. *Cancer discovery.* 2014; 4(10):1198-1213.

212. Dolman MEM, Van Der Ploeg I, Koster J, et al. DNA-dependent protein kinase as molecular target for radiosensitization of neuroblastoma cells. *PLoS One.* 2015; 10(12):e0145744.

213. Tian J, Li X, Si M, Liu T, Li J. CD271+ osteosarcoma cells display stem-like properties. *PloS one.* 2014; 9(6):e98549.

214. Baxter PA, Su JM, Onar-Thomas A, et al. A phase I/II study of veliparib (ABT-888) with radiation and temozolomide in newly diagnosed diffuse pontine glioma: a Pediatric Brain Tumor Consortium study. *Neuro-oncology.* 2020; 22(6):875-885.

215. Su JM, Thompson P, Adesina A, et al. A phase I trial of veliparib (ABT-888) and temozolomide in children with recurrent CNS tumors: a pediatric brain tumor consortium report. *Neuro-oncology.* 2014; 16(12):1661-1668.

216. Chugh R, Ballman KV, Helman LJ, et al. SARC025 arms 1 and 2: A phase 1 study of the poly (ADP-ribose) polymerase inhibitor niraparib with temozolomide or irinotecan in patients with advanced Ewing sarcoma. *Cancer.* 2021; 127(8):1301-1310.

217. Federico SM, Pappo AS, Sahr N, et al. A phase I trial of talazoparib and irinotecan with and without temozolomide in children and young adults with recurrent or refractory solid malignancies. *European Journal of Cancer.* 2020; 137:204-213.

218. Schafer ES, Rau RE, Berg SL, et al. Phase 1/2 trial of talazoparib in combination with temozolomide in children and adolescents with refractory/recurrent solid tumors including Ewing sarcoma: A Children's Oncology Group Phase 1 Consortium study (ADVL1411). *Pediatric blood & cancer.* 2020; 67(2):e28073.

219. Choy E, Butrynski JE, Harmon DC, et al. Phase II study of olaparib in patients with refractory Ewing sarcoma following failure of standard chemotherapy. *BMC cancer.* 2014; 14(1):1-6.

220. Prince EW, Balakrishnan I, Shah M, et al. Checkpoint kinase 1 expression is an adverse prognostic marker and therapeutic target in MYC-driven medulloblastoma. *Oncotarget.* 2016; 7(33):53881.

221. Lowery CD, Dowless M, Renschler M, et al. Broad spectrum activity of the checkpoint kinase 1 inhibitor prexasertib as a single agent or chemopotentiator across a range of preclinical pediatric tumor models. *Clinical Cancer Research.* 2019; 25(7):2278-2289.

222. Goss KL, Koppenhafer SL, Harmoney KM, Terry WW, Gordon DJ. Inhibition of CHK1 sensitizes Ewing sarcoma cells to the ribonucleotide reductase inhibitor gemcitabine. *Oncotarget.* 2017; 8(50):87016.

223. Koppenhafer SL, Goss KL, Terry WW, Gordon DJ. Inhibition of the ATR–CHK1 Pathway in Ewing Sarcoma Cells Causes DNA Damage and Apoptosis via the CDK2-Mediated Degradation of RRM2. *Molecular Cancer Research.* 2020; 18(1):91-104.

224. Southgate HE, Chen L, Tweddle DA, Curtin NJ. ATR inhibition potentiates PARP inhibitor cytotoxicity in high risk neuroblastoma cell lines by multiple mechanisms. *Cancers.* 2020; 12(5):1095.

225. Long GV, Hauschild A, Santinami M, et al. Adjuvant dabrafenib plus trametinib in stage III BRAF-mutated melanoma. *New England Journal of Medicine.* 2017; 377(19):1813-1823.

226. Delattre O, Zucman J, Melot T, et al. The Ewing family of tumors--a subgroup of small-round-cell tumors defined by specific chimeric transcripts. *New England Journal of Medicine.* 1994; 331(5):294-299.

227. Su XA, Ma D, Parsons JV, et al. RAD21 is a driver of chromosome 8 gain in Ewing sarcoma to mitigate replication stress. *Genes & development.* 2021; 35(7-8):556-572.

228. Puigvert JC, Sanjiv K, Helleday T. Targeting DNA repair, DNA metabolism and replication stress as anti-cancer strategies. *The FEBS journal.* 2016; 283(2):232-245.

229. Baillie KE, Stirling PC. Beyond Kinases: Targeting Replication Stress Proteins in Cancer Therapy. *Trends in Cancer.* 2020.

230. Bartkova J, Hořejší Z, Koed K, et al. DNA damage response as a candidate anti-cancer barrier in early human tumorigenesis. *Nature.* 2005; 434(7035):864-870.

231. Bartkova J, Rezaei N, Liontos M, et al. Oncogene-induced senescence is part of the tumorigenesis barrier imposed by DNA damage checkpoints. *Nature.* 2006; 444(7119):633-637.

232. Gorgoulis VG, Vassiliou L-VF, Karakaidos P, et al. Activation of the DNA damage checkpoint and genomic instability in human precancerous lesions. *Nature.* 2005; 434(7035):907-913.

233. Di Micco R, Fumagalli M, Cicalese A, et al. Oncogene-induced senescence is a DNA damage response triggered by DNA hyper-replication. *Nature.* 2006; 444(7119):638-642.

234. Kitao H, Iimori M, Kataoka Y, et al. DNA replication stress and cancer chemotherapy. *Cancer science.* 2018; 109(2):264-271.

235. Zhang J, Dai Q, Park D, Deng X. Targeting DNA replication stress for cancer therapy. *Genes.* 2016; 7(8):51.

236. Gaillard H, García-Muse T, Aguilera A. Replication stress and cancer. *Nature Reviews Cancer.* 2015; 15(5):276-289.

237. Berti M, Vindigni A. Replication stress: getting back on track. *Nature structural & molecular biology.* 2016; 23(2):103-109.

238. Toledo LI, Altmeyer M, Rask M-B, et al. ATR prohibits replication catastrophe by preventing global exhaustion of RPA. *Cell.* 2013; 155(5):1088-1103.

239. Canman CE. Replication checkpoint: preventing mitotic catastrophe. *Current Biology.* 2001; 11(4):R121-R124.

240. Lecona E, Fernández-Capetillo O. Replication stress and cancer: it takes two to tango. *Experimental cell research.* 2014; 329(1):26-34.

241. Laurenti E, Wilson A, Trumpp A. Myc's other life: stem cells and beyond. *Current opinion in cell biology.* 2009; 21(6):844-854.

242. Nesbit CE, Tersak JM, Prochownik EV. MYC oncogenes and human neoplastic disease. *Oncogene.* 1999; 18(19).

243. Schroeder K, Gururangan S. Molecular variants and mutations in medulloblastoma. *Pharmacogenomics and personalized medicine.* 2014; 7:43.

244. Hamperl S, Bocek MJ, Saldivar JC, Swigut T, Cimprich KA. Transcription-Replication Conflict Orientation Modulates R-Loop Levels and Activates Distinct DNA Damage Responses. *Cell.* 2017; 170(4):774-786. e719.

245. Wang JC. Cellular roles of DNA topoisomerases: a molecular perspective. *Nature reviews Molecular cell biology.* 2002; 3(6):430-440.

246. Sollier J, Cimprich KA. R-Loops Breaking Bad. *Trends in cell biology.* 2015; 25(9):514.

247. Korshunov A, Schrimpf D, Ryzhova M, et al. H3-/IDH-wild type pediatric glioblastoma is comprised of molecularly and prognostically distinct subtypes with associated oncogenic drivers. *Acta Neuropathologica.* 2017:1-10.

248. Regairaz M, Zhang Y-W, Fu H, et al. Mus81-mediated DNA cleavage resolves replication forks stalled by topoisomerase I–DNA complexes. *Journal of Cell Biology.* 2011; 195(5):739-749.

249. Seiler JA, Conti C, Syed A, Aladjem MI, Pommier Y. The intra-S-phase checkpoint affects both DNA replication initiation and elongation: single-cell and-DNA fiber analyses. *Molecular and cellular biology.* 2007; 27(16):5806-5818.

250. Satoh MS, Lindahl T. Role of poly (ADP-ribose) formation in DNA repair. *Nature.* 1992; 356(6367):356-358.

251. Ahel I, Ahel D, Matsusaka T, et al. Poly (ADP-ribose)-binding zinc finger motifs in DNA repair/checkpoint proteins. *Nature.* 2008; 451(7174):81-85.

252. Bryant HE, Petermann E, Schultz N, et al. PARP is activated at stalled forks to mediate Mre11-dependent replication restart and recombination. *The EMBO journal.* 2009; 28(17):2601-2615.

253. Min W, Bruhn C, Grigaravicius P, et al. Poly (ADP-ribose) binding to Chk1 at stalled replication forks is required for S-phase checkpoint activation. *Nature communications.* 2013; 4(1):1-14.

254. Murai J, Shar-yin NH, Das BB, et al. Trapping of PARP1 and PARP2 by clinical PARP inhibitors. *Cancer research.* 2012; 72(21):5588-5599.

255. Sin-Chan P, Mumal I, Suwal T, et al. A C19MC-LIN28A-MYCN oncogenic circuit driven by hijacked super-enhancers is a distinct therapeutic vulnerability in ETMRs: a lethal brain tumor. *Cancer cell.* 2019; 36(1):51-67. e57.

256. Haaz M-C, Rivory LP, Riché C, Robert J. The transformation of irinotecan (CPT-11) to its active metabolite SN-38 by human liver microsomes Differential hydrolysis for the lactone and carboxylate forms. *Naunyn-Schmiedeberg's archives of pharmacology.* 1997; 356(2):257-262.

257. Shingyoji M, Takiguchi Y, Watanabe-Uruma R, et al. In vitro conversion of irinotecan to SN-38 in human plasma. *Cancer science.* 2004; 95(6):537-540.

258. Yadav B, Pemovska T, Szwajda A, et al. Quantitative scoring of differential drug sensitivity for individually optimized anticancer therapies. *Scientific reports.* 2014; 4(1):1-10.

259. Gadducci A, Cosio S. Randomized Clinical Trials and Real World Prospective Observational Studies on Bevacizumab, PARP Inhibitors, and Immune Checkpoint Inhibitors in the First-Line Treatment of Advanced Ovarian Carcinoma: A Critical Review. *Anticancer Research.* 2021; 41(10):4673-4685.

260. Litton J, Hurvitz S, Mina L, et al. Talazoparib versus chemotherapy in patients with germline BRCA1/2-mutated HER2-negative advanced breast cancer: final overall survival results from the EMBRACA trial. *Annals of Oncology.* 2020; 31(11):1526-1535.

261. Lord CJ, Ashworth A. PARP inhibitors: Synthetic lethality in the clinic. *Science.* 2017; 355(6330):1152-1158.

262. Xiong Y, Guo Y, Liu Y, et al. Pamiparib is a potent and selective PARP inhibitor with unique potential for the treatment of brain tumor. *Neoplasia.* 2020; 22(9):431-440.

263. Wang H, Ren B, Liu Y, et al. Discovery of pamiparib (BGB-290), a potent and selective poly (ADP-ribose) polymerase (PARP) inhibitor in clinical development. *Journal of Medicinal Chemistry.* 2020; 63(24):15541-15563.

264. Tang Z, Jiang B, Shi Z, et al. BGB-290, a novel PARP inhibitor with unique brain penetration ability, demonstrated strong synergism with temozolomide in subcutaneous and intracranial xenograft models: AACR; 2015.

265. Rouits E, Guichard S, Canal P, Chatelut E. Non-linear pharmacokinetics of irinotecan in mice. *Anti-cancer drugs.* 2002; 13(6):631-635.

266. Bissery M, Vrignaud P, Lavelle F, Chabot G. Experimental antitumor activity and pharmacokinetics of the camptothecin analog irinotecan (CPT-11) in mice. *Anti-cancer drugs.* 1996; 7(4):437-460.

267. Santi DV, Schneider EL, Ashley GW. Macromolecular prodrug that provides the irinotecan (CPT-11) active-metabolite SN-38 with ultralong half-life, low C max, and low glucuronide formation. *Journal of medicinal chemistry.* 2014; 57(6):2303-2314.

268. Fontaine SD, Santi AD, Reid R, Smith PC, Ashley GW, Santi DV. PLX038: a PEGylated prodrug of SN-38 independent of UGT1A1 activity. *Cancer chemotherapy and pharmacology.* 2020; 85(1):225-229.

269. Shi Y, Van der Meel R, Chen X, Lammers T. The EPR effect and beyond: Strategies to improve tumor targeting and cancer nanomedicine treatment efficacy. *Theranostics.* 2020; 10(17):7921.

270. Mishra P, Nayak B, Dey R. PEGylation in anti-cancer therapy: An overview. *asian journal of pharmaceutical sciences.* 2016; 11(3):337-348.

271. Kunos C, Deng W, Dawson D, et al. A phase I-II evaluation of veliparib (NSC# 737664), topotecan, and filgrastim or pegfilgrastim in the treatment of persistent or recurrent carcinoma of the uterine cervix: an NRG Oncology/Gynecologic Oncology Group study. *International Journal of Gynecologic Cancer.* 2015; 25(3).

272. Kummar S, Chen A, Ji J, et al. Phase I study of PARP inhibitor ABT-888 in combination with topotecan in adults with refractory solid tumors and lymphomas. *Cancer research.* 2011; 71(17):5626-5634.

273. Federico SM, Stewart E, Coleman JL, et al. Phase I study of talazoparib and irinotecan in children and young adults with recurrent/refractory solid tumors: American Society of Clinical Oncology; 2017.

274. Bindra RS. Penetrating the brain tumor space with DNA damage response inhibitors. *Neuro-oncology.* 2020; 22(12):1718-1720.

275. Friedlander M, Meniawy T, Markman B, et al. Pamiparib in combination with tislelizumab in patients with advanced solid tumours: results from the dose-escalation stage of a multicentre, open-label, phase 1a/b trial. *The Lancet Oncology.* 2019; 20(9):1306-1315.

276. Piotrowski A, Puduvalli V, Wen P, et al. ACTR-39. Pamiparib in combination with radiation therapy (RT) and/or temozolomide (TMZ) in patients with newly diagnosed or recurrent/refractory (R/R) glioblastoma (GBM); phase 1b/2 study update. *Neuro-Oncology.* 2019; 21(Supplement_6):vi21-vi22.

277. Markham A. Pamiparib: First Approval. *Drugs.* 2021:1-6.

278. Schmidt C, Schubert NA, Brabetz S, et al. Pre-clinical drug screen reveals topotecan, actinomycin D and volasertib as potential new therapeutic candidates for ETMR brain tumor patients. *Neuro-Oncology.* 2017:nox093.

279. Houghton PJ, Cheshire PJ, Hallman JD, et al. Efficacy of topoisomerase I inhibitors, topotecan and irinotecan, administered at low dose levels in protracted schedules to mice bearing xenografts of human tumors. *Cancer chemotherapy and pharmacology.* 1995; 36(5):393-403.

280. Femke M, Goey AK, van Schaik RH, Mathijssen RH, Bins S. Individualization of irinotecan treatment: a review of pharmacokinetics, pharmacodynamics, and pharmacogenetics. *Clinical pharmacokinetics.* 2018; 57(10):1229-1254.

281. Meyer N, Penn LZ. Reflecting on 25 years with MYC. *Nature Reviews Cancer.* 2008; 8(12):976-990.

282. Huang M, Weiss WA. Neuroblastoma and MYCN. *Cold Spring Harbor perspectives in medicine.* 2013; 3(10):a014415.

283. Charron J, Malynn BA, Fisher P, et al. Embryonic lethality in mice homozygous for a targeted disruption of the N-myc gene. *Genes & development.* 1992; 6(12a):2248-2257.

284. Davis AC, Wims M, Spotts GD, Hann SR, Bradley A. A null c-myc mutation causes lethality before 10.5 days of gestation in homozygotes and reduced fertility in heterozygous female mice. *Genes & development.* 1993; 7(4):671-682.

285. Sawai S, Shimono A, Wakamatsu Y, Palmes C, Hanaoka K, Kondoh H. Defects of embryonic organogenesis resulting from targeted disruption of the N-myc gene in the mouse. *Development.* 1993; 117(4):1445-1455.

286. Kenney AM, Cole MD, Rowitch DH. Nmyc upregulation by sonic hedgehog signaling promotes proliferation in developing cerebellar granule neuron precursors. 2003.

287. Morton CL, Wierdl M, Oliver L, et al. Activation of CPT-11 in mice: identification and analysis of a highly effective plasma esterase. *Cancer Research.* 2000; 60(15):4206-4210.

288. Norris RE, Adamson PC, Nguyen VT, Fox E. Preclinical evaluation of the PARP inhibitor, olaparib, in combination with cytotoxic chemotherapy in pediatric solid tumors. *Pediatric blood & cancer.* 2014; 61(1):145-150.

289. Zander SA, Sol W, Greenberger L, et al. EZN-2208 (PEG-SN38) overcomes ABCG2-mediated topotecan resistance in BRCA1-deficient mouse mammary tumors. 2012.

290. Fontaine SD, Ashley GW, Houghton PJ, et al. A Very Long-Acting PARP Inhibitor Suppresses Cancer Cell Growth in DNA Repair-Deficient Tumor Models. *Cancer Research.* 2021; 81(4):1076-1086.

291. Arif WM, Elsinga PH, Gasca-Salas C, et al. Focused ultrasound for opening blood-brain barrier and drug delivery monitored with positron emission tomography. *Journal of controlled release.* 2020; 324:303-316.

292. Brabetz S. *Molecular and preclinical evaluation of patient-derived orthotopic xenograft models of pediatric brain tumors*. Heidelberg: Combined Faculty of Natural Sciences and Mathematics, Ruperto Carola University Heidelberg; 2018.

293. Skoda AM, Simovic D, Karin V, Kardum V, Vranic S, Serman L. The role of the Hedgehog signaling pathway in cancer: A comprehensive review. *Bosnian journal of basic medical sciences.* 2018; 18(1):8.

294. Nüsslein-Volhard C, Wieschaus E. Mutations affecting segment number and polarity in Drosophila. *Nature.* 1980; 287(5785):795-801.

295. di Magliano MP, Hebrok M. Hedgehog signalling in cancer formation and maintenance. *Nature reviews cancer.* 2003; 3(12):903-911.

296. Varjosalo M, Taipale J. Hedgehog: functions and mechanisms. *Genes & development.* 2008; 22(18):2454-2472.

297. Lowry W, Richter L, Yachechko R, et al. Generation of human induced pluripotent stem cells from dermal fibroblasts. *Proceedings of the National Academy of Sciences.* 2008; 105(8):2883-2888.

298. Beachy PA, Karhadkar SS, Berman DM. Tissue repair and stem cell renewal in carcinogenesis. *Nature.* 2004; 432(7015):324-331.

299. Plotnikova OV, Golemis EA, Pugacheva EN. Cell cycle–dependent ciliogenesis and cancer. *Cancer research.* 2008; 68(7):2058-2061.

300. MacDonald TJ. Hedgehog pathway in pediatric cancers: they're not just for brain tumors anymore. *American Society of Clinical Oncology Educational Book.* 2012; 32(1):605-609.

301. Booms P, Harth M, Sader R, Ghanaati S. Vismodegib hedgehog-signaling inhibition and treatment of basal cell carcinomas as well as keratocystic odontogenic tumors in Gorlin syndrome. *Annals of maxillofacial surgery.* 2015; 5(1):14.

302. Onodera S, Nakamura Y, Azuma T. Gorlin Syndrome: Recent Advances in Genetic Testing and Molecular and Cellular Biological Research. *International journal of molecular sciences.* 2020; 21(20):7559.

303. Sheng T, Li C, Zhang X, et al. Activation of the hedgehog pathway in advanced prostate cancer. *Molecular cancer.* 2004; 3(1):1-13.

304. Bailey JM, Mohr AM, Hollingsworth MA. Sonic hedgehog paracrine signaling regulates metastasis and lymphangiogenesis in pancreatic cancer. *Oncogene.* 2009; 28(40):3513-3525.

305. Ma X, Sheng T, Zhang Y, et al. Hedgehog signaling is activated in subsets of esophageal cancers. *International journal of cancer.* 2006; 118(1):139-148.

306. Karhadkar SS, Bova GS, Abdallah N, et al. Hedgehog signalling in prostate regeneration, neoplasia and metastasis. *Nature.* 2004; 431(7009):707-712.

307. Taipale J, Beachy PA. The Hedgehog and Wnt signalling pathways in cancer. *nature.* 2001; 411(6835):349-354.

308. Hahn H, Wicking C, Zaphiropoulos PG, et al. Mutations of the human homolog of Drosophila patched in the nevoid basal cell carcinoma syndrome. *Cell.* 1996; 85(6):841-851.

309. Roma J, Almazán-Moga A, Sánchez de Toledo J, Gallego S. Notch, wnt, and hedgehog pathways in rhabdomyosarcoma: from single pathways to an integrated network. *Sarcoma.* 2012; 2012.

310. Girardi D, Barrichello A, Fernandes G, Pereira A. Targeting the Hedgehog pathway in cancer: current evidence and future perspectives. *Cells.* 2019; 8(2):153.

311. Amakye D, Jagani Z, Dorsch M. Unraveling the therapeutic potential of the Hedgehog pathway in cancer. *Nature medicine.* 2013; 19(11):1410.

312. Romer JT, Kimura H, Magdaleno S, et al. Suppression of the Shh pathway using a small molecule inhibitor eliminates medulloblastoma in Ptc1+/− p53−/− mice. *Cancer cell.* 2004; 6(3):229-240.

313. Robinson GW, Orr BA, Wu G, et al. Vismodegib exerts targeted efficacy against recurrent sonic hedgehog–subgroup medulloblastoma: results from phase II pediatric brain tumor consortium studies PBTC-025B and PBTC-032. *Journal of Clinical Oncology.* 2015; 33(24):2646.

314. Lee Y, Kawagoe R, Sasai K, et al. Loss of suppressor-of-fused function promotes tumorigenesis. *Oncogene.* 2007; 26(44):6442-6447.

315. Atwood SX, Sarin KY, Whitson RJ, et al. Smoothened variants explain the majority of drug resistance in basal cell carcinoma. *Cancer cell.* 2015; 27(3):342-353.

316. Zheng T, Ghasemi DR, Okonechnikov K, et al. Cross-species genomics reveals oncogenic dependencies in ZFTA/C11orf95 fusion-positive supratentorial ependymomas. *Cancer Discovery.* 2021.

317. Raleigh DR, Reiter JF. Misactivation of Hedgehog signaling causes inherited and sporadic cancers. *The Journal of clinical investigation.* 2019; 129(2):465-475.

318. Kupp R, Ruff L, Terranova S, et al. ZFTA-translocations constitute ependymoma chromatin remodeling and transcription factors. *Cancer discovery.* 2021.

319. Rudin CM, Hann CL, Laterra J, et al. Treatment of medulloblastoma with hedgehog pathway inhibitor GDC-0449. *New England Journal of Medicine.* 2009; 361(12):1173-1178.

320. Yauch RL, Dijkgraaf GJ, Alicke B, et al. Smoothened mutation confers resistance to a Hedgehog pathway inhibitor in medulloblastoma. *Science.* 2009; 326(5952):572-574.

321. Buonamici S, Williams J, Morrissey M, et al. Interfering with resistance to smoothened antagonists by inhibition of the PI3K pathway in medulloblastoma. *Science translational medicine.* 2010; 2(51):51ra70-51ra70.

322. Sharpe HJ, Pau G, Dijkgraaf GJ, et al. Genomic analysis of smoothened inhibitor resistance in basal cell carcinoma. *Cancer cell.* 2015; 27(3):327-341.

323. Wang C, Wu H, Katritch V, et al. Structure of the human smoothened receptor bound to an antitumour agent. *Nature.* 2013; 497(7449):338-343.

324. Atwood SX, Sarin KY, Li JR, et al. Rolling the genetic dice: neutral and deleterious Smoothened mutations in drug-resistant basal cell carcinoma. *The Journal of investigative dermatology.* 2015; 135(8):2138.

325. Pricl S, Cortelazzi B, Dal Col V, et al. Smoothened (SMO) receptor mutations dictate resistance to vismodegib in basal cell carcinoma. *Molecular oncology.* 2015; 9(2):389-397.

326. Pusapati GV, Kong JH, Patel BB, et al. CRISPR screens uncover genes that regulate target cell sensitivity to the morphogen sonic hedgehog. *Developmental cell.* 2018; 44(1):113-129. e118.

327. Kong JH, Young CB, Pusapati GV, et al. A membrane-tethered ubiquitination pathway regulates Hedgehog signaling and heart development. *Developmental Cell.* 2020; 55(4):432-449. e412.

328. Zhou X, Edmonson MN, Wilkinson MR, et al. Exploring genomic alteration in pediatric cancer using ProteinPaint. *Nature genetics.* 2016; 48(1):4-6.

329. Bader JC, Razak ARA, Shacham S, Xu H. Pharmacokinetics of selinexor: the first-in-class selective inhibitor of nuclear export. *Clinical Pharmacokinetics.* 2021:1-13.

330. Tremblay G, Daniele P, Breeze J, et al. Quality of life analyses in patients with multiple myeloma: results from the Selinexor (KPT-330) Treatment of Refractory Myeloma (STORM) phase 2b study. *BMC cancer.* 2021; 21(1):1-10.

331. Smith MA, Lock R, Carol H, et al. Pharmacodynamic and genomic markers associated with response to the XPO1/CRM1 inhibitor selinexor (KPT-330): a report from the Pediatric Preclinical Testing Program: AACR; 2015.

332. Hau P, Frappaz D, Hovey E, et al. Development of randomized trials in adults with medulloblastoma—the example of eortc 1634-btg/noa-23. *Cancers.* 2021; 13(14):3451.

333. Wall ME, Wani MC, Cook C, Palmer KH, McPhail Aa, Sim G. Plant antitumor agents. I. The isolation and structure of camptothecin, a novel alkaloidal leukemia and tumor inhibitor from camptotheca acuminata1, 2. *Journal of the American Chemical Society.* 1966; 88(16):3888-3890.

334. Rodriguez-Galindo C, Radomski K, Stewart CF, Furman W, Santana VM, Houghton PJ. Clinical use of topoisomerase I inhibitors in anticancer treatment. *Medical and Pediatric Oncology: The Official Journal of SIOP—International Society of Pediatric Oncology (Societé Internationale d'Oncologie Pédiatrique.* 2000; 35(4):385-402.

335. Turner CD, Gururangan S, Eastwood J, et al. Phase II study of irinotecan (CPT-11) in children with high-risk malignant brain tumors: the Duke experience. *Neuro-oncology.* 2002; 4(2):102-108.

336. Friedman HS, Petros WP, Friedman AH, et al. Irinotecan therapy in adults with recurrent or progressive malignant glioma. *Journal of Clinical Oncology.* 1999; 17(5):1516-1516.

337. Hughes P, Marshall D, Reid Y, Parkes H, Gelber C. The costs of using unauthenticated, over-passaged cell lines: how much more data do we need? *Biotechniques.* 2007; 43(5):575-586.

338. Bhimani J, Ball K, Stebbing J. Patient-derived xenograft models—the future of personalised cancer treatment: Nature Publishing Group; 2020.

339. DeRose YS, Wang G, Lin Y-C, et al. Tumor grafts derived from women with breast cancer authentically reflect tumor pathology, growth, metastasis and disease outcomes. *Nature medicine.* 2011; 17(11):1514-1520.

Publications

Ongoing work:

Krausert S.*, Brabetz S.*, Mack N.L., Schmitt-Hoffner F., Schwalm B., Peterziel H., Mangang A., Holland-Letz T., Sieber L., Korshunov A., Oehme I., Jäger N., Witt O., Pfister S.M. and Kool M. **Predictive modeling of resistance to SMO-inhibition in a patient-derived orthotopic xenograft model of SHH medulloblastoma**; Neuro-Oncology; *in revision*

* Sonja Krausert and Sebastian Brabetz are joint first authors.

Authorships in peer-reviewed journals:

Keller K.M.*, **Krausert S.***, Gopisetty A.*, Luedtke D., Koster J., Schubert N.A., Rodríguez A., van Hooff S.R., Stichel D., Dolman E.M., Vassal G., Pfister S.M., Caron H.N., Stancato L.F., Molenaar J.J.**, Jäger N.**, and Kool M.**. **Target Actionability Review: a systematic evaluation of replication stress as a therapeutic target for pediatric solid malignancies**; European Journal of Cancer; *in press*

* Kaylee M. Keller, Sonja Krausert and Apurva Gopisetty are joint first authors.

** Jan J. Molenaar, Natalie Jäger and Marcel Kool are joint senior authors.

Ballhausen A., Przybilla M.J., Jendrusch M., Haupt S., Pfaffendorf E., Seidler F., Witt J., Hernandez Sanchez A., Urban K., Draxlbauer M., **Krausert S.**, Ahadova A., Kalteis M.S., Pfuderer P.L., Heid D., Stichel D., Gebert J., Bonsack M., Schott S., Bläker H., Seppälä T., Mecklin J.P., Ten Broeke S., Nielsen M., Heuveline V., Krzykalla J., Benner A., Riemer A.B., von Knebel Doeberitz M. and Kloor M. (2020). **The shared frameshift mutation landscape of microsatellite-unstable cancers suggests immunoediting during tumor evolution**; Nature Communications *11* (1): 1-13.

Fresnais M., Muck A., Majewsky M., Statz B., **Krausert S.**, Benzel J., Castel D., Le Dret L., Pfister S.M., Haefeli W.E., Burhenne J. and Longuespée R. (2020). **Rapid and sensitive drug quantification in tissue sections using matrix assisted laser desorption ionization-ion mobility-mass spectrometry profiling**; Journal of the American Society for Mass Spectrometry *31* (3): 742-751.

Lambo S., Gröbner S.N., Rausch T., Waszak S.M., Schmidt C., Gorthi A., Romero J.C., Mauermann M., Brabetz S., **Krausert S.**, Buchhalter I., Koster J., Zwijnenburg D.A., Sill M., Hübner J.M., Mack N., Schwalm B., Ryzhova M., Hovestadt V., Papillon-Cavanagh S., Chan J.A., Landgraf P., Ho B., Milde T., Witt O., Ecker J., Sahm F., Sumerauer D., Ellison D.W., Orr B.A., Darabi A., Haberler C., Figarella-Branger D., Wesseling P., Schittenhelm J., Remke M., Taylor M.D., Gil-da-Costa M.J., Łastowska M., Grajkowska W., Hasselblatt M., Hauser P., Pietsch T., Uro-Coste E., Bourdeaut F., Masliah-Planchon J., Rigau V.,

Alexandrescu S., Wolf S., Li X.N., Schüller U., Snuderl M., Karajannis M.A., Giangaspero F., Jabado N., von Deimling A., Jones D.T.W., Korbel J.O., von Hoff K., Lichter P., Huang A., Bishop A.J.R., Pfister S.M., Korshunov A. and Kool M. (2019). **The molecular landscape of ETMR at diagnosis and relapse;** Nature *576* (7786): 274-280.

Pusch S., **Krausert S.**, Fischer V., Balss J., Ott M., Schrimpf D., Capper D., Sahm F., Eisel J., Beck A.C., Jugold M., Eichwald V., Kaulfuss S., Panknin O., Rehwinkel H., Zimmermann K., Hillig R.C., Guenther J., Toschi L., Neuhaus R., Haegebart A., Hess-Stumpp H., Bauser M., Wick W., Unterberg A., Herold-Mende C., Platten M. and von Deimling A. (2017). **Pan-mutant IDH1 inhibitor BAY 1436032 for effective treatment of IDH1 mutant astrocytoma in vivo;** Acta neuropathologica *133* (4): 629-644.

Acknowledgements

The preparation of the thesis would not have been possible without the support of many people and I would like to thank all of them. Not only their technical and scientific contribution but also their mental and psychological support made the last 4.5 years as enjoyable as they were.

First of all I want to thank Marcel Kool for giving me the chance to join his group as a PhD student. Thank you so much for the supervision and the guidance to develop as a scientist. It was great to get the freedom to decide independently but also know that you were always available for help to discuss open questions and arising problems. You also never lost sight of the goal of the projects and encouraged me to summarize the results for publications. Moreover, your support was not only scientifically and you also promoted group outings, which ensured a good spirit in the group. This contributed a lot that I enjoyed the time of my PhD in the group as much as I did. Thank you very much!

Furthermore, I want to thank Stefan Pfister for all his support and guidance. I enjoyed a lot being part of the department "Pediatric Neurooncology" and was delighted by the great and familial atmosphere. The flat hierarchy contributed to a great working environment within the department and facilitated team work. Furthermore, the KiTZ Christmas parties, summer parties and lab outings contributed that the department still felt as a team even though it grew a lot the last years.

My gratitude goes to Michael Boutros for being the faculty supervisor of my PhD and supporting me as a member of my thesis advisory committee. Furthermore, I want to thank Christel Herold-Mende for her helpful input and comments in the TAC meetings. In addition, I thank Karin Müller-Decker and Moritz Mall for their willingness to participate in my PhD defense examination.

Since a lot of work of my PhD project was related to *in vivo* work, I am deeply grateful for the great work and support of Norman Mack and Benjamin Schwalm. Thank you both for all the support and help with the *in vivo* studies and the work related to mice. A special thank goes to Norman for always doing the treatments in the morning, doing IVIS and taking care of the mice, which took much work off my shoulders. It was always great and helpful to hear your experience for any question that came in my mind related to mouse work (but also be able to talk with you about any other topic) and have your support for the project. Thank you very much!

I also want to thank Olaf Witt and Cornelis van Tilburg for their great support and regular discussions that stimulated the project and pushed the project forward. It was great to collaborate with you and I am very grateful that I could always count on you, your quick reply to emails and your input.

Additionally, I am thankful for all the work contributed by Ina Oehme, Heike Peterziel, Aileen Mangang and Alexandra Stroh-Dege of the Translational Drug Screening Unit at the KiTZ. Thank you so much for all your help and, especially Heike, answering my thousands of questions and giving me the opportunity for screening the cell lines and PDX models.

For the support with all questions related to animal protocols I want to thank Kerstin Dell. All your comments and experiences did not only improve and speed up the writing of animal protocols but also helped me to assess the different arising questions related to the *in vivo* work. Moreover, I want to thank Mattea Durst and all animal caretakers for their great work. All the preclinical *in vivo* work wouldn't have been possible to this extent without your everyday work.

For all the great help, meetings, discussions and support related to my *in vivo* CRISPR-screen project (even though time was unfortunately too short to finish it) I want to thank Luisa Henkel, Benedikt Rauscher and Katharina Imkeller. Luisa, thanks for all your patience and the explanations to my numerous questions. Benedikt and Katharina, thanks for your quick help with all the bioinformatic questions.

I am very thankful for the great collaboration with Kaylee Keller and Apurva Gopisetty for the TAR. Ladies, it was a ton of work reading all the papers and struggling with the limitations, but I am very proud of us that we managed it and compiled the review paper. And I am really happy that we went through the process together – it was a real team-effort!

A big thank goes to all members of B06x. You all contributed to the great atmosphere; the Christmas parties and defense celebrations were always fun. Most importantly, it was amazing to always know that helpful people were around and every arising question for help/antibodies/enzymes was answered. A special thanks goes to Laura Sieber and Britta Statz. You both helped me so much with the stainings and always gave me the feeling that I, as an "unexperienced stainer", can ask every question no matter how basic it was. In addition, I want to say a big "thank you" to Andrea Wittmann. Witti, thank you for always being helpful and contributing to a great mood in the lab and it was always great knowing that you have a sympathetic ear and to chat with you.

Furthermore, I want to thank Anna-Lisa Böttcher and Iris Oezen. You helped me so much with all administrative work and I always enjoyed our lunch breaks a lot. We could not only discuss problems and concerns, but also chatted and laughed about any other topic and you ensured me relaxing and

recovering lunch and coffee breaks. I missed seeing you in “real life” the last almost two years. Additionally, I want to thank Kendra Maaß for all the great talks and nice evenings we had. It was always good and fun chatting with you – I still have a bottle of Gin that needs to be emptied ☺.

Even though, as probably for most PhD projects, not everything went perfectly from the beginning on and there were always ups and downs, I will always remember the last four years as an amazing time and never lost the motivation to go to work (well, on some days it was harder than on other days). A large share for this has the amazing Kool group: Marcel Kool, Felix Schmitt-Hoffner, Norman Mack, Benjamin Schwalm, Aylin Camgöz, Annette Büllesbach, Monika Mauermann, Anne Jenseit, Enrique Blanco Carmona, Anke Heit-Mondrzyk, Aniello Federico, Shanzheng Wang, Joudi Khal, Pascal Johann, Johannes Gojo and our alumnis Sebastian Brabetz, Sander Lambo, Sjoerd van Rijn and Jens-Martin Hübner. I enjoyed so much that we could not only talk and discuss about topics related to work, but also about other random topics and enjoyed time together outside of work, be it in Amsterdam, at Bräustadl, at the Christmas market, hiking to the brewery in Ziegelhausen or having a BBQ together. And I hope a lot that we can finally go skiing together in January. I am really happy that I did my PhD in this great group - it’s definitely the “kool”est group ☺ - and I want to thank all of you for making these 4.5 years to such a great chapter in my life!

Furthermore, I want to thank Stefan Pusch for giving me in 2012 the chance to work with him as a Hiwi. Thank you so much for everything I learned and was able to do under your supervision. Your trust in my skills and all the different experiments and lab work encouraged me to proceed with my studies and let my motivation for brain tumor research grow. Also during my PhD it was great to know that I could always count on your support and help.

However, I enjoyed my time of the PhD not only because of work but also made great friends, for which I am really thankful. Britta Ismer and Jasmin Mangei, thank you so much for motivating me to do triathlons. It was great to challenge ourselves in a sporty way and experience all this together. But not only sport, it is also always great to chat with you and enjoy time together. Thank you so much for being great friends! I am already looking forward to all upcoming adventures we will do together. Moreover, a big “thank you” also to Felix Schmitt-Hoffner, Norman Mack, Benjamin Schwalm, Jens-Martin Hübner, Annette Büllesbach and Alexander Sommerkamp. Whatever we did together, be it a trip to Manchester, a Tough Mudder, a trip to Freiburg, cooking, Gin-tasting, Squash, discussions about dairy goods (☺), or whatever. I always enjoyed the time together and the talks about any possible topic a lot. You all contributed so much that I had such a great time the last 4.5 years. But of course I hope that we will do many more great things together (we still have many vouchers to redeem anyway ☺).

In addition, I want to thank my friends in Heidelberg and at home to always be there for me and ensure that I didn't get lost in work and always found a balance between work and life besides work. A special thank goes to Laura, who motivated me to join sport courses, even though it was at 7 am in the morning, and I am very proud of us that we hold on to it even on rainy, cold days in winter. Thank you very much for preventing that I got stuck to my desk.

Finally, I am very grateful and a big "thank you" to my parents Dagmar and Norbert and my sister Bettina. Not only during the time of my PhD but for all my life you always fully supported me and are the best family I can wish for. Whatever I decided or wanted to do, you gave me the trust and freedom to give it a try and do it. I am so happy that we have such a good relation and can talk about everything. Thank you so much for everything! And Bettina: I am very sure that my sister is the best sister in the world!

One person that went through the time of my PhD completely together with me and was always at my side is Damian. Thank you so much for all your support, motivation, help, distraction (if necessary) and patience. You did not only help me a lot with proof-reading of the thesis, programming with R, interpretation of sequencing data and were patient with all the mouse work on weekends, but also supported me in everything besides work to find a good work-life balance. There are not enough words to describe how thankful I am.